PEOPLE'S DEMOCRATIC REPUBLIC OF ALGERIA

MINISTRY OF HIGHER EDUCATION

AND SCIENTIFIC RESEARCH

Universityof Kasdi Merbah – Ouergla

FACULITY OF APPLIED SCIENCES

DEPARTMENT OF PROCESS ENGINEERING

Thesis submitted in part fulfillment of the requirement for the degree of

Doctorate LMD

in Process Engineering

Specialty: Chemical Engineering

Application of cellulose/ZnO nanocomposite on the removal of toxic pollutants from aqueous solutions

Presented by

TEREA Hafidha

Before the jury composed of

ACHI Fethi	**Professor**	**University of Ouargla**	**President**
SELLOUM Djamel	**Professor**	**University of Setif**	**Supervisor**
REBIAI Abdelkrim	**Professor**	**University of El-Oued**	**Co- Supervisor**
MENNOUCHE Djamel	**Professor**	**University of Ouargla**	**Examiner**
GHIABA Zineb	**Professor**	**University of Ouargla**	**Examiner**
BACHA Oussama	**Professor**	**University of Ouargla**	**Examiner**

2022-2023

Abstract

Peanut (*Arachis hypogaea*) and pea (*Pisum sativum*) shells are among the most abundant plant waste found in agricultural regions.This residue contributes to environmental pollution if not repurposed and used in other fields.

The objective of this study is valorise these residues and use them as crude material to produce nanocrystalline cellulose.This compound was prepared by extracting pure cellulose (Cs) from the residues and converting it into nanocrystalline cellulose (CNCs), as well as hybridizing this substance with zinc oxide (ZnO) using two different methods. In order to study the properties of these new materials and validate their nature, several characterisation techniques were used, including optical (UV-visible, FTIR), structural and morphological (XRD, SEM) techniques.The analysis showed, the crystal size of the compounds (CNC/ZnO NPs) varied between 19.64 and 27.31 nanometers, while the gap bands ranged between 3.27 and 3.66 v for the first and second methodsm respectivety.

In this research work, the adsorption of methylene blue dye in an aqueous solution onto the cellulose and CNC/ZnO NPs prepared were studied. Five adsorption operation parameters were studied to optimize these adsorbents (adsorbent mass, contact time, initial concentrationof dye solution, initial solution pH, and temperature). Empirical data were analyzed using adsorption isotherm by Langmuir, Freundlich, and Temkin isotherm models to evaluate the maximum adsorption capacities. Kinetic data were tested with pseudo first-order model and pseudo second-order model.Thermodynamic parameters were also calculated.

Furthermore, the antibacterial activity of CNCs and CNC/ZnO NPs were tested using the agar well diffusion method, which has shown significant antibacterial activity against both Gram-positive, Gram-negative bacteria and fungi.

The remarkable output of this research can open a window for other possible significant applications such as removal of heavy metal ions and treatment of real wastewater.

Keywords: *Arachis hypogaea, Pisum sativum,*pure cellulose, nanocrystalline cellulose,zinc oxide.

الملخص

تعتبر قشور الفول السوداني و قشور البازلاء من بين أهم المخلفات النباتية المتواجدة بكميات كبيرة في المناطق الزراعية و تعد هذه الأخيرة كنفايات ملوثة للبيئة إن لم يتم استغلالها و استثمارها في مجالات أخرى. تهدف هذه الدراسة إلى إعادة تدوير هذه المخلفات واستخدامها كمواد خام لإنتاج السليلوز البلوري النانوي . تم الحصول على هذا المركب من خلال استخراج مادة السيليلوز النقية (Cs) من المخلفات و تحويلها إلي السيليلوز النانوي (CNCs), بالإضافة إلى تهجين هذه المادة بأكسيد الزنك (ZnO) بطريقتين مختلفتين. تم استخدام عدة تقنيات توصيف منها البصرية (**FTIR, UV-visible**) ,الهيكلية و المرفولوجية (**SEM ,XRD**) لدراسة خصائص هذه المواد المصنعة و كذا التأكد من طبيعتها. أظهرت التحاليل أن الحجم البلوري للمركب (CNC/ZnO NPs) يتراوح مابين 19.64-27.31 نانومتر , في حين بلغت طاقات فجوة النطاق من 3.27 إلى 3.66 فولت لكل من الطريقة الاولى و الثانية على الترتيب.

في هذا العمل البحثي، تمت دراسة امتزاز صبغة الميثيلين الزرقاء في محلول مائي على السليلوز وCNC/ZnO NPs المحضرة. تمت دراسة خمس معاملات لعملية الامتزاز لتحسين هذه الممتزات (كتلة المادة المازة، زمن التلامس، التركيز الأولي لمحلول الصبغة، الرقم الهيدروجيني الأولي للمحلول، ودرجة الحرارة). تم تحليل البيانات التجريبية باستخدام ايزوثرم الامتزاز بواسطة نماذج لانجمير وفريندليتش وتيمكين لتقييم السعات القصوى للامتزاز. تم اختبار البيانات الحركية باستخدام نموذج الدرجة الأولى الزائف ونموذج الدرجة الثانية الزائفة.كما تم حساب المعلمات الديناميكية الحرارية.

علاوة على ذلك، تم اختبار النشاط المضاد للبكتيريا لـ CNCs وCNC/ZnO NPs باستخدام طريقة الانتشار في أبار الاغار، والتي أظهرت نشاطًا مضادًا للبكتيريا كبيرًا ضد كل من البكتيريا إيجابية الجرام وسالبة الجرام و الفطريات.

يمكن أن تفتح النتائج الرائع لهذا البحث نافذة لتطبيقات مهمة أخرى محتملة مثلازالة أيونات المعادن الثقيلة و معالجة مياه الصرف الصحي الحقيقية.

الكلمات المفتاحية: قشور الفول السوداني,قشور البازلاء , السيليلوز النقي, السيليلوز النانوي, أكسيد الزنك.

Résumé

Les coques *Arachis hypogaea* et de *Pisum sativum* font partie des déchets végétaux les plus importants, présents en grandes quantités dans les zones agricoles. Ces déchets contribuent à la pollution de l'environnement s'ils ne sont pas exploités et utilisés dans d'autres domaines. L'objectif de cette étude est de valoriser ces résidus et de les utiliser comme matière brute pour élaborer de la cellulose cristalline nanométrique. Ce composé a été préparé par l'extraction de la cellulose pure (Cs) des déchets et en la convertissant en cellulose nanocristalline (CNCs), ainsi qu'en hybridant cette substance avec de l'oxyde de zinc (ZnO) à l'aide de deux méthodes différentes.Afin d'étudier les propriétés de ces nouveaux matériaux et de confirmer leur nature, plusieurs techniques de caractérisation ont été utilisées, y compris des techniques optiques (UV-visible, FTIR), structurelles et morphologiques (XRD, SEM). Les résultats ont montré que la taille cristalline du composé (CNC/ZnO NPs) variait entre 19,64 et 27,31 nanomètres, tandis que les bandes gap se situaient entre 3,27 et 3,66 v pour la première et la deuxième méthode respectivement.

Dans ce travail de recherche, l'adsorption du colorant bleu de méthylène en solution aqueuse sur la cellulose et les NP CNC/ZnO préparées a été étudiée. Cinq paramètres d'opération d'adsorption ont été étudiés pour optimiser ces adsorbants (masse d'adsorbant, temps de contact, concentration initiale de la solution de colorant, pH initial de la solution et température). Les données empiriques ont été analysées à l'aide de l'isotherme d'adsorption par les modèles isothermes de Langmuir, Freundlich et Temkin pour évaluer les capacités d'adsorption maximales. Les données cinétiques ont été testées avec un modèle de pseudo premier ordre et un modèle de pseudo second ordre. Les paramètres thermodynamiques ont également été calculés.

En outre, l'activité antibactérienne des CNC et des NP CNC/ZnO a été testée à l'aide de la méthode de diffusion dans des puits de gélose, qui a montré une activité antibactérienne significative contre les bactéries Gram-positives et Gram-négatives et les champignons.

Les résultats remarquables de cette recherche peuvent ouvrir la voie à d'autres applications importantes possibles, telles que l'élimination des ions de métaux lourds et le traitement des véritables eaux usées.

Mots clés :*Arachis hypogaea*,*Pisum sativum*,cellulose pure,cellulose nanocristalline,oxyde de zinc.

Acknowledgements

First and foremost, I would like to thank Almighty ***God*** *for granting me the strength and patience to complete this modest work.*

My heartfelt thanks go to Professor ***Djamel Selloum*** *, my thesis supervisor. Thank you for your guidance, your advice and for the trust you have shown me all along this study.*

I have a deep sense of gratitude to Professor ***Abdelkrim Rebiai,*** *my co-supervisor, for his advice and participation throughout this research, and his always enriching discussions.*

My thanks also go to the members of the jury for accepting to examine this work.

*Mr.****ACHI Fethi****, Professor at the University of Ouergla, who honoured me by agreeing to chair the jury.*

*Mr .****MENNOUCHE Djamel*** *and Mr.* ***BACHA Oussama****, Professors at the University of Ouergla, for agreeing to devote part of their time to evaluating this work as examiners.*

We would like to thank Mrs. ***GHAIBA Zineb****, Professor at the University of Ouergla, for his kind attention to this work and for agreeing to judge it.*

I wish to extend my special thanks to Professor ***Omar Ben Mya,*** *Professor* ***Belfar Mohamed Lakhder,*** *Professor* ***Dehamchia Mohamed****, Dr.****Djamila Berra****, Dr.* ***Abderrhmane Bouafia,*** *Dr.* ***khaoula Zaiz*** *, Dr.* ***Mohammed Laid Tedjani****, and Dr.* ***Louafi Okba*** *for their help and assistance.*

I am infinitely indebted to my family, my mother and my sisters and brothers, and I would like to express my heartfelt gratitude for your unconditional support, your unfailing encouragement and your constant love.

I will not forget my colleagues in the Pedagogical laboratory at the University of El-oued, ***Karima Beloul*** *, Dr.* ***Allag Nassiba,*** *Dr.* ***Dia Ouahida,*** *and* ***Gherbi Aicha.***

for their kindness, warm welcome during these unforgettable years, encouragement and support during the most challenging moments. Thank you for being an essential part of my academic journey.

Table of Contents

CHAPTER TWO

WATER POLLUTION AND ADSORPTION METHODE

CHAPTER THREE

MATERIALS AND METHODS

List of figures

List of tables

List of Abbreviations

Cs, CNCs	Cellulose, cellulosenanocrystals
CNCs, CNFs	Cellulose nanocrystals, Cellulose nanofibers
CNC/ZnO NPs.M1	Cellulose/Zinc oxide nanocomposite by first method from peanut shells.
CNC/ZnO NPs.M2	Cellulose/Zinc oxide nanocompositeby second method from peanut shells.
CNC/ZnO NPs.T1	Cellulose/Zinc oxide nanocomposite by first method from pea shells.
CNC/ZnO NPs.T2	Cellulose/Zinc oxide nanocomposite by second method from pea shells.
CrI	Crystallization Index
CrS	Crystal Size
Eg	Band gap energy
UV-Vis	Ultraviolet–visiblespectroscopy
FTIR	TransformInfraredspectroscopy
XRD	X-RayDiffraction
SEM	ScanningElectronMicroscopy
EDX	EnergyDispersiveX-ray analysis
C_0	Initial concentration
Ce	Equilibrium concentration
MB	Methyl Bleu
K_1	Pseudo first-order adsorption rate constant (min^{-1})
K_2	Pseudo second -order adsorption rate constant (g/mg.min)
KL	Langmuir constant (L/mg)
KF	Freundlinch constant
KT	Temkin constant
Qe	Quantity adsorbed at equilibrium (mg/g)
Qmax	Capacity of adsorption at saturation (mg/g)
R^2	Coefficientofdetermination

General Introduction

Water pollution is a significant environmental challenge, primarily due to the discharge of industrial effluents into water bodies. These effluents contain various contaminants, including dyes used in industries such as textiles, leather production, pulp and paper, and paints [1]. These dyes consist of persistent organic molecules that are difficult to degrade into non-toxic compounds, contributing to water pollution when they become bioavailable. Dye molecules are resistant to chemical oxidizing agents, light, heat, aerobic digestion, biological processes, and photochemical degradation. To address water contaminated with toxic metals and dyes, adsorption and photocatalysis are widely recognized as effective techniques due to their simplicity, environmental friendliness, and applicability to different water sources. However, the success of these technologies depends on the appropriate selection of water treatment materials[2].

While chemically synthesized water treatment products have been used, they have drawbacks, including the potential leaching of hazardous chemicals back into the water. Therefore, there is an increasing demand for non-toxic, biodegradable, cost-effective, and highly efficient materials to ensure the complete removal of contaminants from water[3].

The world is witnessing an increasing production of agricultural by-products, which are materials that accumulate as a result of farming and food processing processes. The exploitation and recycling of these wastes are crucial for achieving sustainable development and preserving the environment.

Cellulose, the most abundant natural polymer on Earth, is an organic material found in plant cell walls. It holds great importance in the fields of biotechnology and nanotechnology[4]. Cellulose possesses excellent properties, including high mechanical strength, heat resistance, and chemical resistance.

One promising method for extracting cellulose nanoparticles is utilizing agricultural residues as the primary source of cellulose. By converting these waste materials, we can obtain cellulose and utilize it in the production of nanomaterials.

Cellulose nanocrystals (CNCs) with diameters ranging from 1 to 100 nm are commonly prepared through the selective hydrolysis of the less-ordered regions of natural cellulose [5].

In the past twenty years, CNCs have attracted great interest because of their renewable nature, are exceptional in many ways, such as their excellent safety profile, biocompatibility, high specific surface area, high elastic modulus, and high aspect ratio[6], biodegradability, availability, as well as the accessibility and affordability of their pristine materials [7, 8].

Nanocellulose offers a wide range of potential applications in areas such as electronics, medicine, food, energy, and many other industries [9-12].

As a result, the cellulose surface's nano-properties, notably OH groups, adsorption capacity, and mechanical strength are all benefits of enabling strong binding of inorganic substances like metal oxide nanoparticles (NPs), facilitating the excellent permanence of nanomaterials [13-15].

CNs may function as a polymer base to augment the efficacy of metal/metal oxide NPs. The consequential hybrids are worthy substances that exhibit novel in several applications [16].

In food engineering applications, ZnO nanoparticles (NPs) have garnered considerable attention due to their stability, robustness, intrinsic antimicrobial properties, and long shelf life [17]. Moreover, they are considered safe for human consumption and fall under the category of GRAS substances (i.e., "Generally Recognized as Safe"), as recognized by the U.S. Food and Drug Administration [18].

To mitigate particle agglomeration and enhance the dispersibility of ZnO nanoparticles, one of the most effective approaches is the addition of surfactants or polymeric ligands to the system. Sustainable cellulose, particularly nanocellulose with its abundant hydroxyl groups, is among the preferred carriers for hybrid materials [19, 20]. The incorporation of ZnO nanoparticles into nanocellulose matrices yields nanocellulose/ZnO hybrids, which find applications in various fields, including photocatalysis, antibacterial treatments, and reinforcing fillers [21].

In this thesis, we will specifically address the exploitation and recycling of agricultural waste to extract the nanocomposite cellulose/zinc oxide (CNC/ZnO NPs) and study its adsorption to remove organic pollutants from aqueous solutions in addition to studying its biological activity. The peels of each of the fruits of peanuts and peas were used in the process of extracting nanocellulose (CNCs) using primary chemical treatment in order to obtain cellulose and convert it into nanocellulose and were used two different methods to prepare the nanocomposite cellulose/zinc oxide (CNC/ZnO NPs).

This work consists of four chapters:

The first chapter is a review of the literature on nanoparticles, their composition, classifications, properties, and applications with a critical study focusing on the chemistry of cellulose, nanocellulose, its types, methods of extraction, and its broad application in many fields. In addition to the synthesis and properties of the multifunctional zinc oxide nanocellulose composite, and its excellent application possibilities in various fields.

The second chapter briefly describes water pollution, in addition to a comprehensive study of the adsorption process, in addition to the factors affecting it.

The fourth chapter presents the material and methods to the synthesis of the nanocomposite cellulose/zinc oxide (CNC/ZnO NPs).

The fourth chapter presents the results and discussion of the physicochemical characterization, the adsorption study for removal methyl blue dye (BM) of cellulose and nanocomposite cellulose/zinc oxide prepared from peanut shells and pea shells. followed by discussions and explanationsand the evaluation of the the antimicrobial activities of cellulose and nanocomposite cellulose/zinc oxide prepared from peanut shells and pea shells.

Finally, the general conclusion summarizes the main findings obtained during this thesis and proposals for further study.

CHAPTER ONE:

OVERVIEW ON THE NANOMATERIALS, CELLULOSE AND CELLULOSE/ZNO NANOPARTICLES

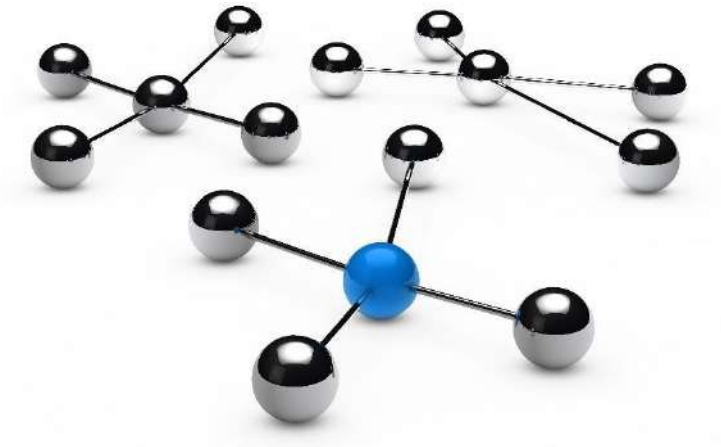

ntroduction

Over the past few decades, nanotechnology has emerged as an exciting field in modern science and applications. The concept of nanotechnology was first given by renowned physicist Richard Feynman in 1959 and earned Nobel Prize [22], and involves designing and producing objects at nanoscale size (~1 to 100 nm) [23].

Nanomaterials are one of the main products of nanotechnology as nanoparticles, nanotubes, nanorods, etc. It is also explained as nanoparticles have a high surface to volume ratio [24].

One material that has gained significant attention in nanoresearch is cellulose, which is a fundamental component naturally found in plants. Cellulose is a type of sugar polymer consisting of long chains of glucose molecules and is considered one of the most abundant and renewable biomaterials in the natural world.

Nanotechnology represents a significant advancement in enhancing the properties of cellulose and expanding its applications. One key innovation in this field is nanocellulose, which is an advanced form of cellulose at the nanoscale level. Nanocellulose is obtained by breaking down cellulose into extremely small particles, leading to increased surface area and improved mechanical and chemical properties. This makes it an ideal material for nanotechnology applications.

In this chapter, we will explore more details about cellulose and nanocellulose, along with an overview of hybrid nanocomposites that incorporate nanocellulose and zinc oxide. These hybrid materials combine the organic properties of cellulose with the inorganic properties of zinc oxide, and we will delve into their methods of extraction, preparation, and their advantages in various applications.

1. Nanomaterials and Nanoparticles

1.1. Definition

Nanotechnology , can be defined as the design, synthesis, and application of materials and devices whose size and shape have been engineered at the nanoscale to create new and unique materials [25] for various industrial and biomedical applications [26].

Nanoparticlesare organic or inorganic [23] can be produced from the destruction of a macroscopic material, or by the development of a group of atoms or molecules and can have different shapes such as nanospheres, nanotubes, nanowires, cells, and single crystals [26]

Nanoparticles can have amorphous or crystalline form. To some degree, nanoparticulate matter should be considered a distinct state of matter, in addition to the solid, liquid, gaseous, and plasma states. Nanoparticles have various special and distinct properties than other particles, are higher surface/volume ratio and melting temperature which provides tremendous driving force for diffusion[27, 28].

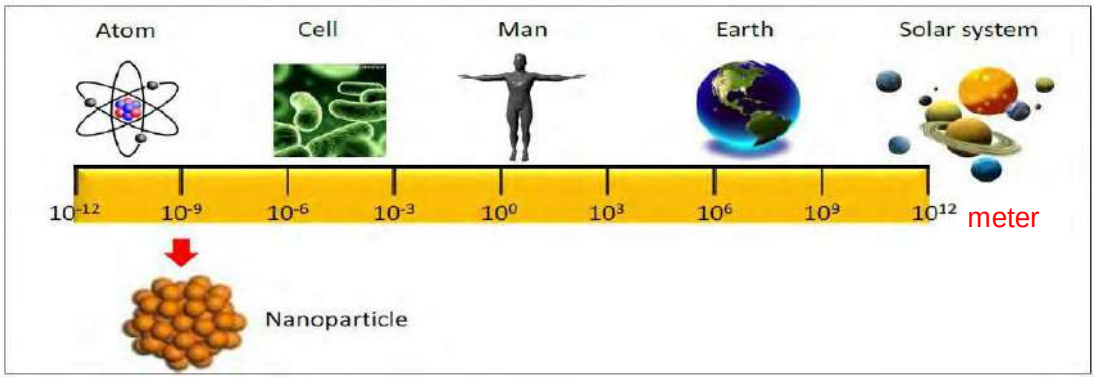

Figure I.1: *Logarithmicallengthscale showingsize of nanomaterials compared tobiological components and definition 'nano'and 'micro' sizes.*

1.2. Nanoparticle classification

Nanoparticles are generally classified based on their dimensionality, morphology, chemical composition, sources (natural and/or anthropogenic), uniformity, and agglomeration.

1.2.1. Dimensionality

1.2.1.1. Zero dimensional nanomaterials "0D" materials in dispersed, random or organized form as in colloidal crystals for optics or magnetic fluids[29].

1.2.1.2. One dimensional nanomaterials "1D" materials with one dimension in the nanometer scale are typically thin films or surface coatings, and include the circuitry of computer chips and the antireflection and hard coatings on eyeglasses [30]and can be grown controllably to be only one atom thick, a so-called monolayer.

1.2.1.3. Two dimensional nanomaterials "2D" have two dimensions in the nanometer scale. These include 2D nanostructured films, with nanostructures firmly attached to a substrate, or nanopore filters used for small particle separation and filtration[30]. Thick coatings obtained by plasma spraying or electrochemical[29].

1.2.1.4. Three dimensional nanomaterials "3D" Materials that are nanoscaled in all three dimensions are considered 3D nanomaterials. These include thin films deposited under conditions that generate atomic-scale porosity, colloids [31], and nanoparticles in compact form as in ceramics and metal nanostructures [29].

1.2.2. Nanoparticle morphology

Morphological characteristics to be taken into account are: flatness, sphericity, and aspect ratio. A general classification exists between high- and low-aspect ratio particles(**Figure I.2**) [32] . High aspect ratio nanoparticles include nanotubes and nanowires, with various shapes, such as helices, zigzags, belts, or perhaps nanowires with diameter that varies with length. Small-aspect ratio morphologies include spherical, oval, cubic, prism, helical, or pillar. Collections of many particles exist as powders, suspension, or colloids [33].

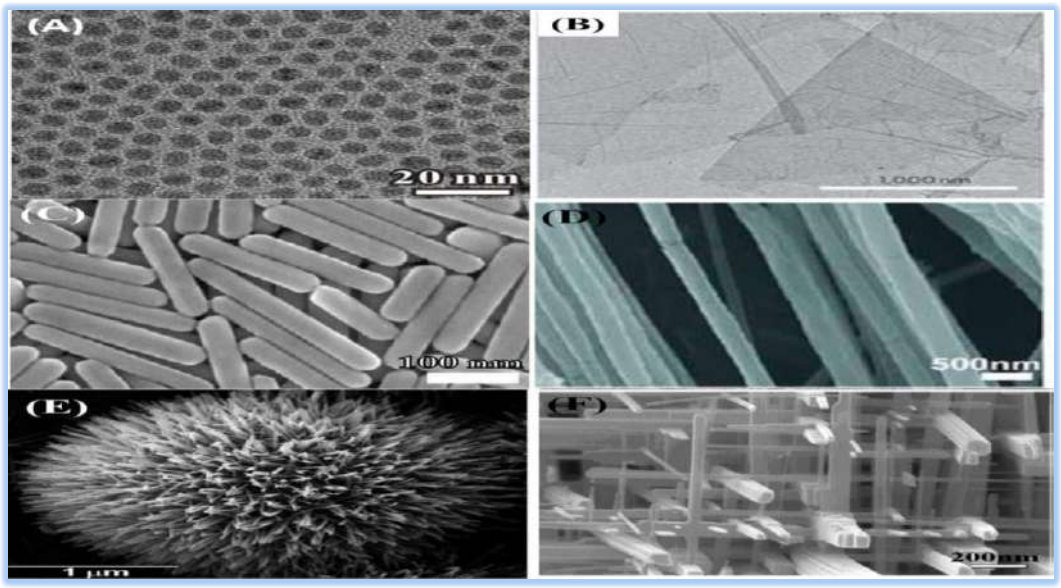

Figure I.2:*The different morphologies of Nanomaterials: (A) non-porous Pd NPs, (B) Graphene nanosheets, (C) Ag nanorods, (D) poly(ethylene oxide) nanofibers), (E) ZnO nanowires looking like sea urchins, (F) WO3 nanowire array* [32].

1.3. Nanoparticle composition

The nanoparticles are generally classified into the organic, inorganic and carbon based:

1.3.1. Organic nanoparticles

This class comprises NPs that are made of proteins, car- bohydrates, lipids, polymers, or any other organic com- pounds

- ***Organic polymers:*** which represent a new class of the organic nanoparticles or polymers with controlled structure and nanometric dimensions. These nanoparticles are biodegradable, non-toxic, and are sensitive to thermal and electromagnetic radiation such as heat and light,. These unique characteristics make them an ideal choice for drug delivery[34, 35].
- ***Biologically inspired nanoparticles:*** are very diverse but normally group together structures in which a biological substance is encapsulated, trapped or absorbed on the surface [34].

1.3.2. Inorganic nanoparticles

Inorganic nanoparticles are particles that are not made of carbon. They can be classified into metals, metal oxides and quantum dots.

- ***Metal based***

Nanoparticles that are synthesized from metals to nanometer sizes by either destructive or constructive methods are metal-based nanoparticles [36]. Metallic nanoparticles (gold (Au), copper (Cu), silicon, iron (Fe), silver (Ag), zinc (Zn) and cobalt (Co) etc.) are widely used in catalysis, electronics, sensors, photonics, environmental remedies and medicine [36]. The latter have distinctive properties such as sizes as small as 10-100 nm, surface characteristics such as high surface-to-volume ratio, pore size, crystalline and amorphous structures, shapes like spherical and cylindrical and colors, reactivity and sensitivity to environmental factors such as air, humidity, heat and sunlight [37].

- ***Metal oxides based***

Metal oxide-based nanoparticlesare synthesized to modify the properties of their respective metal based nanoparticles due to their increased reactivity and

efficiency . Different metal oxides have appeared in various forms: nanotubes, nanorods, nanoflakes...etc[38].

These nanoparticles have possess an exceptional properties when compared to their metal counterparts, some structures demonstrate interesting properties for virtual applications in fields such as sensors, optoelectronics, transducers, medicine[34].

1.3.3. Carbon based nanoparticles

This class comprises NPs that are made solely from carbon atoms. Famous examples of this class are: quantum dots [39], Fullerenes (C60) [40, 41], Carbon nanotubes (CNTs) [42], Carbon nanofibers (CNFs) [35], and Carbon black (CB) [35].

1.4. Nanoparticle production processes

In recent years, many techniques have been developed to manufacture nanomaterials. The choice of techniques to be used is based on several criteria, such as conditions and synthesis methods. From an industrial point of view, the cost, duration and reproducibility of the synthesis represent important criteria. In general, there are two main approaches "bottom-up" and "top-down". Although both approaches play a very important role in the fabrication of nanoparticles, but each has advantages and disadvantages. Therefore, one should choose them according to the requirement very carefully.

1.4.1. Bottom-up method “ascendant”

The Bottom-up or ascendant method involves building material from the "bottom". it is the build-up of material from atom to clusters to nanoparticles. The assembly or positioning of atoms, molecules or aggregates is carried out in a precise and controlled manner, thus allowing the manufacture of materials whose structure is perfectly controlled, with new and useful properties. The motivation for bottom-up approaches comes from biological systems, where nature has harnessed chemical forces to create all the structures necessary for life. The most commonly used bottom-up methods for nanoparticle production.

The sol-gel method: The "sol" a colloidal solution of solids suspended in a liquid

phase. The "gel" a solid macromolecule submerged in a solvent. Sol-gel is the most preferred bottom-up method due to its simplicity and as most of the nanoparticles can be synthesised from this method. It is a wet chemical process containing a chemical solution acting as a precursor for an integrated system of discrete particles. Metal oxides and chlorides are the typically used precursors in sol-gel process [43]. The precursor is then dispersed in a host liquid either by shaking, stirring or sonication and the resultant system contains a liquid and a solid phase. A phase separation is carried out to recover the nanoparticles by various methods such as sedimentation, filtration and centrifugation and the moisture is further removed by drying [44]. Allows obtaining an ultrafine powder of the metal hydroxide. Subsequent heat treatments of this metal hydroxide results in an ultrafine powder corresponding to the desired metal oxide[45].

In addition to this method there are: Chemical Vapour Deposition (CVD)[35, 46, 47], Biosynthesis is a "green chemistry" approach [48-50], Pyrolysis[51, 52], and Spinning [38, 53].

1.4.2. Top-down method “destructive”

The Top-down or destructive method is the reduction of a bulk material to nanometric scale particles of the desired size and shape. This technique cannot be used for large scale production of nanoparticles because it is a slow and expensive process, the most widely used nanoparticle synthesis methods are: Thermal decomposition [37], Laser ablation [54][42], Sputtering method [55-57], mechanical milling [58], and Nanolithography [59, 60].

1.5. Properties of nanoparticles

1.5.1. Surface properties

Nanoparticles possess unique properties that are primarily attributed to the high proportion of surface atoms compared to the core atoms comprising the particle. Assuming nanoparticles have a spherical shape, the ratio of their surface area to volume increases, along with the proportion of surface atoms in relation to the total number of atoms constituting a nanoparticle (**Table I.1**). However, as particle size decreases to the nanoscale, the proportion of surface atoms becomes increasingly

significant, thereby playing an increasingly important role that can alter the properties of the nanoparticles [61].

Table I.1: Relationship between particle size and the number of surface atoms [62]

Nanoparticle size Diameter(nm)	Number of atoms on particle	The percentage of the number of atoms on the surface of the particule (%)
1	30	99
2	$2,5.10^2$	80
4	4.10^3	60
5	$4,2.10^3$	50
10	3.10^4	20

1.5.2. Optical properties

The optical characteristics of nanoparticles, including transmission, absorption, reflection, and light emission, exhibit dynamic behavior and are distinct from their bulk material counterparts. The interaction between electrons and light in nanoparticles differs from that in bulk materials. The confinement of electrons in nanoparticles, due to their extremely small size, restricts their free movement, leading to quantum confinement effects of electrons [63, 64]. By altering the shape, size, and surface functionality of nanoparticles, a wide range of optical properties suitable for various applications can be achieved. These modifications directly influence the observed color of nanoparticles. For instance, spherical gold nanoparticles with a diameter of 100 nm appear orange, whereas the same size range of gold nanoparticles exhibits a green color when their diameter is reduced to 25 nm. Similarly, spherical silver nanoparticles with a diameter of 100 nm display a yellow color [63].

1.5.3. Electronic properties

The electronic properties of metallic nanoparticles are intermediate between those of an atom which exhibits discrete states and those of bulk metal which exhibits an electronic structure in energy bands. The electrical resistance increases when the

particle size decreases due to the large proportion of atoms on the surface of the particles [65].

1.5.4. Mechanical properties

Includes the mechanical properties in nanometric dimension. an increase in the elastic limit is observed, flexibility that play a significant factor in their application. the nanoparticles therefore have good ductility, have extremely high hardness and also impact resistance [66].

1.6. Metal oxides nanoparticles (Zinc oxide nanoparticles)

Metal oxides play a significant role in the various areas of chemistry, physics, and materials science. Metallic elements can form a large diversity of oxide compounds, which can adopt a vast number of structural geometries with electronic structures that can exhibit metallic, semiconductor, or insulator character [67].

Metal oxides are interesting class of materials formed between metals and oxygen. Some of them have been considered to be important and widely characterized solid catalysts, and their catalytic property is further enhanced when the materials are reduced to nanometer scales. Metal oxide nanoparticles become even more beneficial nanomaterials when empty voids or pores are introduced into their structures to enhance their surface area. The porosity of the metal oxides could be classified as micro, meso or macroporous if the pore sizes are <2nm, 2–50 nm and > 50 nm, respectively [68, 69].

Zinc oxide is an inorganic and is a very promising material in the development of new materials for renewable energy and for the environment. It has established itself in recent years in planar technologies as a transparent conductive oxide (TCO) for solar and photo electrochemical cells, widely used as an additive in many materials and biomedical products [70, 71].

1.6.1. The properties nanostructures of ZnO NPs

a. Structural properties

ZnO NPs preferentially crystallizes in the compact hexagonal structure of the Würtzite type [72, 73] and belongs to the 6mm crystal class, however, It exists in three different crystalline forms. The first is the cubic structure (Rock-Salt), which

appears under very high pressures, the second is the blende structure which is unstable and which appears under high pressures, the third is the stable hexagonal structure under normal conditions. These structures are illustrated in **Figure (I.3)** [74]. ZnO also has the property, under certain conditions, of having interstitial atoms, generated by the empty space between the zinc and oxygen atoms which only fill 40% of the crystal space [75].

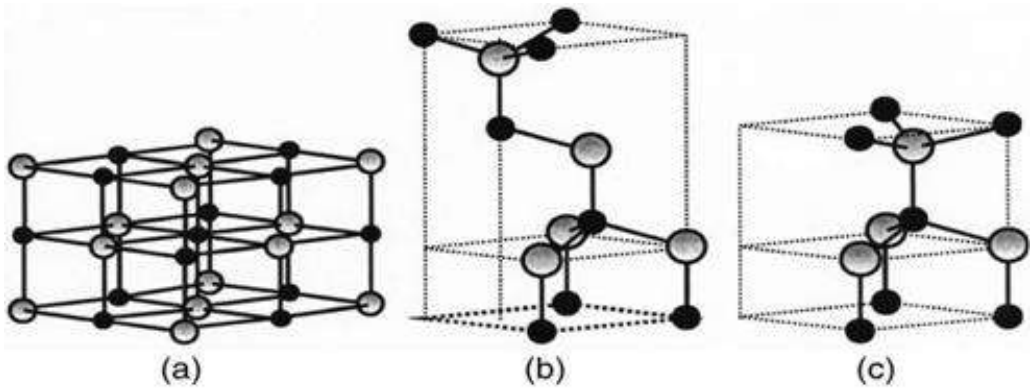

Figure I.3:*Representation of ZnO structures: (a) cubic NaCl, (b) blende, (c) hexagonal wurtzite*

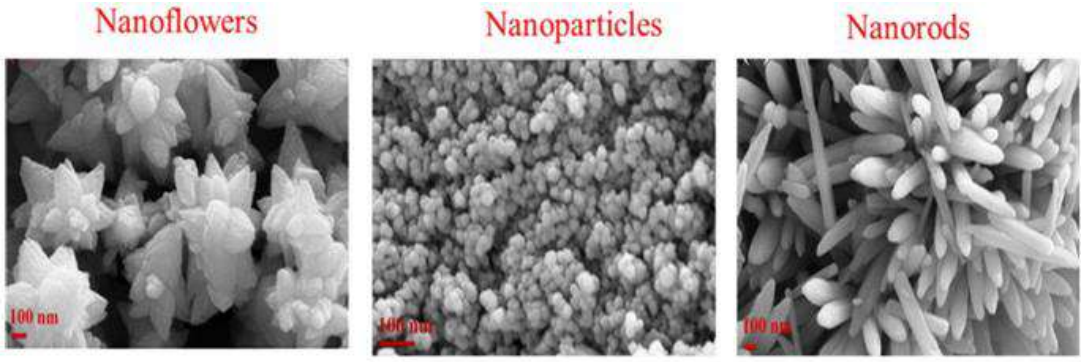

Figure I. 4: *The SEM images of different forms of ZnO Nanoparticles.*

b. Physico-chemical properties:

The physicochemical properties of zinc oxide are as follows [16, 76]:

- ✓ ZnO is a white powder, but in nature it occurs as the rare mineral zincite, which usually contains manganese and other impurities that confer a yellow to red color.
- ✓ Crystalline zinc oxide is thermochromic, changing from white to yellow when heated in air and reverting to white on cooling. This color change is caused by a small loss of oxygen to the environment at high temperatures.

- ✓ Chemically, zinc oxide is amphoteric, meaning it can react as both an acid and a base. It can react with both acids such as hydrochloric acid and alkalis to form zinc salts, This property makes it useful in various chemical processes and applications.

$$ZnO + 2\ HCl \rightarrow ZnCl_2 + H_2O$$

$$ZnO + 2\ NaOH + H_2O \rightarrow Na_2[Zn(OH)_4]$$

- ✓ ZnO reacts slowly with fatty acids in oils to produce the corresponding carboxylates, such as oleate or stearate. ZnO also forms cement like material when treated with phosphoric acid; related materials are used in dentistry. A major component of zinc phosphate cement produced by this reaction is hopeite, $Zn_3(PO_4)_2 \cdot 4H_2O$
- ✓ ZnO decomposes into zinc vapor and oxygen at around 1975 °C with a standard oxygen pressure. In a carbothermic reaction, heating with carbon converts the oxide into zinc vapor at a much lower temperature (around 950 °C).

$$ZnO + C \rightarrow Zn_{(Vapor)} + CO$$

- ✓ One of the notable physical properties of zinc oxide is its ability to absorb ultraviolet (UV) radiation. This property makes it a common ingredient in sunscreens and other skincare products.

In addition to the Physico-chemical properties of ZnO, its have:
Molar mass: 81.406 g/mol, Density: 5.606 g/cm3, not soluble in water (0.0004% at 17.8°C), Band gap: 3.3 eV, Melting temperature: 1975°C, and chemical bond strength O-Zn:66Kcal/mol.

1.6.2. Application of Zinc Oxides NPs (ZnO NPs)

In recent years, the applications of ZnO nanostructures have received a lot of attention due to its multiple interesting properties (structural, optical, electrical, etc.); which makes it a very promising material for a wide range of devices, it is currently used by several 100,000 tons per year, we present some of them below [77].

a- ZnO powder

The rubber industry is the biggest consumer of zinc oxide, with 57% of the market. It is used to improve the thermal conductivity and resistance and slow down

the aging of rubber. The paint industry also uses it a lot because it provides great hiding power, better color retention, greater durability and protection against ultraviolet rays, due to its ability to absorb these rays. It also enters the ceramics industry, by participating in the manufacture of glass, because it makes it possible to reduce the coefficient of expansion [78]. In the presence of small amounts of metal oxides (bismuth), zinc oxide exhibits excellent electrical properties. This allows it to be widely used in the protection of electronic devices and in particular in high-voltage electrical stations [79].

b- ZnO in thin layers

Thanks to its semiconductor, piezoelectric, optical and catalytic properties, zinc oxide in thin layers has multiple applications. It occupies an important place in the electronics industry. Due to their piezoelectric properties, ZnO films can be used as pressure sensors [80] or in electronic devices such as rectifiers, filters, resonators for radio communications and in electronic devices. Thin layers of zinc oxide can also serve as very sensitive chemical sensors in gas detectors[81]. Zinc oxide coatings can be deposited on polymers and thus increase their durability [82, 83].

c- ZnO in Biomedical

NPs synthesized by biological methods are known to have immense applications in the field of medicine and in a biological system due to their stability in various biological media[84]. One of the most important characteristics of ZnO nanomaterials is their low toxicity and biodegradability. Due to their size, giving them new properties. They are used in many everyday products. They are products of the pharmaceutical and cosmetic industry, well-known antiseptic [85]. Mainly as targeted drug delivery systems to minimize and negative effects of different chronic degenerative diseases like delay [86]. For example, they are commonly found in sun care products to provide broad spectrum UV light protection [84]. They were used in powder (baby powder), or incorporated into ointments for skin complaints, and also used in the form of medicinal balms for the treatment of open wounds or eye irritations, because it neutralizes acid productions while destroying the greatest number of bacteria present on the skin and antiseptic ointments [85].

Today, researchers are trying to use drugs in the form of more effective nanoparticles for the treatment of various diseases. Many reports exist in the literature on the use of ZnO nanomaterials in different biological and medical applications. In an interesting study [87], presented the desirable properties of ZnO nanomaterials which have generated enormous interest in biomedical applications.

D. Rania et al 2019 [88], carried out a study aimed at measuring and optimizing the microcidal activity of ZnO NPs, in particular for the decontamination of surfaces. Which have shown that, even at low concentrations, ZnO NPs exhibit bacterial activity. Because at the nanometric scale, nanoparticles have improved efficiency compared to the same larger materials due to their specific surface. Also Afaf D. et al. (2018) [89], used ZnO NPs as a therapy against coccidiosis, which is a protozoan infection of animals that causes growth retardation and high mortality in rabbits.

2. Lignocellulosic biomass

Lignocellulosic biomass includes various natural organic matters which mostly refer to the plants or plant based materials which is the largest amount of sustainable carbon material group and the most promising feedstock for the sustainable production of biochemical, bioethanol and biofuels [90].

Especially, lignocellulosic biomass is a source of natural fiber which can substitute the petroleum-based polymers due to its outstanding environmentally friendly properties. Furthermore, the wastes from biomass such as agricultural wastes and forest residues have high potential for reuse as fuel or feedstock for production of high value-added materials without the competition with human and animal food chains. Cell wall structure of lignocellulosic biomass mainly consists of three kinds of polymer, i.e. lignin, hemicelluloses, and cellulose **Figure I.5**.

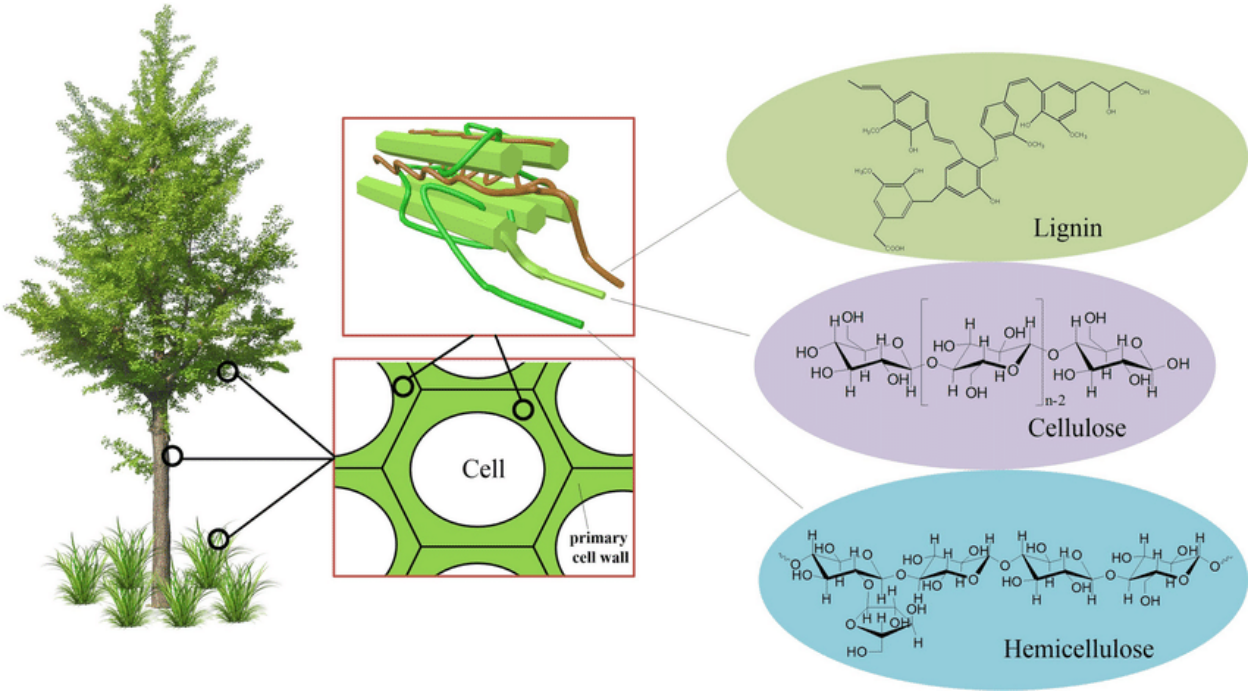

Figure I.5: The cellulose, hemicellulose and lignin in the cell wall of lignocellulosic biomass.

- **Hemicellulose**

Hemicellulose represents about 20–35% in lignocellulosic biomass [91-93]. Hemicellulose is the hetero polymer which is composed by the short, linear, and branched chains of different kinds of monomers such as pentoses and hexoses [94, 95]. Hemicellulose adheres to the cellulose fibrils through hydrogen bonds and Vander Waal's interactions **Figure II.1**. In addition, it also cross-links with lignin [96]. Theimbedding of hemicellulose with cellulose and lignin relates to the strength in structure of plant cell wall. Hemicellulose can be hydrolyzed By using acid, alkaline or enzymatic hydrolysis in mild conditions for production of fuel ethanol and the valuable chemicals from its oligomers or monomers which can be used for food, cosmetic, pharmaceutical industries, mining industries and so on [96, 97].

- **Lignin**

Recently, the isolation of lignin from lignocellulosic biomass and the depolymerization of lignin are mainly studied for the production of bio fuels and chemicals from natural materials [98, 99]. Lignin represents about 10–25% by weight

of dry lignocellulosic biomass[91-93]. In plant cell walls, lignin serves as the binder which holds between and around cellulose and hemicellulose complexion **Figure II.1**. With its binding function, lignin provides the stiffness, compressive strength, resistant to decay, and water impermeability to plant cell wall. Lignin consists of the cross-linked amorphous copolymer synthesized from the random of three different phenylpropane monomers the ratio of these three primary monomer units depends on the species and sources of lignocellulosic biomass[98, 100, 101]. Lignin-based carbon materials are applied for catalysis, energy storage, and pollutant removal, which are attractively developed [101].

- **Cellulose**

The word “cellulose” originates from a French word called “cellule”, meaning a living cell and glucose. This was discovered by a French chemist called Anselme Payen in 1838 [102]. Cellulose is the major component in lignocellulosic biomass which is mainly localized in the plant fiber walls at around 35–50% [91-93] such as in wood, hemp, cotton, cereal straws and other plant-based materials[103, 104].

Cellulose is an environmentally friendly and is a natural stable polymer, the polymers are formed by building block unit d-glucopyranose (glucose) molecules, which are linked together by β-1,4-glucosidic bonds [105] through an oxygen covalently bonded to the C1 of one glucose ring and the C4 of the adjoining. The chemical formula of cellulose is $(C_6H_{10}O_5)_n$ (n = 10 000 to 15 000) , where n is the number of repeating sugar) [106-109],

The cellulose is containing hydrogen bond network, which does not dissolve in common aqueous solvents and does not exhibit a melting point [110]. Ultimately, some of the cellulose chains will agglomerate to form fibril or microfibrils due to the strong intra molecular and intermolecular hydrogen bonding, which makes the cellulose molecule highly stable [111]. The structure of cellulose is composed of three hydroxyl groups, the primary (- OH) at the C-6 position and the secondary (- OH) at C-2 and at C-3 which are hydrophilic [104, 112, 113]. However, cellulose is insoluble in water and some solvents [114].

Furthermore, the strong hydrogen bonding due to the hydroxyl functional groups leads to the formation of a crystal structure, each cellulose molecule contains

several crystalline and amorphous parts thus making cellulose a semi crystalline polymer comprising ordered and disordered regions within a single microfibril [115].

with a production capacity of and approximately 700 billion tons annually [116]. The global market indicates that the cellulose market's size was estimated to be USD 211.68 billion in 2019 with an expected increase of compound annual growth rate (CAGR) by 2.9% from 2020 to 2026 [117].

3. Cellulose in nanoscale (Nanocellulose)

Micro and nanocellulose are the common sizes of cellulose used in industrial applications by chemical, mechanical and biological methods [118, 119]. These methods can be used separately or in sequence in order to achieve the preferred morphology, structure, dimensions, composition and properties [119]. Depending on the technique and synthesis conditions of nanocellulose, it can be divided into three main categories or type: nanocrystalline cellulose, nanofibrillated cellulose, and bacterial nanocellulose ones. Although all types are similar in chemical composition, they are different in morphology, particle size, crystallinity, and some properties due to the difference of sources and extraction methods [120, 121].

3.1. Cellulose nanocrystals (CNCs)

Cellulose nanocrystalsalso known as cellulose whiskers nanocellulose or rod-like cellulose nanocrocrystals are whisker-shaped material isolated by the biosynthesis process from cellulose, CNCs are commonly produced using acid hydrolysis of cellulosic materials dispersed in water. Both the reaction conditions such as the nature of the acid and the source of cellulosic material have a great impact on the obtained properties of CNC, for example, aspect ratio, degree of crystallinity, structural and morphological properties, and size and dimensional dispersity [122]. They show relatively width of 3–50 nm and length varies between 100 nm to several micrometers [123], it contains 54 to 88% in crystallinity and are 100% cellulose chemical composition[120, 121]. With higher thermal stability value (~260 °C), larger aspect ratio (10 to 70), and lower density value (1.5–1.6 g/cm3) [123, 124]. CNCs are obtained from cellulosic biomass such as wood and cotton fibres [125]. CNCs also exhibit several unique properties such as high crystallinity index, high-magnetic response, high strength and large surface area[126].

3.2.Cellulose nanofibrils (CNFs)

Also known as nanofibrillated cellulose (NFC), microfibrillated cellulose (MFC) or cellulose nanofibers, can be expressed as a natural cellulosic material, It's the long, flexible and strongly entangled of nanofibrils [107, 127]. Unlike CNCs, which have near perfect crystallinity (c.90%), CNFs contain both amorphous as well as crystalline cellulose domains within the single fibers [128]. CNFs are isolated using the mechanical disintegration [129], which require high energy consumption usually involves and involve different types of equipment and processes which are not cost-effective [130]. Also, chemically, enzymatically or treated by solvents of cellulose fibres [131]. The resulting product of CNF is high volume and large surface area cellulose fibers, having diameter in nanometer range (nm) and several micrometer of micrometres (µm) lengths [132]. Comparing with nanocrystalline cellulose, nanofibrillated cellulose has the longer length with high aspect ratio (length to diameter), high surface area, and high extensive of hydroxyl groups which is easily accessible for surface modification [120].

The basic properties of obtained in CNFs depend on the natural source of the cellulose materials including cotton stalk [133], banana [134], corn husk [135], and soft and hardwoods [136], rice straw [137], and sugar beet pulp[138] Similarlythe methods employed vary the degree of crystallinity, the intensity of fibrillation, morphological and structural properties of the resulting CNFs[139].

3.3. Bacterial nanocellulose (BNCs)

Also known as microbial nanocellulose or bionanocellulose and electrospun cellulose nanofibers (ECNFs). BNCs is another type of nanocellulose differed from CNF and CNC particles, displays the same molecular formula as plant's cellulose. synthesized from several bacterial species such as Gluconoacetobacter (e.g., Acetobacter xylinium) species within several days cultivation in aqueous culture media containing carbon and nitrogen sources [140]. The glucose chains are supplied inside the bacterial body and expelled out through minor pores present on the cell wall [132]. Those bacteria are capable of altering glucose into cellulose materials through a biofabrication assembly process [141], from building up of low molecular weight of sugars by bacteria mainly by bottom-up process, resulting in a three dimensional network of nanofibers [142].

As such, the bacterial nanocellulose is always in the pure form without other components from lignocellulosic biomass and does not require additional processing to remove contaminants like lignin, pectin, and hemicelluloses [143]. It is twisting ribbons in the form of nanofiber system with the average diameters of 20 to100 nm and micrometer of lengths with large surface area per unit[127, 144].

The advantages of bacterially derived cellulose microfibrils are as lightweight, non-toxic as well as controllable microfibril formation (3D). BNCs has native cellulose I crystal structure with high molar mass, a higher degree of polymerization, higher crystallinity (70–80%), similarly, have the ability to form an extremely ultrafine web structure (3D) that allows them to not to be dispersed in water [145, 146]. BNCs is regarded to have higher Young's modulus value (78 GPa), higher molecular weight (8000 Da), reported to have excellent water holding capacity (content 90%) [140], and high thermal and mechanical stability [142, 147]. Because of excellent characteristics, BNCs is extensively used in biomedical applications [148]. In addition, biomedical materials have claimed attention because of the increased interest in tissue engineering materials for wound care and regenerative medicine [149]. Nonetheless, it is economically unattractive due to its highly expensive carbon source [109].

4. The extraction of Nanocellulose from different biomass

4.1. Cellulose pretreatments methods

Cellulose is occurred in nature as assemblies of individual cellulose long chain-forming fibers, instead of an isolated molecule or individual cellulose particle. Several individual cellulose particles make one large unit called as protofibrils (elementary fibrils) that are packed into larger sections, generally named as microfibrils [150]. Plants, the natural major source of cellulose are consist of cell walls cellulose molecules and other closely packed polysaccharide moieties, which results in a complex morphology of the cellulose fibers. The pretreatment process has become an important step for improve the degree of nanofibrillation with increase in production of cellulose fibers [151].

The aim of the pretreatment process is to remove ashes, waxes, lignin, hemicellulose, and other noncellulosic compounds, which are crucial and an

important step for improve to produce pure cellulosic products such as CNFs and CNCs [106, 152].

4.1.1. Alkaline-acid hydrolysis pretreatment

In this pretreatment process, the biomass is treated mostly with an alkali solution for extraction the cellulose fibers. This treatment process is famous for the surface modification of natural fibers which involves the solubilization and removal of hemicellulose, lignin, extractives, and waxes [153] before mechanical isolation of nanocellulose NFCs [154-158]. Alkali treatment cause the breakage of intermolecular α- and β-aryl ether linkages between hemicellulose and lignin, causing swelling of the biomass pores, disruption of the lignin structure, an increase in available surface area and ductility [159, 160].

Alkaline extraction needs to be controlled to avoid cellulose degradation [161]. Depending on the type of biomass, different working conditions are established for the alkaline treatment in relation to NaOH concentration, time and temperature.
Alkaline pretreatment is an effective method that can improve cellulose yield from 43% to 84% [154] wherein lignin and hemicellulose are hydrolyzed [162]. However, if lignin content is high in the cellulosic source, the cellulose and nanocellulose yield is low [162, 163].

4.1.2. Enzyme hydrolysis pretreatment

Enzymatic pretreatment is a biological treatment that used for modification of biomass cellulose fiber by used enzymes are used in the assistance of the restrictive hydrolysis of several particles or the selective hydrolysis of specified elements in the cellulose fibers [164]. The enzymatic treatment mechanism is complex, but the enzyme action is based on the catalysis of the H-bonding linkage between cellulose microfibers [118] it's can degrade or modify the noncellulosic (lignin and hemicellulose) contents without disturbing cellulose content [165, 166].
Generally, the reaction time required for enzymatic pretreatment is much higher as compared to the acid hydrolysis process [164]. Several reports [167, 168] have been done for the CNF production from bleached softwood pulp by using enzymatic pretreatment process with homogenization and refinement. [169, 170].

4.1.3. Ionic liquids pretreatment (ILs)

ILs are organic salts having special properties such as nonflammability, thermal and chemical stability, and infinitely low vapor pressure [171, 172] no corrosive properties, as well as lower melting temperature (below 100 °C), and low viscosities[173]. Except for enzymatic and alkali acid pretreatments, ionic liquids have also been extensively reported to be used [173, 174] Ionic liquids dissolve cellulose and render a wide range of particle morphologies. The ionic liquid breaks intra molecular hydrogen bonds, whereas the cations attack the O atom of the –OH, and anions attack the hydrogen atoms of the -OH group [173], by using an ionic liquid 1-butyl-3-methylimidazolium chloride [(Bmim)Cl] , after that high-pressure homogenization (HPH) technique was used to isolate nanocellulose fibers (CNFs) after precipitation these fibers in water solution and regenerated by freezedrying [173].

Generally, the power of the microwave, reaction time, temperature, and the weight ratio of cellulose to ionic liquid have agreat influence on the solubilization of cellulose [175]. The most important advantage of using IL as pretreatment is the minimal loss in solvent recovery, which can also be used many times. For example, it has been possible to recover more than 90% of BmimCl by reusing it four times without losing its activity [176]. The most common anions employed are: $(Al_2Cl_7)^-$, $(AlCl_4)^-$, BF_4^-, PF_6^-,$(SbF_6)^-$, $(CF_3CO_2)^-$, $(GeCl_3)^-$, $(ClO_4)^-$ and $(OTS)^-$[177, 178].

4.1.4. Bleaching Process

The bleaching process, related to cellulose purification to improve ageing resistance avoiding yellowing and brittleness, these defects are mainly related to the presence of lignin. After pretreatment and obtain an accurate removal of lignin This step provides a more homogeneous end product.

Different compounds are commonly used for cellulose bleaching and purification techniques these include: sodium acetate and chlorite [179], the treatment with tetraacetylethylenediamine (TAED) [180], hydrogen peroxide (H_2O_2), chlorine dioxide (ClO_2), ozone (O_3), peracetic acid, and $NaClO_2$[181].

In most cases, bleaching is achieved by treating the fiber with chlorine in an acid medium, where it can be remove most of the lignin from lignocellulosic biomass. The process temperature is 70–80 °C, and treatment time can vary between 4 and 12

h, and it was based on performing a in one or more steps This allows us to obtain pure white cellulose microfibers[179].

The final purification of the cellulose fibers obtained not only increases the removal of lignin but also reduces the diameter and improves some properties such as crystallinity or surface area [179]. However, this procedure is not environmentally friendly and other more ecological but perhaps less efficient bleaching processes should be applied, such as the use of ozone or hydrogen peroxide.

4.2. Isolation of Nanocellulose

After the chemical purification of natural biomass materials, the sec- ond process is the conversion of purified cellulosic content to nanoscale particles (CNC or CNF) to obtain the desired characteristics of the nano- particles [182], by using several techniques especially acid hy- drolysis and mechanical treatments separately or in a combination of the various methods. In this section, the main extraction methods are categorized to several techniques:

4.2.1. Chemicals process (acid hydrolysis)

Acid hydrolysis is one of the main processes for the extraction of nanocellulose from cellulosic materials. Fabrication of CNCs by chemical treatment methods using hydrochloric acid and sulfuric acid is the most common method used for decades [122, 181, 183]. The first isolation of CNCs using sulfuric acid was reported by Rånby and co-workers in 1949 [184].

The main process for the preparation of CNCs is based on strong acid hydrolysis under strictly controlled conditions of concentration, temperature, agitation, and time by acid solution [185, 186], the major influencing factors regarding the structural and dimensional properties of the obtained fibers [120, 182]. The mineral acid breaks the β-1,4 glycosidic bonds in cellulose. During hydrolysis, the amorphous regions are attacked to dissolve her and permit longitudinal cutting of microfibrils, leaving the crystalline regions intact [187]. The CNCs have a degree of crystallinity from 55% to 90%. Moreover, the degree of crystallinity, aspect ratio, and morphology depends on the source of cellulosic material and preparation conditions [188]. Smaller CNCs are obtained by increasing hydrolysis time and acid concentration [162]. The main drawback of acid hydrolysis is the acid wastewater

generated from the washing process in order to neutralize the pH value of the nanocellulose suspension [189].

4.2.2. Mechanical process

The mechanical treatments is separately or in a combination of the various methods to obtain the desired characteristics of the nanoparticles [190, 191]. Mechanical methods are followed by chemical treatments to decompose or remove the amorphous material, it's help in widening the space between hydroxyl groups to break the hydrogen bonding of the cellulose fibers (interfibrillar materials), increased the reactivity of obtained fibers which helps boost the reactivity of the fibers [191, 192]. There are Several mechanical methods to convert cellulose fibers into nanofibers particles such as: High-pressure homogenization (HPH) [193-198], High-intensity ultrasonication (HIUS) [195, 199], Ball milling [200, 201], Microfluidizers [202, 203]. Grinding [196], and Cryocrushing [195]. [196, 204].

4.3. Applications of nanocellulose

Nanocellulose is believed to be a replacement for synthetic materials in more environmentally friendly materials, and is an addition to completely new types of biomaterials, i.e., cellulose nanocomposites. There are plenty of application areas for nanocellulose-based materials derived from natural resources (agricultural, biomass, and forestry residues) showing extensive and inclusive prospect in daily life (**Figure I.6).**

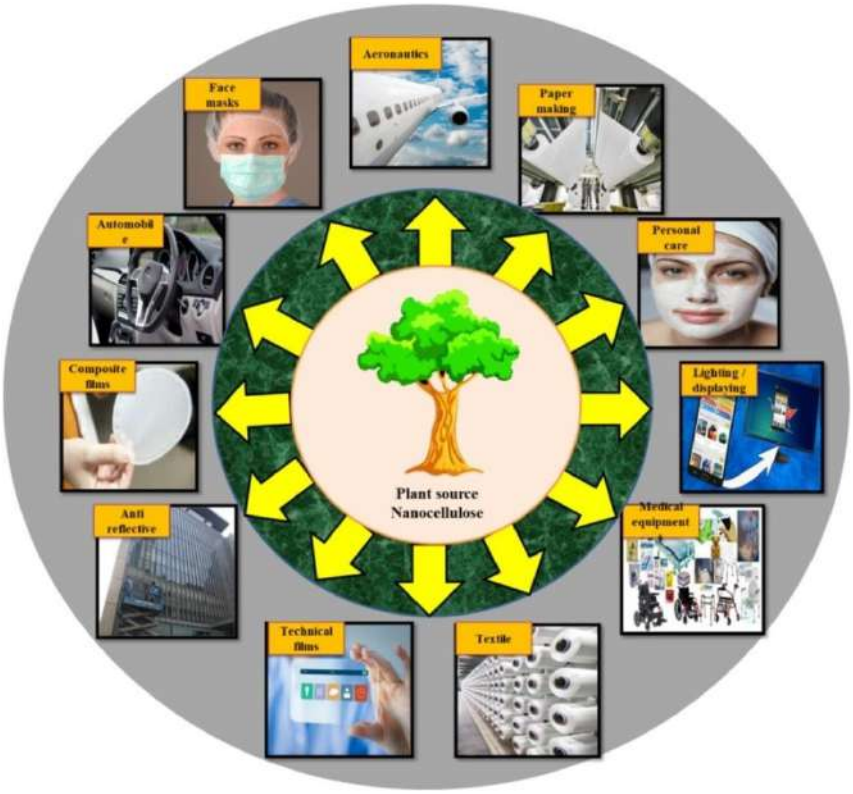

FigureI.6*.Different applications of nanocellulosemateris.*

All applications of nanocellulose are associated to their excellent properties, lightweight, and the application specifications and standards [127].

Recently, nanocellulose particles in printing applications have become the subject of increasing study. Researchers found that CNFs material could improve the ink density and the quality of print when it was subjected to be used as a coating agent to enhance the print quality of synthetic fiber sheet [205]. As well as for extensive applications in food packaging [206]. Because of the small diameter of CNCs, it is useful in the medical, pharmaceutical, cosmetic, hygienic [207], field applications, especially in the vascular graft [208], wound healing, burn, and ulcer dressings[102]. As well as used in producing highly porous materials with higher tensile strength such as nanocellulose papers making and films for varied purposes[209, 210].

It is also used in tissue engineering, electronic [211], optical, sensor, and as a supporting agent in metal nanoparticles in catalysis applications [212], synthetic plastic or polymers, fuel cells, filtration, solar cells, and lithium-ion batteries [213]. The CNCs bionanocomposites can also be implemented in automotive components [214] and fire extinguishers [215] due to their high thermal stability and tensile strength.

5. Cellulose/ZnO Nanocomposites materials

The field of metal oxide-cellulose (MOC) nanocomposites is an emerging area that offers unique advantages in incorporating inorganic nanoparticles into natural-based materials for various applications. It is crucial to carefully synthesize MOC nanocomposites to ensure the proper dispersion of metal oxide nanoparticles within the cellulose matrix, preventing their aggregation. Cellulose, a natural polymeric material, possesses abundant OH groups that can be modified with other functional groups to enhance its properties. The combination of metal oxides and cellulose nanoparticles in the composite structure offers significant benefits. Metal oxide nanoparticles provide an increased surface area for various reactions, such as photocatalysis. On the other hand, nanocellulose exhibits intriguing properties including biodegradability, biocompatibility, nontoxicity, ion-adsorption capacity, high thermal strength, sensitivity, and stability [216].

5.1. Preparation of Cellulose/Zinc Oxide nanocomposites

Generally, severals methods for preparations a cellulose/ZnO nanocomposite using metal or metal oxides nanoparticles and nanocellulosic materials especially:

- Cellulose and metal oxide nanoparticles mixing without using any external reducing elements.
- By using an external reducing agent with metal/metal oxide NPs and CNFs particles.
- Nanoparticles composite materials synthesis without any reducing agent.
- Nanoparticles preparation by chemical surface modification of nanocellulosic materials as shown in **Figure I.7.**

which includes the hydrothermal or wet chemical, solvothermal, electrospinning sol-gel, coprecipitation, and microwave synthesis methods [205, 210], spray pyrolysis, precipitation, and pulsed laser [217]. For cellulose/ZnO NPs preparation usually, chemical methods are preferred to physical ones because of simple equipment used, milder reaction conditions, and facile scale up.

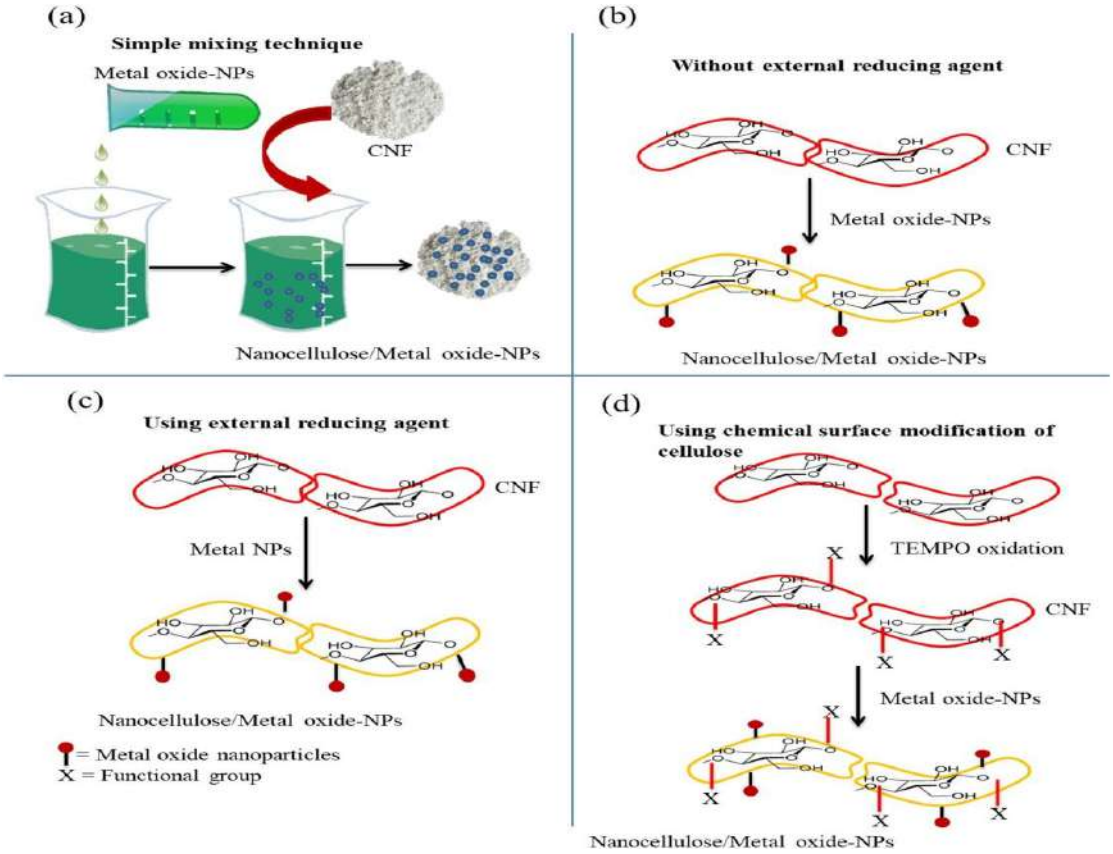

Figure I.7: *Schematic presentation for the synthesis of nanocellulose/metal NPs hybrid composite. (a) Simple blinding of prepared inorganic NPs and cellulose source (b) Synthesis of NPs using nanocelluloses without using external reducing agents, (c) Preparation of NPs composite using an external reducing agents, and (d) Synthesis of NPs composite through nanocellulose surface modification.*

5.2. Application of Cellulose/Zinc Oxide nanocomposites

Recently, polymers based metal oxides have been reflected as important materials due to their extensive range of applications like solar photo-catalysis, cells, waste water treatment, photodetector, sensors [218, 219], nano-composite films [220].

5.2.1. Application in water treatment

Metal nanocomposites are known to have physiochemical properties such as high reactivity for the separation, extraction, and removal of pollutants in water. The incorporation of metal oxides or inorganic materials into cellulose is an interesting way of improving material properties and could act as a platform in the purification of water. Different cellulose / metal oxides nanocomposites like cellulose/ZnO NPs

have been prepared and used in photodegradation of dye components in water. The degradation of methylene blue dye using ZnO/cellulose nanocomposites has been reported by Lefatshe et al [221], and according to their reports, the nanocomposites showed better efficiency compared to the ZnO nanoparticles alone.

5.2.2. Biomedical applications

ZnO NPs were shaped into a composite form by using biodegradable and biocompatible hydroxyethyl cellulose as a stabilizing agent through facile technique. The results of environmental friendly synthesis of nanoparticles lead to a new generation of nanomaterial for treatment of diabetic complications[222]. The antimicrobial properties of bacterial cellulose-zinc oxide nanocomposites were tested against common burn pathogens[223]. Hybrid nanocomposites exhibited 90.9%, 94.3%, 90.0%, and 87.4% activity against Citrobacter freundii, Staphylococcus aureus, Escherichia coli, and Pseudomonas aeruginosa, respectively. Recently, the nanocomposite films of CNFs and ZnO nanoparticles showed greater antimicrobial ability against Gram- positive Staphylococcus aureus, recommending the CNF/ZnO films can be used in a targeted biomedical application. The scaffolds of ZnO NPs and CNF are also synthesized and proven to be degradable (in vitro) in nature due to swelling and degradation nature of TEMPO oxidized CNF resulting in high blood absorption in significant bleeding inhibition[224].

5.2.3. Application in food packaging

The reports in a study revealed that the food packaging materials established with nanotechnology are the largest group of current nanotechnology applications for food sector[225]. Currently, Zinc oxide is listed as safe material by the food and drug administration and is also used as a food additive. ZnO NPs have been incorporated with different polymers to improve the properties of the nanocomposites resulted in the improvement of barrier and mechanical properties as well as heat resistance properties when compared with the original polymers itself or conventional composites[226]. A composite containing bacterial cellulose (an interesting ecofriendly biomaterial), zinc oxide and polypyrrole (a famous conducting polymer) has been prepared and considered as a suitable candidate for applications in smart packaging in the food industry[227].

5.2.4. Ultra-violet (UV) sensing properties

ZnO nanoparticles have strong UV response that generally depends on the surface area and crystalline size in case of powder form the morphology and nature and of the surface in case of ZnO films. The ZnO nanostructure composite with suitable polymers can significantly enhance its activity in sensors[228, 229]. Cellulose/ZnO NPs powder is reported to be synthesized by growing ZnO nanorods on the cellulose fibers (powder) surfaces at different temperatures using aqueous chemical method for the fabrication of UV sensor[230]. Composite involves the advantages of cellulose in terms of sustainability, flexibility, transparency, and low price as well as exploitation of synergetic effects of ZnO functionality; characteristic results proved that it can be used for wearable sensors that can detect the UV component of sunlight with great sensitivity and stability[231]. There are many reports on the applications of CNF/ZnO NPs nanocomposites as UV sensors[230, 232-234]. The study revealed that cellulose was crucial for development of the porosity of the ZnO surface and a higher porosity leaded to an improved absorption of UV radiation[230].

Conclusion and future perspectives

Advances in nanotechnology are driven by rapid commercialization of products containing nanostructures and nanoparticles with remarkable properties. This is reflected in the enormous number of publications on nanotechnology. The conclusion highlights the utilization of plant fibers in conjunction with zinc oxide nanoparticles and discusses the current state of research findings and future developments in nanocellulose applications. The controllable properties and reproducible production methods of bio-compatible nanocellulose are essential for its acceptance as a commercially available material in multiple applications.

Furthermore, the incorporation of zinc oxide nanoparticles with cellulose or nanocellulose particles can significantly enhance the physical, morphological, and catalytical properties of the matrix. These nanocellulose/zinc oxide composites are considered multifunctional materials with improved modulus, strength, antibacterial properties, and photocatalytic capabilities.

In the future, the demand for nanocellulose/ZnO-NPs-based materials will increase, particularly in flexible and wearable electronics in the biomedical field, due to their lightweight and non-toxic properties. Therefore, further investigations are

necessary to facilitate the industrialization of nanocellulose/ZnO-NPs nanocomposites to meet human needs effectively.

CHAPTER TWO:

WATER POLLUTION AND ADSORPTION METHODE

Introduction

Environmental pollution is one of the utmost global concerns with exacerbation of industrial, urban, and agricultural activities due to population escalation. jeopardizes the human health and balance of ecosystem[235].

Water is essential for life. Its role is fundamental for the economic development of human civilization given its use in many sectors including industry and agriculture. This vital resource is well known for its great fragility. Hence the need to improve effective means for its protection against pollution [236].

The pollution of water by various organic materials: dyes (e.g., methylene blue, basic violet 3, reactive yellow 145), heavy metals (e.g., lead (II), chromium (VI), cadmium (II)) and other toxic substances is a global problem and a real danger for aquatic flora and fauna and causes serious problems for mankind[235]. Reducing the content of these toxic micropollutants is extremely important in terms of protecting natural environments and improving water quality. In this chapter we present some generalities on pollution and water treatment.

1. Water pollution by heavy metals and dyes

The rapid growth of industrial and agricultural activities has resulted in considerable discharge of pollutants into the environment, particularly dyes and heavy metals thus causing major concern worldwide [237]. Underground water is the major source of drinking water. This underground water is being polluted by the wastewater containing a large number of contaminants like acids, bases, toxic organics, inorganics, heavy metals[238].

1.1. Contamination of water by dyes

Dyes are basically coloured chemical compounds that a water-soluble, and can connect themselves to surfaces or fabrics to impart color [239]. which have mutagenic and carcinogenic impacts [240] which affects the environment due to the presence of toxic pollutants resistant to microbial biodegradation [241, 242]. The majority of dyes are complex organic molecules and consist of two components which are chromophores(the part of a molecule responsible for its color, e.g: -N=O, -C=C-, -

C=O) and auxochromes (A functional group that modifies the light absorbance,e.g: -OH,$-NH_2$, −COOH.) [243].The dye molecules persist in the aquatic environments due to their low biodegradability, stability to photolysis and oxidizing agent [1].

1.2. Classification of dyes

There are two types of dyes that are natural and synthetic. The natural sources are plants, animals, minerals and insects without any chemical treatment [244, 245]. Synthetic dyes are synthesized chemically, which are highly stable and toxic to living organisms.

There are many ways that can be classified for the classification of Commercial synthetic dyes. Classification can be done concerning color [246], molecular structure, and methods of application[1, 247].

Dyes can also be classified generally based on charge when dissolved in the aqueous medium [248, 249], such as cationic dyes (all basic dyes), anionic dyes (direct, acid, and reactive dyes), and non-ionic dyes (dispersed dyes), and the following (**Table II.1**) shows various types of dyes.

Table II.1:*Different types of dyes and their Health impacts, water solubility, and applications.*

Type	Water Solubility	Applications	Health impacts	Example
Acid	*Soluble*	Cosmetics,food,leather ,modifiedacrylics,nylon ,paper,printingink ,silkandwool	carcinogens Asthma Allergenic effects	AcidYellow36 Methyl Orange (MO) Congo Red (CR)
Basic	*Soluble*	Inks,medicine,modified nylon,modifiedpolyester ,paper,polyacrylonitrile,poly ester	carcinogens Skin Allergies Respiratory toxicity	Basic yellow-28 MethyleneBlue(MB) Malachite green
Direct	*Soluble*	Cotton,leather,nylon, rayon,silkandpaper	bladder carcinoma	DirectOrange26 Violet, blue, and
Disperse	*Insoluble*	Acetate,acrylicfibers, cellulose,celluloseacetate	DNA damage Splenic sarcomas	Disperse yellow, bleue, and Red
Reactive	*Soluble*	Cellulosic,cotton,nylon, silkandwool	/	ReactiveBlue5
Azo	*Soluble/insoluble*	Acetate,cellulose,cotton , rayonandpolyester	/	BluishRedazodye

- **Methylene blue (BM)**

Among these kinds of dyes The Methylene blue (BM) dye (or methylthioninium chloride) which was highlighted in this research as a representative model of medium-sized organic pollutants. MB is a cationic (basic) dye and one of the most widely used synthetic dyes in various fields. It is used as a colorant in the textile industry because of its properties such as water solubility [250], simplicity in utilization, and resistance to degradation [251] as it has widely been applied to cotton substrates, providing a wide range of bright and colorful tones [252]. It serves as a redox color indicator (its oxidized form is blue, while its reduced form is colorless), As an antiseptic in aquariums, and as a means of combating methemoglobin. It is harmful if ingested and irritating to the eyes, respiratory tract, and skin [253]. Table: 1.2 and Figure: 1.1 display some chemical properties and chemical structure of BM dye [253, 254].

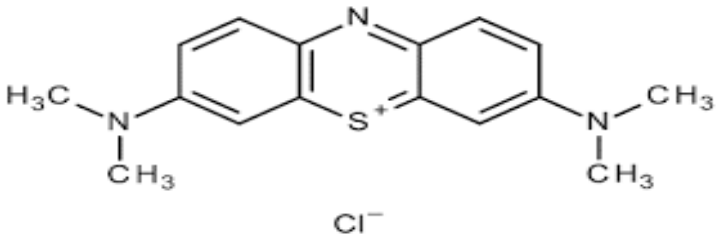

Figure II.1: *Chemical structure of methylene blue dye [255].*

Table II.2: *chemical properties of methylene blue dye.*

Nom	Bleu de méthylène (BM)
Famille	Colorants Basiques
Formule brute	$C_{16}H_{18}N_3SCl$
Appellation chimique	3,7-bis-(dimethylamino) phenazathionium
Masse molaire (g/mol)	320 g/mol
Dimensions (A°)	15 (diamètre)
λmax	663 nm

2. Water treatment methods

The remediation of aqueous solutions and wastewater requires treatment technologies which are robust, efficient, simple to operate and affordable such as adsorption [256]. Water treatment technologies for the removal of toxic metals and dyes The use of any water treatment technology in dyes and heavy metals removal depends on the basis for the treatment or kind of contaminant to be removed. For example, water treatment techniques suitable for the removal of dyes might be unsuitable for heavy metals removal to the extent of acceptable discharge limit. The concurrent removal of these coexisting most common and highly hazardous pollutants is difficult due to their persistent environmental nature [235]. There are several methods to remove pollutants from water classified as chemical, physical, and biological methods (Figure 4).

- Chemical methods can be such as precipitation (via chemical reaction, electrochemical), complexation, degradation (via chemical reaction (oxidation, reduction).
- The water treatment via physical methods includes adsorption, sedimentation, filtration, extraction, floating, and degradation via light (photocatalysis), or heat (pyrolysis).
- The biological methods including enzymatic degradation, and flocculation can be also used for the removal of pollutants such as organic contaminants

3. Adsorption

Adsorption is a phenomenon that occurs at the surface's interfaces, a surface process that leads to the accumulation of a substance (an atom an ion, or molecule) on the solid surface from its gaseous or liquid surroundings. The solid surface on which the adsorption process occurs is called the adsorbent, and the substance that accumulates on the surface of the solid is called the adsorbate [257].

Several definitions have been given by various authors, the most common among these are: Adsorption is a physicochemical phenomenon resulting in a modification of the concentration at the interface of two immiscible phases: (liquid / solid) or (gas / solid), we will therefore speak of the couples (adsorbate/adsorbent), This is a process of the greatest importance with regard to the behavior of both

inorganic and organic substances in natural waters because it influences both the distribution of dissolved and particulate substances and the properties of the particles in its suspension [258].

3.1. Types of adsorption

The nature of the bonds formed as well as the amount of energy released during the retention of a molecule on the surface of a solid makes it possible to distinguish two types of adsorption; physique sorption (Physisorption) and chemical sorption (chemisorption) [259, 260].

3.1.1. Physical sorption (or Physisorption)

It is usually called natural adsorption and also called van der Waals adsorption because It illustrates the nature of the weak link between the adsorbate and adsorbent including hydrogen bonding without a chemical change of the adsorbed molecules, and it occurs at low temperatures and within the limits of energies (mole / Kcal 10) at most. It is a process characterized by low binding energy and produces energy less than 40 kj /mol [24], usually rapid and readily reversible. Although weak individually[261].

3.1.2. Chemical sorption (or chemisorption)

Chemisorption is a process that results from the formation of a chemical bond that occurs between the adsorbent surface and molecules or ions of adsorbate [262]. As changes occur in the molecular structure and it is characterized by high binding energy [20-200 kj /mol] [263]. It is characterized by high binding energy (greater than 40 kJ mol-1) and corresponds to the more permanent ionic or covalent bonds between the adsorbent and the adsorbed molecule. This type occurs This interaction occurs between various organic molecules and the surface of the adsorbent material that can lead to the formation of a complex [264] and at high temperatures

3.2. Factors Experimental Influencing the Adsorption Process

There are principal factors that affect the adsorption effectiveness for instance: adsorbent dosage, contact time, pH, the initial dye concentration, and temperature [265]. Before applying an adsorbent material on an industrial scale, it is first

optimized in batch mode experiments; then if it possesses a high removal efficiency, it can be employed in industrial adsorption [266, 267].

In the next section, some of the factors affecting the adsorption process of dyes in wastewater [266, 268, 269]:

3.2.1. Effect of solution pH

The pH of adsorbate is vital in the determination of the active site's charge [270]. The efficiency of adsorption is dependent on the solution pH since variation in pH leads to the variation in the degree of ionization of the adsorptive molecule and the surface properties of the adsorbent [271]. At lower pH values, $H3O^+$ ions concentration is high and protonates carboxylate as well as amino groups making the adsorbent surface more positive [272]. This makes $-COO^-H^+$ and $NH3^+$ groups lose affinity for dyes by creating an electrostatic repulsive effect between surface sites of adsorbate and the dye ions resulting in a decrease in the adsorption capacity of dye s [273, 274]. To obtain maximum removal capacity, optimum pH is very important [275].

3.2.2. Effect of contact time

The interaction time is a vital parameter as adsorption is dependent on residence time [276]. At the initial stages, there are available adsorbent surface sites that rapidly adsorb dyes [277]. At equilibration time, active sites are exhausted limiting the capacity of adsorbent of dyes that can be adsorbed [278]. Completion of adsorption occurs when equilibration time is achieved at a specific time of adsorption [279]. Which means the active sites of the adsorbent are saturated with adsorbate molecules and no further adsorption can take place.61Therefore, obtaining optimal residence time of adsorption is important [240].

3.2.3. Effect of temperature

The effect of temperature on the adsorption process is another significant Physico-chemical process parameter because the temperature will change the adsorption capacity of the adsorbent it is either exothermic or endothermic [280] depending on the nature of the materials used in the adsorption process due to the kinetic energy of its molecules, and this requires adjusting the process temperature from the beginning [281]. Thus, if the amount of adsorption increases with increasing

temperature then the adsorption is an endothermic process. Increasing the temperature enhances chemical adsorption processes. Whereas the decrease of adsorption capacity with increasing temperature indicates that the adsorption is an exothermic process, the temperature enhances physical adsorption [282].

3.2.4. Effect of initial dye concentration

The initial concentration of sorbate is another important parameter, which affects the adsorption phenomenon and the amount of adsorption for dye removal. The effect of initial dye concentration depends on the immediate relation between the concentration of the dye and the available sites on an adsorbent surface. In general, the percentage of dye removal decreases with an increase in the initial dye concentration, which may be due to the saturation of adsorption sites on the adsorbent surface. On the other hand, the increase in initial dye concentration will cause an increase in the capacity of the adsorbent and this may be due to the high driving force for mass transfer at a high initial dye concentration [283].

3.2.5. Effect of dosage of adsorbent

Adsorbent dosage is an important process parameter to determine the capacity of an adsorbent for a given amount of the adsorbent at the operating conditions. Generally, the percentage of dye removal increases with increasing adsorbent dosage, where the quantity of sorption sites at the surface of the adsorbent will increase by increasing the amount of the adsorbent. The effect of adsorbent dosage gives an idea of the ability of dye adsorption to be adsorbed with the smallest amount of adsorbent, to recognize the capability of a dye from an economical point of view [280].

4. Kinetics study

4.1. The adsorption mechanism of a dye

Knowledge of the adsorption kinetics is of considerable practical interest in the optimal use of an adsorbent during an industrial operation, and in the knowledge of the factors to be optimized to manufacture or improve an adsorbent leading to the kinetics of the adsorbent fastest possible.

From a kinetic point of view, adsorbents can be divided into two categories[284]:

- homogeneous adsorbents whose porous structure is homogeneous over the entire scale of grain, for example, Silica gels, activated aluminas, and most activated carbons
- heterogeneous adsorbents with double porosity (micro and macropores) resulting from the accumulation of crystals or microparticles, for example, zeolites and carbonaceous molecular sieves.

The transfer of material takes place from the fluid phase to the active sites of the adsorbent, after the transfer of material from the solution to the boundary layer surrounding the particle in the agglomerated and dispersed adsorbents having a double porosity [284] structure through the following four steps (**Figure II.2**) [285]:

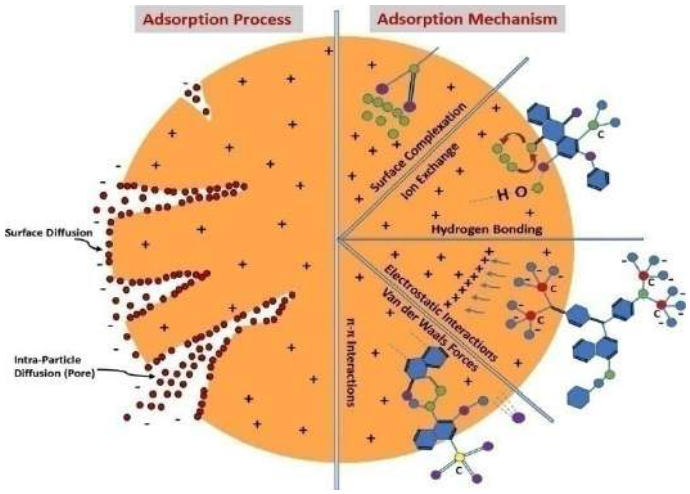

Figure II.2: *Mechanism and process of adsorption for the elimination of dye [286].*

a- External mass transfer (external diffusion): the molecules must cross the boundary layers (film) around the grains of the adsorbent to arrive at the surface of the latter; which corresponds to the transfer of the solute (a dye) from the breast of the solution to the outer surface of the particles. The transfer of the external material depends on the hydrodynamic conditions of the flow of a fluid in an adsorbent bed..

b- Internal mass transfer in the pores (internal diffusion): these transfers generally occur in the fluid phase filling the pores. fluid particles penetrate inside the pores macropores and mesopores formed between the crystallites or the microparticles of the adsorbent from the surface of the grains towards the center.

c- Microporous internal material transfers: adsorbed molecules diffuse through networks of micropores with an activated process mechanism (jumping of adsorbed

molecules between adsorption active sites) and this corresponds to the attachment of the particles to the surface of the pores.

d- Intrinsic adsorption kinetics: the molecules adsorb on the surface with a finite speed [287].

4.2. Modeling ofKinetic study

Kinetic study of adsorption illustrates how the uptake rate of solute controls the time of residence of the adsorbate at the interface of solution. This rate becomes significant when the adsorption system is designed and calculated from the kinetic study [288, 289]. So, to investigate the efficiency of the sorbent and to study the controlling component of the sorption, pseudo first and second order kinetics models.

4.2.1. Pseudo-First-Order Kinetics

The pseudo-first-order model, proposed by Lagergren in 1898, is based on a linear relationship between the amount of solute (adsorbate) attached to the surface of the material (adsorbent) and time. This model has been widely used by many authors to describe the adsorption of organic and inorganic solutes on heterogeneous solid surfaces. However, it is often not suitable for the entire range of contact times in elimination kinetics studies and is generally applicable only at the initial stages of adsorption, typically within the first 20 or 30 minutes [290]. Beyond that, the experimental data may not be accurately extrapolated using this model. The pseudo-first-order model can be linearized using the following expression [291-293].

$$\frac{dq_t}{dt} = K_1(q_e - q_t) \quad (II.1)$$

$$ln\,(q_e - q_t) = ln\,q_e - K_1 t \quad (II.2)$$

Where:

q_t: the quantity of adsorbate adsorbed at time t (mg.g-1). q_e: the quantity of adsorbate adsorbed at equilibrium (mg.g-1). k_1: the rate constant of the pseudo-first-order adsorption model (min-1). *t*: time (min)[294]. A linear plot of *ln(qe - qt)* versus t indicates that the pseudo-first-order kinetic model is applicable to the adsorption process.

4.2.2. Pseudo-Second-Order Kinetics

The pseudo-second-order model assumes that the adsorption capacity is directly proportional to the number of active sites occupied by the adsorbate. This model is expressed by equation **(II. 4),** and its linearity was developed by [295]. It accurately describes the adsorption of solute molecules on the solid surface of the material. Analysis of kinetic data indicates that an irreversible second-order model yields higher-quality results compared to lower-order models [290]. The linearization of the equation **(II. 4)** leads to the equation **(II. 3)**. The linear equation allows for the determination of qe (mg.g-1) and k_2 (g.min-1.mg-1) from the slope and the y-intercept of the line $\frac{t}{q_t} = \mathbf{F}(t)$[296].

$$\frac{d\,q_t}{dt} = K_2(q_e - q_t)^2 \qquad (II.3)$$

$$\frac{t}{q_t} = \frac{1}{q_e}t + \frac{1}{K_2 {q_e}^2} \qquad (II.4)$$

With: $k_2$is the pseudo second order kinetic constant (g.mg-1min-1); q_t: the adsorption capacity at time t (mg.g-1); q_e: the adsorption capacity at equilibrium (mg.g-1), and *t*: the time (min)[297].

5. Adsorption isotherms

Generally speaking, all adsorbent/adsorbate systems do not behave in the same way. Adsorption phenomena are often approached by their isothermal behavior. This adsorption isotherm is a curve that represents the relationship between quantity adsorbed Qe (mg/g) per unit mass and the concentration Ce (mg/L) of the solute in the solution at equilibrium Qe = f (C_e) Such curves are obtained in the laboratory at a constant temperature [47].

The adsorption capacity was calculated using the following relation **(II. 5)** [47]:

$$Qe = \left(\frac{(C_0 - C_e) \times V}{m}\right) \qquad (II.5)$$

Where: Qe is the amount of adsorbed at equilibrium (mg/g), V is the volume of the solution (L), C_0 and C_e are the initial and equilibrium dye concentrations (mg/L), respectively, and m is the amount of the adsorbent (g).

The adsorbed quantities can also be estimated by R %, which is the removal percentage defined by the following equation **(II. 6)** [100]:

$$\boldsymbol{R}\,(\%) = \frac{(\boldsymbol{C_0} - \boldsymbol{C_e})}{\boldsymbol{C_0}} \times \mathbf{100} \qquad (\boldsymbol{II.6})$$

5.1. Classification of adsorption isotherms

Several authors, including Gilles and Coll, have proposed a classification of sorption isotherms based on their shape and their initial slope [298, 299]. The shape of the isothermal curve varies according to the adsorbate–adsorbent couple studied [285, 300], the review by [301] presents a more or less detailed summary of this classification. Among the forms of isotherms, these authors distinguish (**Figure II.3**):

- ✓ **Type "H" isotherms:** called "high affinity" isotherms, is a special case of the "L" shape. This case is distinguished from the others because the solute sometimes shows such a high affinity for the solid, where the initial slope is very high that the initial slope cannot be distinguished from infinity, even though it does not make sense from a thermodynamic point of view.
- ✓ **Type "L" isotherms:** called "Langmuir", would rather correspond to low concentrations of solute in water. The isotherm is convex in shape, which suggests a progressive saturation of the solid. When Ce tends to zero, the slope of the isotherm is constant. This model indicates flat adsorption of bi-functional molecules.
- ✓ **Type "S" isotherms:** called "sigmoidal", has a revealing inflection point, this type of isotherm is always the result of at least two opposing adsorption mechanisms. This is the case, for example, when the first layer of solute is first adsorbed and then when the adsorption of one or more additional layers becomes favored.
- ✓ **Type "C" isotherms:** known as "constant partition", is a straight line passing through zero which means that the qe/Ce ratio (called distribution coefficient Kd) is constant[282].

The "L" and "H" forms are the most observed, especially in the case of the adsorption of organic compounds in an aqueous solution on activated carbons.

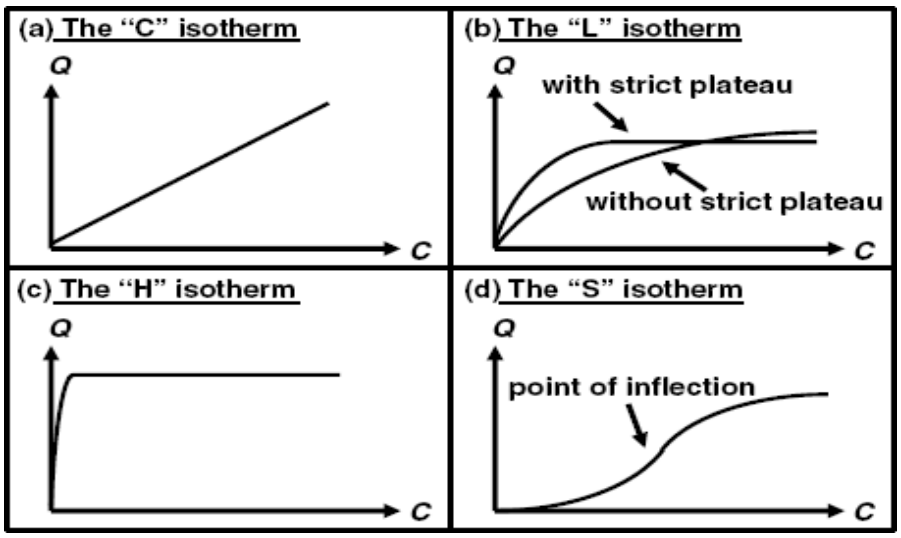

Figure II.3: *Types of isothermes [301].*

5.2. Modeling of adsorption isotherms

The most frequently used models in the literature to describe solid-liquid adsorption are the two-parameter models (Freundlich, Langmuir, Dubinin-Radushkevich and Temkin, Elovich).

5.2.1. Langmuir Isotherm:

The best-known model for representing adsorption phenomena in the aqueous phase is the one developed by Langmuir [302]. The Langmuir model is based on two key assumptions: firstly, that the number of adsorption sites on the material's surface is fixed and each site can only adsorb one molecule; secondly, that the surface is uniform and there are no interactions between adsorbed molecules, which allows for constant adsorption energy. The linear form of the Langmuir isotherm can be expressed using the following relationship **(II. 7)** [302-304]:

$$Qe = \frac{Qmax\ KLCe}{1 + KL\ Ce} \qquad (II.7)$$

Where *Qe* (mg/g) is the adsorbed amount of the solute at equilibrium, *Qmax* is the maximum adsorption capacity are expressed in (mg/g), C_e is the solute concentration at equilibrium of the adsorbate (mg/L), and *KL* is Langmuir equilibrium constant is expressed in (L/mg). The linear form of Langmuir equation is **(II. 8)**:

$$\frac{Ce}{Qe} = \frac{1}{KL\ Qmax} + \frac{Ce}{Qmax} \qquad (II.8)$$

If the equation of Langmuir is checked, we must obtain while placing our experimental points in $C_e/Q_e = f(Ce)$, a line whose slope and ordinate in the beginning enable us to determine *Qmax* and *KL*. The essential characteristic of Langmuir isotherm can be expressed by the dimensionless constant called equilibrium parameter R_L, defined by:

$$R_L = \frac{1}{1 + KL\ C_0} \qquad (II.9)$$

Note that some authors define the R_L ratio **(II. 9)** as a quantity without a unit. According to the value of R_L, we can say that [305]:

- the isotherm is irreversible: $R_L = 0$.
- the isotherm is favorable: $0 < R_L < 1$.
- the isotherm is linear: $R_L = 1$.
- the isotherm is unfavorable: $R_L > 1$.

5.2.2. Freundlich Isotherm

The Freundlich model was established by Freundlich in 1926 as a very satisfactory isotherm that can be successfully applied to the adsorption of gases but has mainly been used for adsorption in dilute solutions [306]. He found that the mechanism of this process is quite complex, as the adsorption isotherm of Freundlich occurs on a heterogeneous surface through a multilayer mechanism of adsorption, which results in variable heat of adsorption [307]. Additionally, he observed that the adsorbed quantity increases with the concentration. The mathematical expression of the Freundlich isotherm equation is written as follows:

$$Qe = K_F\ Ce^{1/n} \qquad (II.10)$$

Where K_F (L/mg) is Freundlich constant and n is the heterogeneity factor. The K_F value is related to the adsorption capacity; while the *1/n* value is related to the adsorption intensity. 1/n values indicate the type of isotherm to be irreversible ($1/n = 0$), favorable ($0 < 1/n < 1$), an unfavorable ($1/n > 1$) can be rearranged to linear form [307]:

$$Log\ Qe = Log\ K_F + \frac{1}{n} Log\ Ce \qquad (II.11)$$

5.2.3. Temkin Isotherm

Temkin adsorption isotherm discusses interaction of sorbent and sorbate, and the model is based on assumption that heat of adsorption will not remain constant. Temkin model is assumes that the decay of adsorption heat with recovery rate is linear rather than logarithmic (as in Freundlich's equation) . It decreases due to interaction between sorbent and sorbate during adsorption phenomenon [31]. Temkin's isotherm model is usually applied in the following form:

$$Qe = \frac{RT}{b}\ln(a\,Ce) \qquad (II.12)$$

$$Qe = B\,\ln a + B\,ln\,Ce \qquad (II.13)$$

Where: $B = \frac{RT}{b}$

R the perfect gas constant: 8.314 J. mol-1. K-1. In addition, T is the absolute temperature (K) and the constant *B* is related to the heat of adsorption [308].

a And b are characteristic constants of the adsorbate/adsorbent system By setting (qe) as a function of $(lnCe)$ we obtain a straight line with slope *B* and ordinate at the origin *B ln a*, this allows the determination of the two Temkin parameters, *a* and *b*[309].

6. Thermodynamics of adsorption

The concept of thermodynamics supposes that in an isolated system where energy cannot be gained or lost. The adsorption phenomenon is always accompanied by a thermal process, either exothermic or endothermic due to the transfer of the unit of the body dissolved starting from the solution to the solid-liquid interface [310].

The measurement of the heat of adsorption is the main criterion that makes it possible to differentiate Chemisorption from physisorption.

The thermodynamic parameters which must be considered to determine the process are changes in the standard enthalpy (ΔH°), the standard entropy (ΔS°), and free standard energy (ΔG°) The thermodynamic parameters values were calculated by using the equation of Van't Hoff [311]:

$$ln\,K_d = \frac{\Delta S}{R} - \frac{\Delta H}{RT} \qquad (II.14)$$

$$K_d = \frac{Qe}{Ce} \qquad (II.15)$$

Where K_d: is the distribution thermodynamic constant; Qe : quantity adsorbed on the solid with balance (mg/g), and Ce : concentration with balance (mg/L).

R: is the molar gas constant (R = 8.314 J/mol .K), T: absolute temperature of solution (K).

$\Delta G°$*:* standard Gibb's free energy (J/mol); $\Delta H°$*:* standard enthalpy change (J/mol) and $\Delta S°$*:* standard entropy change (J/mol/K)

$\Delta H°$ is used to explain the endothermic or exothermic adsorption nature[312, 313]. Positive $\Delta H°$ values above 40 kJ/mol implies chemisorption involving strong electrostatic coordination of metal ions by the active sites[314]. The negative ΔG° values at different temperatures are an indication of a favorability and spontaneity of adsorption process [315-317].

The $\Delta S°$ provides information about the disorderliness of an adsorbent surface during adsorbent-adsorbate interactions [277] . $\Delta H°$ and $\Delta S°$ are determined by plotting a graph of lnkd versus1/T .$\Delta G°$ can be calculated below by using the relation (II. 16 and II. 17):

$$\Delta G = -RT \ln K_d \qquad (II.16)$$

$$\Delta G = \Delta H - T\Delta S \qquad (II.17)$$

CHAPTER THREE:

MATERIALS AND METHODS

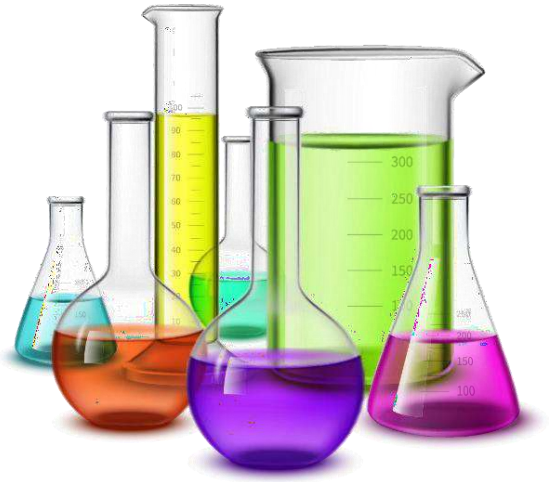

Introduction

Cellulose, the most abundant natural polymer on earth, [4]. Cellulose nanocrystals (CNCs) prepared by hydrolysis of cellulose in an acidic medium are typically, depending on the biomass source, with high crystalline content with diameters varying from 1-100 nm and lengths of several hundreds nm [5]. In the past twenty years, CNCs have attracted great interest because of their renewable nature, biodegradability, low toxicity, low density16, biocompatibility, high specific surface area, high elastic modulus,high crystallinity, and high mechanical strength, availability and reproducibility18 and high aspect ratio [6]. Besides the application of unmodified cellulose products, cellulose can be converted into regenerated cellulosic materials, which have been widely applied in many fields [318, 319].

Zinc oxide (ZnO) is a versatile inorganic metal oxide, which is considered as a GRAS substance (i.e. “Generally Recognized as Safe”) by the U.S. Food and Drug Administration [18].

ZnO nanoparticles are widely used in many [17]. However,ZnO nanoparticles have the tendency to aggregate in solution due to their large specific surface area and high surface energy, the catalytic ability of NPs is directly related to the surface area of the catalyst, so this aggregation process will reduce the catalytic activity. To overcome this drawback and improve the dispersibility of ZnO nanoparticles, one of the most effective methods is adding surfactants or polymeric ligands into the system, scientists are very interested in synthesizing ZnO NPs on the basis of another material, acting as a carrier to improve the dispersion of ZnO NPs at the nanometer level.. Sustainable cellulose and nanocellulose in particular, with abundant hydroxyls groups become a few of the preferred carriers for hybrid materials[20, 320]. Nanocellulose could even self-assemble to form 3D network structure to inhibit the agglomeration of ZnO nanoparticles further. The nanocellulose-ZnO hybrids have a wide range of applications in photocatalysis, antibacterial and reinforcing fillers [21].

This chapter, aims to present a simple protocol for the synthesis of the organic/inorganic nanocomposite. In this work we used two different methods for synthesis of the biocomposite cellulose/Zinc oxide nanoparticles (CNC/ZnO NPs) from peanut shells and pea shells. As well as in this chapter, for confirm the synthesis and the nature of the final products obtained of cellulose/zinc oxide nanoparticles and study their properties, were analyzed using standard techniques such as, Fourier

transform infrared (FTIR), X-ray diffraction (XRD), UV-visible (UV-Vis), scanning electron microscopy (SEM), and energy dispersive X-ray analysis (EDX). Meanwhile, this synthesis by two different methods aims to obtain the optimal conditions for CNC/ZnO NPs synthesis to use in many applications and novel fields.

Functionalized cellulose (Cs) and cellulose/zinc oxide nanocomposite (CNC/ZnO NPs) has been used as adsorbents for removing MB dye from aqueous solution by adsorption technique. We studied the effects of various parameters influencing the adsorption capacity, that affect the adsorption process in wastewater treatment such as adsorbent dose, initial dye concentration, contact time, initial pH dye solution, and temperature under the aspects of thermodynamic study, adsorption isotherms, and adsorption kinetics.

1. Materials and methods

This work was carried out at the level of the Laboratory ofValorization and Promotion of Saharan Resources (VPRS), Kasdi Merbah University in Ouargla, Algeria and the pedagogical laboratories in the Department of Chemistry, Faculty of Exact Sciences, University of Echahid Hamma Lakhdar El-Oued, Algeria.

1.1. Plant waste collection (peanut shells and pea shells)

Peanut and pea shells were gathered from a local farm in Bagouza, Taghzout, 20 kilometers from the provincial capital, El Oued. The shells were collected on the 2020. Additional information about the collection of peanut and pea are shown in **Table III.1** and **Figure III.1.**

Table III. 1:*Information about the collection of peanut and pea shells.*

Location	SiteName	Geographicalcoordinates	Altitude (m)	Bioclimatic zone	Collectiondate
El-Oued, Algeria	**Bagouza Taghzout**	**Latitude:33°, 49N Longitude: 06°, 72E**	**68**	**Arid**	**03/2020**

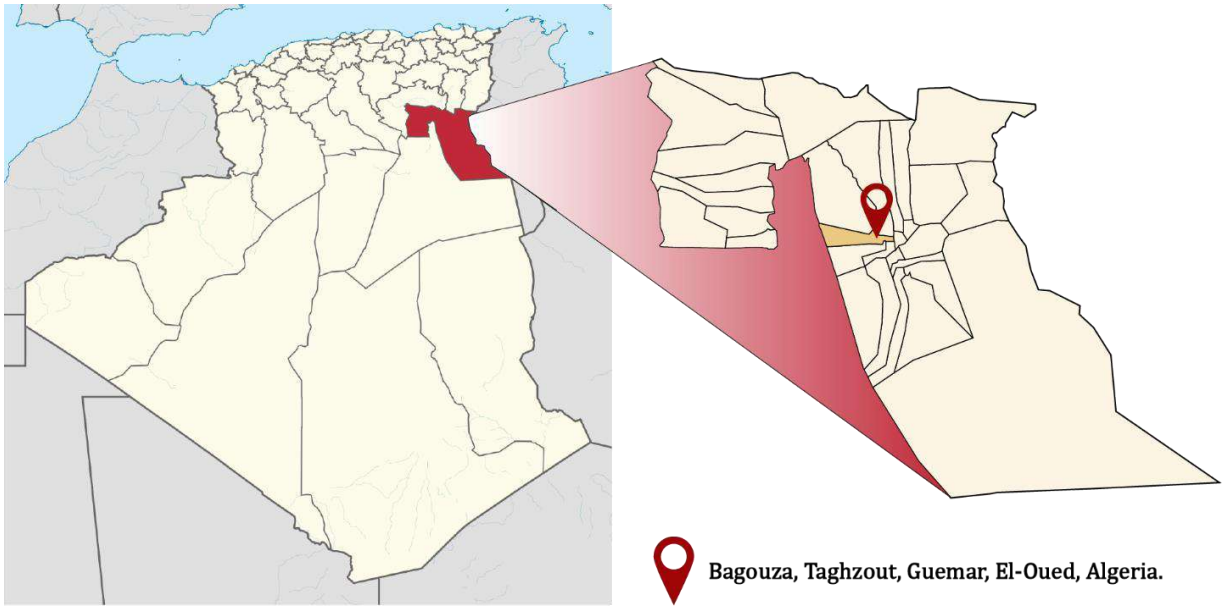

Figure III. 1:*Geographic map showing the collection Bagouza Taghazout El-Oued area.*

1.2. Preparation of the plant waste (drying, grinding, and preservation technology)

To obtain cellulose and determine the percentage of its presence in each of the peanut shells and pea shells, once the fruits are harvested and the husks are separated for the 2020 season. we have collected samples, where the peanut shells were dry, while the pea shells were still soft. Then, An operation of dusting and washing the leaves of the plants with distilled water, then they are spread on aluminum foil and left to dry at room temperature for a few days and dried away from sunlight and ventilated in the open air at room temperature for several days. After it is completely dry, the cutting of the leaves of the plants was carried out using a pair of scissors in the form of fragments of approximately 5-10 mm in length. We put the dried and chopped leaves in an electric grinder to grind to the finest possible particle size and sieve it with a porous manual sieve to obtain a sample in the form of fine fibers and of equal size so that all molecules are chemically treated to the same degree. After drying and grinding, the powder has been kept in tightly closed boxes in order to basically keep its color, taste and properties. The box was carefully stored in a dry place until powder analysis [321, 322] **(Figure III.2).**

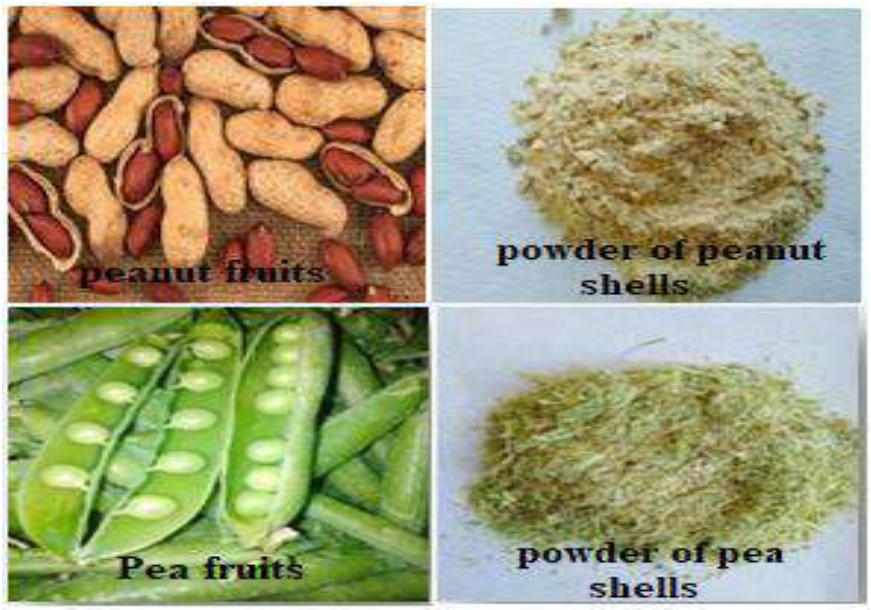

Figure III. 2:*Pictures of the raw material of peanut and pea shells.*

1.3. Chemical products used

All the chemicals used in this work are stored away from light and in an inert atmosphere. The origin and purity of the reagents used in this work are described in **Table *III.* 2.**

Table III. 2:*Chemical products used in this work.*

Chemical products, Reagents and solvents	Chemical formula	N°CAS [Reg.Num]	Purity (%)	M(g/mol)	
Hydroxydede sodium	NaOH	215-185-5	97	40	BIOCHEM
Hydrochloric acid	HCl	7647-01-0	37	36.46	BIOCHEM
Sodium Chlorite	$NaClO_2$	7758-19-2	80	90.44	/
Acide sulfurique	H_2SO_4	7664-93-9	96	98.08	BIOCHEM
Urea	CH_4N_2O	57-13-6	99-101	60.06	SIGMA-ALDRICH
Zinc Acetate	$Zn(NO_3)_2$	5970-45-6	99.7	219.5	BIOCHEM
Zinc Chloride	$ZnCl_2$	7646-85-7	98 -100.5	136.30	SIGMA-ALDRICH
Zinc Nitrate	$Zn(NO_3)_2.6H_2O$	10196-18-6	98	297.49	SIGMA-ALDRICH
Dimethyl sulfoxide (DMSO)	$(CH_3)_2SO$	67-68-5	99.9	78.13	SIGMA-ALDRICH
(dimethylamino)-3,7 phenazathionium chloride Methyl Bleu (MB)	$C_{16}H_{18}N_3SCI$	61-73-4	96-101	319.85	BIOCHEM

2. Synthesis of cellulose zinc oxide nanoparticules (CNC/ZnO NPs)

2.1.1. Isolation of Cellulose (Cs)

For extraction the cellulose and cellulose nanocrystals, we go through several successive stages:

a- Elimination of soluble matter in hot water:

We soaked a weight of 300 g of each sample in distilled water at a temperature of 100 °C by 10% of the dry matter under stirring for 10 minutes, after which each sample was filtered separately and we spread it on aluminum foil and put it in an oven at a temperature not exceeding 70 °C until it is completely dry, as shown in the following ***Figure* III. *3(A)*.**

b- Acid treatment with hydrochloric acid (HCl):

The dry matter from the first step is put in Arlène Mayer and an acid chlorine solution is added to it at a concentration of 1M in a ratio (solid / liquid) (mg / ml) (1/80) and left under stirring using a magnetic rod at a temperature of 85 °C for 30 minutes. After the required time has elapsed, we filter the mixture and separate the solid part from the liquid part. This step is repeated under the same previous conditions by changing the concentration of the hydrochloric acid solution from 1M to 0.5M. After completion of the second filtration, the filtrate obtained is dried by placing it in an electric oven at a temperature not exceeding 70 °C. By acid treatment of the filtrate, the bacterial sugars are eliminated. as shown in the following **Figure III. 3(B).**

c- Basic treatment with sodium hydroxide (NaOH):

The main role of the soda lye treatment is the elimination of the majority of hemicelluloses and the lignin stuck to the cellulose fibrils. At this point, both samples were treated with NaOH solution. We put the dry matter resulting from the acid treatment process into the flask and add sodium hydroxide solution into the flask with a solid to liquid ratio (1:2) (g/ml) under stirring using a magnetic rod to facilitate the stirring process of the mixture and at a temperature of 85 °C for 1 hour. Then we filter the mixture and completely separate the solid sample from the liquid this sample

undergoes the same treatment with NaOH solution several times until a filtrate is obtained with a pale color and the resulting extract is almost transparent to ensure the elimination of hemicellulose and lignin. After having separated the solid matter by filtration one last time, and washing the sample with distilled water several times until a neutral pH (pH=7) after which the solid matter is dried in an oven at a temperature of 60 °C. as shown in the following **Figure III. 3 (C).**

d- Blashing with Sodium hypochlorite($NaClO_2$):

The sample obtained after basal treatment with NaOH is yellow color, hence the need to bleach it with $NaClO_2$ at a concentration of 2% [323] in order to eliminate the lignin residue and obtain pure cellulose as shown in the following **Figure III.3 (D).**

This step was carried out by placing the dry matter from the basic treatment in an erlyn mayer and then adding a $NaClO_2$ solution in a solid/liquid ratio (1:6) (g/ml) in addition to drops of acetic acid to obtain the pH = 5. The mixture is stirred at a temperature of 85 °C for one hour (1h) after the necessary time has elapsed, the sample is filtered and this step is repeated with a solution of $NaClO_2$ solution until a white filter is obtained, then the filter obtained is washed several times with distilled water using a centrifuge (speed = 5000 rpm, t = 15 min and T = 25 °C) to ensure the complete separation of the solid part from the liquid part and not to lose mass. We monitor the total disappearance of the chlorine effect in the washing water using a dilute solution of Silver nitrate $AgNO_3$. Then, the sample is treated with ultrasound for 30 minutes at a temperature of 25 °C to eliminate agglomerates and dried in an oven at a temperature of 60 °C. Finally, the sample is ground to obtain the final product, which is the pure white cellulose powder

Figure III. 3:*A photos showing the different stages of cellulose extraction (A: Washing, B: acid treatment, C: basic treatment, and D: bleashing)*

2.1.2. Preparation of Cellulose Nanocrystals (CNCs)

Cellulose nanocrystals (CNCs) was isolated by the acid hydrolysis of obtained cellulose from peanut husks and pea husks are shown in **Figure III. 4.**

1g of cellulose was mixed with 50 ml of sulfuric acid solution (H_2SO_4) solution with a concentration 40% in the ratio powder/ solution (20:1) (mg/mL) [324]. The reaction was carried out using reflux assembly with continuous stirring for 4 hours at room temperatur. Resultant suspension was diluted 10 times with cold water. The insoluble part was separated by centrifugation (5,000 rpm; 25 °C, 20 min) to reduce its water content, washed several times with distilled water at room temperature until a neutral pH=(7 or 8) and treated with ultrasonic waves (9 kHz) during 20 min and the solid product obtained dried between 70/50°C.

The size and the morphology of the nanoparticles generally depend on several factors such as the plant species, the amount of sample used, the concentration of solutions, the temperature and the reaction time. In this work, we focused on the study of the effect of the acid concentration (H_2SO_4), the same previous procedures were used each time for the cellulose nanocrystals (CNCs) extraction with a change in acid concentration (40%, 38%, 36%).

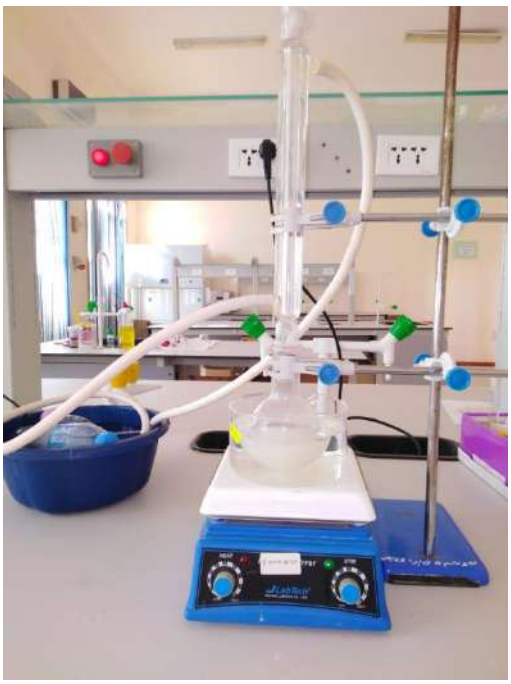

Figure III. 4:*A photo showing the assembly of synthesis of cellulose nanocrystals (CNCs)*

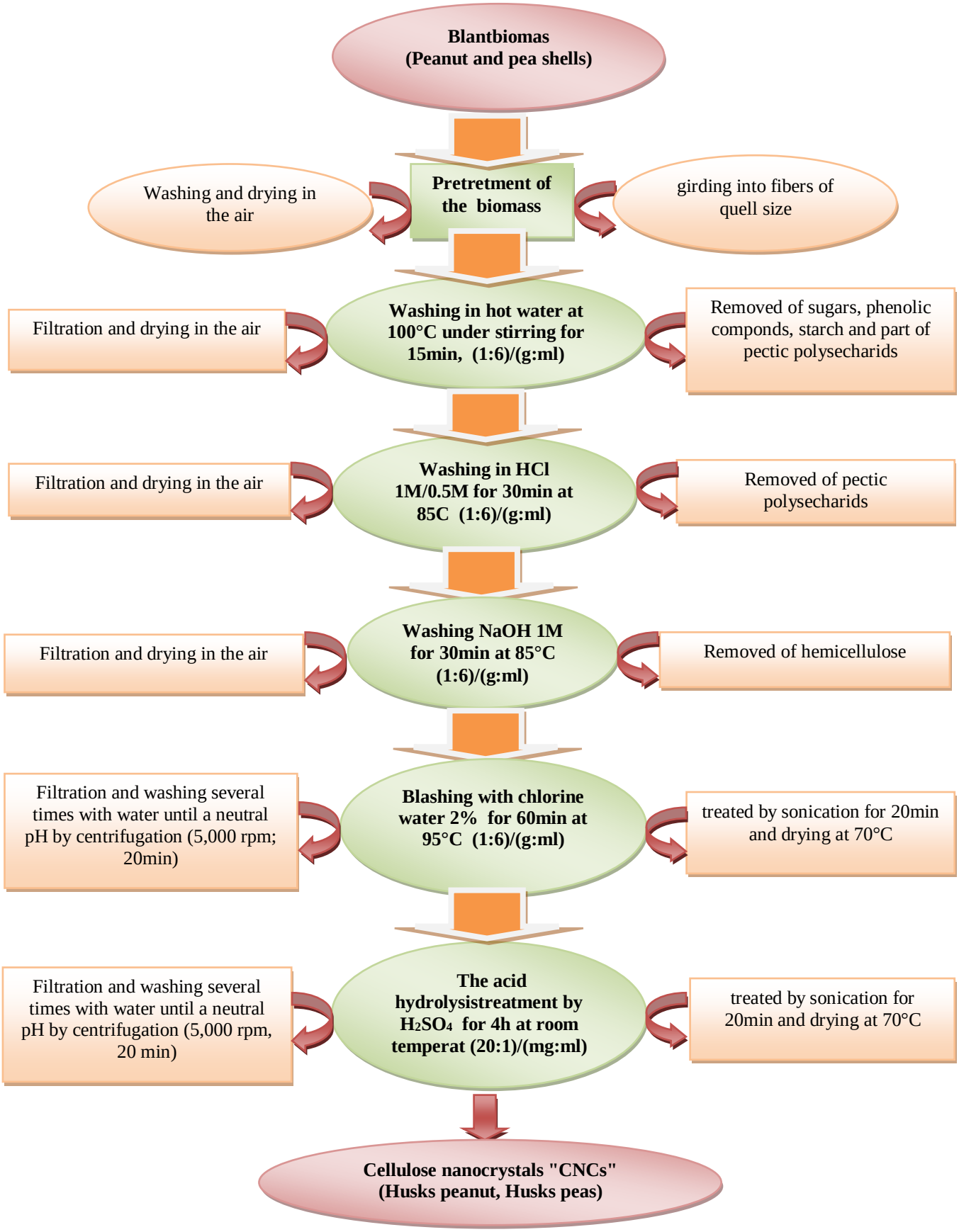

Figure III. 5:*Aschematic representation showing the stagesof CNCs preparation from plant waste (peanut and pea shells).*

2.1.3. Synthesis of zinc oxide nanoparticles (ZnO NPs)

The zinc oxide (ZnO) nanoparticles were prepared by wet chemical method using zinc chloride and sodium hydroxide as precursors.

In this experiment, an aqueous solution of $ZnCl_2$ (V/C), (100ml / 1 M) was kept under constant stirring using a magnetic stirrer to completely dissolve the zinc chloride and an aqueous solution of NaOH (V/ C), (100 ml/ 5 M) was also prepared in the same way. After complete dissolution of the zinc chloride, an aqueous solution of 5 M NaOH was added under constant stirring at high speed (slowly for 30 min), drop by drop without touching the walls of the vessel. The reaction was carried out by rising under reflux with continuous stirring for 2 hours at 80° C after complete addition of sodium hydroxide. After the completion of the reaction, the solution was allowed to stand overnight and further, using a needle, the supernatant solution was discarded carefully. The remaining solution was centrifuged at at 5000 rpm for 10 min, and the precipitate removed. Thus obtained ZnO NPs were washed a few times using distilled water to eliminate the byproducts which bound to the nanoparticles. After washing, the nanoparticles were dried in an oven at 80°C for overnight. Finally, the powder subjected to calcination in a muffle furnace at a temperature of 500°C for 3,5 h in order to eliminate all the organic functions that may be present in the powder (Na, CL, water, etc.). During drying, $Zn(OH)_2$ is completely converted into ZnO takes place.

2.1.4. Synthesis of cellulose zinc oxide nanoparticules (CNC/ZnO NPs)

In this work, was used two methods to synthesis the cellulose/ZnO nanoparticules

2.1.4.1. The first method (CNC/ZnO NPs M1 and CNC/ZnO NPs.T1)

In this method, We dissolved the Cellulose nanocrystals by a mixture aqueous solution as solvent of cellulose (CNCs) was prepared by directly mixing alkali hydroxide, urea and distilled water. the concentrations were weight percent (NaOH/Urea) (7%/12%) [325] amount of dried cellulose nanocrystals was immersed in the solvent and stirred for about 30 min at ambient temperature until to transparent cellulose solution without any native fibers, the cellulose was considered being dissolved completely. After that was freezed the mixture to -20°C.

After 17h, was heating and melting the mixture to a temperature of 80°C , a zinc nitrate solution (50 mM) was added drop-wise (by sol-gel method) to the dissolved

mixture solution until color change to milky white. The reaction was carried out using reflux mounting under continuous gentle stirring at 80°C for 4 hours. After that we stopped the reaction by diluting the mixture and cooling it **Figure III. 6**

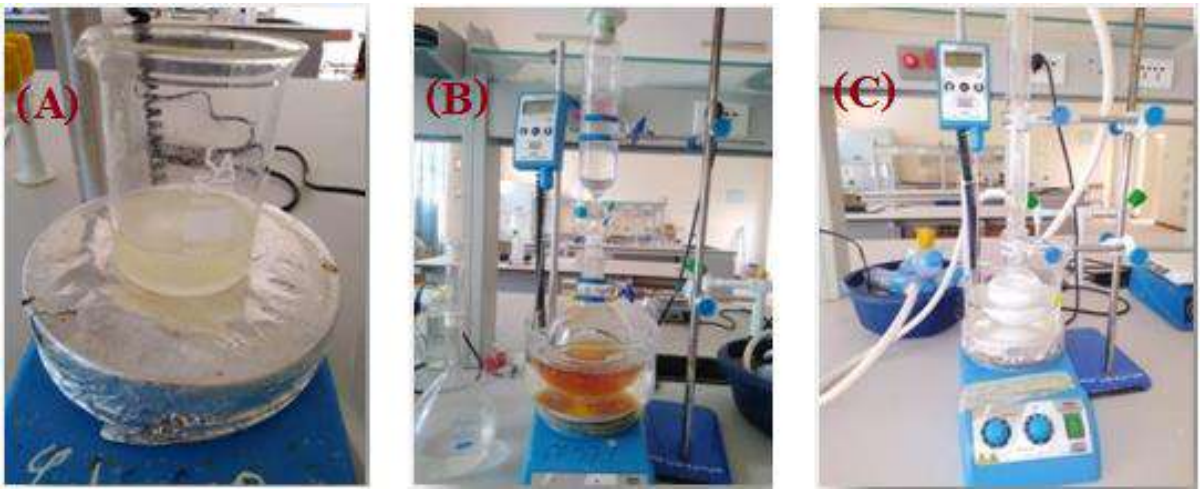

Figure III. 6:*A photos showing the different synthesis stages of CNC/ZnO NPs for the first method (A: dissolving, B: added zinc nitrate solution, and C: stirring for 4h)*

2.1.4.2. The second method (CNC/ZnO NPs M2 and CNC/ZnO NPs.T2)

For this method, we use nanocellulose as an undissolved solid. In a reflux assembly, 1g of ground CNCs are added with $ZnCl_2$ solution (50 ml/0.2 M) is added, the mixture is left under stirring and heating up to 80° C (almost 30 min).

After 30 minutes, NaOH (50 ml/1M) is lowered drop by drop, then the composition is connected and left under vigorous and continuous stirring and heating at the same temperature 80° C for 2 hours. Then, the reaction is stopped and the mixture is cooled and the precipitate is recovered using a centrifuge .

The white solid product (CNC/ZnO NPs) was collected from the two methods separately by centrifugation (5000 t/min et 10 min) at room temperature and washed several times with distilled water until a neutral pH. Then treated with ultrasonic waves for 30min and dried at 70 °C for complete transformation of the remaining zinc hydroxide to zinc oxide.

3. Characterization techniques

The following techniques were used for the characterization of Cellulose/Zinc oxide nanoparticles: UV-Vis, FT-IR, XRD, SEM and EDX.

3.1. Structural and morphological properties

3.1.1. X-ray diffraction (XRD)

X-rays are electromagnetic waves with wavelengths ranging from 0.01 to 10 °A. This is the most common and widely used non-destructive technique for determining the properties and structure of crystallized products. Furthermore, X-ray diffraction provides access to physical information about the crystal, such as its size and orientation [326].

- **Principle:**

This technique is based on the interaction of a sample's crystal structure with short-wavelength monochromatic radiation.

The monochromatic X-ray beam is directed onto a polycrystalline material and reaches the crystal lattice planes, where they come into contact with the electronic clouds of atoms that comprise this plane, in which case the X-ray beam is partially reflected in the first plane, or they do not encounter any obstacle and can continue to partially reflect the second plane. These planes are separated by specified distances that vary depending on the nature of the substance under consideration (grid distance). The beams' interference would be either constructive or destructive. Bragg's law can be used to determine the directions in which the interferences are constructive, known as diffraction peaks [326].

- **Bragg's law:**

When a crystalline species is irradiated by X-radiation of wavelength λ under an incidence θ the radiation is diffracted if Bragg's law is verified, as shown in **Figure III.7**.

$$n\lambda = 2dhklsin\theta \qquad \textbf{(III. 1)}$$

Where: n is an integer representing the order of the reflection.

λ: is the wavelength of the X-rays.

d: is the interarticular distance.

θ: is the angle of incidence of the X-rays.

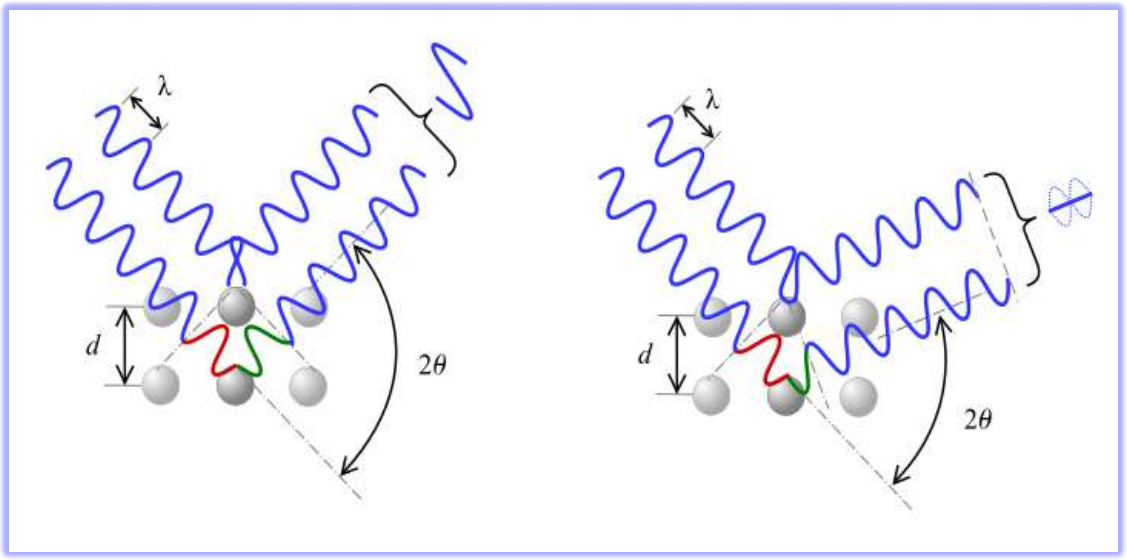

Figure III. 7:*Diagram illustrating the principle of Bragg's law.*

In general, the diffractogram is a recording of the diffracted intensity as a function of the angle 2θ formed with the direct beam. The study of the diffractogram makes it possible to trace a large amount of information on the structural and microstructural characteristics of the sample such as the crystalline structures, crystalline size (D), crystallinity index (CrI), and morphology crystallites.

- **Crystalline size determination (D):**

Although many approaches have been described for size determination using XRD, the Debye-Scherrer equation is the most commonly used for crystalline size determination [327].

$$\boldsymbol{D = k\lambda/\beta cos\theta} \qquad \textbf{(III. 2)}$$

Where: D is the grain size in nm.

λ is the wavelength of the X-ray beam.

θ is the diffraction angle.

β is the width at half height expressed in radians.

As part of our study, X-ray diffraction (XRD) was used, using the Miniflex 600 with Cu-kα radiation of wavelength = 1.5418. The diffractometer reflections were taken at room temperature and the 2θ value was varied from 10 to 80°.

- **Crystallinity index (CrI):**

The crystallinity index (CrI) of cellulose was calculated from the XRD patterns according to the Segal method [328]:

$$\boldsymbol{CrI}\ (\%)\ = \left((\boldsymbol{I_{002} - I_{am}})/\boldsymbol{I_{002}}\right) \times \mathbf{100} \qquad \textbf{(III. 3)}$$

Where I_{002} is the maximum (002) lattice diffraction intensity at 2θ = 23° and I_{am} is the diffraction intensity at 2θ = 18°.

3.1.2. Scanning electron microscopy (SEM)

Scanning electron microscopy (SEM) is a technique that allows observation of the surface morphology of solid material and is a testing process that scans a sample with an electron beam at high magnifications to produce images magnified high resolution for analysis and accurately measures very small objects. The method is used very effectively in microanalysis and failure analysis of solid inorganic materials, so this technique offers many advantages in morphology and dimensional analysis.

The morphology of the samples was analyzed using a TESCAN VEGA3 scanning electron microscope (SEM). Attached is a chemical element determination system (EDS).

- **principle:**

Scanning electron microscopy is a technique using electron-matter interactions to observe the surface topography of massive samples. SEM provides images of the surface of the mode of electron scattering by the sample. These images are formed mainly using surface electron emissions (secondary electrons and backscattered electrons). The interaction between the beam of electrons with energy E0 (primary electrons) and the sample generates low-energy electrons called "secondary electrons". These are then accelerated towards a detector which has the role of amplifying the electrical signal received (at each point, the intensity is converted into an electrical signal). The different particles are analyzed by different detectors which makes it possible to reconstruct a three-dimensional image of the surface. It uses, in addition, the other interactions of primary electrons with the sample: the emergence of backscattered electrons, absorption of primary electrons, as well as the emission of X photons. Each of these interactions is often significant for the topography, and the composition of the surface and It gives information on the relationships between the different structures of the tissue [329].

It is not strictly speaking a conventional microscope in the optical sense of the term:

- There is no formation of an image by an objective lens (as is the case in optical microscopy and in transmission electron microscopy).

- Here, the image is formed sequentially by scanning the surface of the sample with an electron beam and collecting the secondary electrons, i.e. the backscattered electrons[330].

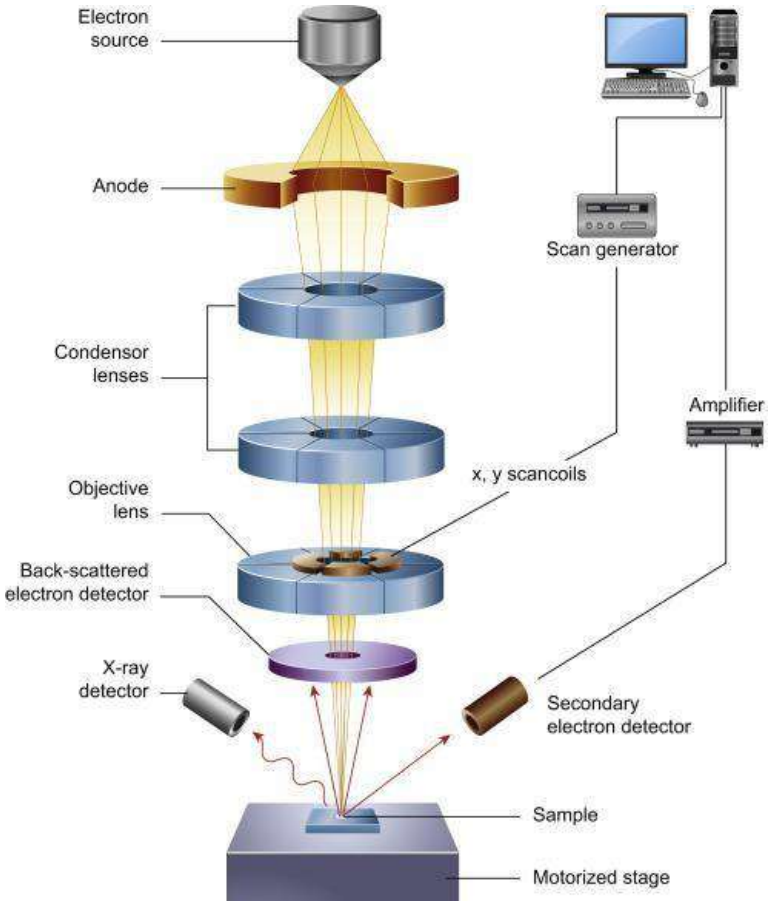

Figure III. 8:*Schematic Diagram of Scanning Electron Microscope [331].*

3.2. Optical properties

3.2.1. UV-visible absorption spectroscopy

Ultraviolet-visible (UV-vis) spectroscopy is used to obtain absorbance spectra of a compound in solution or solid form. What is observed spectroscopically is the absorbance of light energy or electromagnetic radiation, which excites electrons from the ground state to the first singlet excited state of the compound or material. The UV-vis energy region for the electromagnetic spectrum covers 1.5 to 6.2 eV, which corresponds to a wavelength range of 800 to 200 nm. were studied using visible UV transmittance spectroscopy using the Shimadzu 3101PC double beam spectrophotometer [332].

Principle:

UV-visible absorption spectrometry is based on the transition of valence electrons that pass from a ground state to an excited state after absorption of a photon in the UV-visible.

The principle of the UV spectrophotometer follows the Beer-Lambert law. This law states that each time a beam of monochromatic light passes through a solution with an absorbing substance, the decreasing rate of the intensity of the radiation as well as the thickness of the absorbing solution is proportional to the concentration of the solution and incident radiation. This law is expressed through this equation [333]:

$$A = log\left(I_0/I\right) = \varepsilon cl \quad \textbf{(III. 4)}$$

Where I_0: Intensity of incident light.

I: Intensity of light transmitted by the sample solution.

c: Represents the solute concentration.

l: Represents the length of the sample cell.

ε: Represents the molar absorption coefficient.

The ratio (I/I_0) is known as the transmittance (T) and the logarithm of the ratio inverse (I_0/I) is known as the absorbance (A). Therefore:

$$A = -log\left(I/I_0\right) = -logT = \varepsilon cl \textbf{ (III. 5)}$$

Where: $$A = -logT \quad \textbf{(III. 6)}$$

So: $$A = log\left(1/T\right) \quad \textbf{(III. 7)}$$

- Determining optical band gap (optical energy bands) (Eg) :

The theory of optical energy bands **(Figure VI. 9)** estimated (Eg) can be determined by extrapolation from the absorption edge which is given using the Tauc relation [334]:

$$(\alpha hv) = A(hv - Eg^{opt})^n \quad \textbf{(III. 8)}$$

Where α is the absorption coefficient, A is constant, hv is the energy of light and n is a constant depending on the nature of the electronic transition, Eg^{opt} is the optical band gap energy, and the exponent n=1/2 for the direct allowed transition, while n=2 for the indirect allowed transition.

We obtained the energy gap from the intersection of the edge of the absorption linear part with the energy axis.

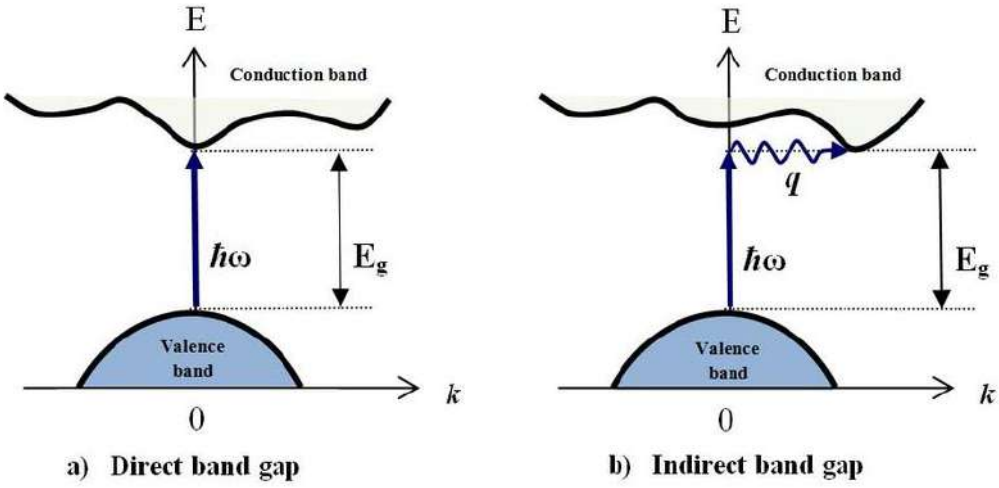

Figure III. 9:*Transition electronics in the case of a semiconductor (a) to an indirect gap and (b) to a direct gap.*

3.2.2. Fourier Transform Infrared Spectroscopy (FTIR)

Infrared spectroscopy allows the rapid and simple analysis of both organic and inorganic compounds. It is a technique that can obtain information about the different functional groups from the peak positions in the spectrum and information about the identification and stabilization of nanoparticles can also be inferred from this analysis. absorption of infrared radiation by the analyzed material, it allows, via the detection of the characteristic vibrations of the chemical bonds, the analysis of the chemical functions present in the material. During the analyses, we generally place ourselves in the mid-infrared between 4000 and 400 cm^{-1}[335]. It is done by depositing a layer of the product to be analyzed in contact with a crystal with a high refractive index and is based on the existence of an evanescent wave that propagates in a region very close to the surface of the crystal. Our samples being a powder, the required contact between the ATR crystal and the sample is obtained so that it is necessary to add additional pressure [335].

- **Principle:**

The principle of FTIR is based on the absorption of single or double-beam infrared radiation by the sample to be analyzed. It allows via the detection of the

characteristic vibration frequencies of the chemical bonds, to carry out the analysis of the chemical functions present in the material.

The infrared beam is directed towards the Michelson interferometer which will modulate each wavelength of the beam at a different frequency. In the latter, the incident light beam is split into two by a splitter. These two parts will be reflected on mirrors, one of which is fixed and the other mobile. When the two beams recombine, destructive or constructive interferences appear depending on the position of the mobile mirror. The modulated beam is then reflected from the two mirrors towards the sample, where absorptions occur. The beam then arrives at the detector to be transformed into an electrical signal [336].

4. Study of removal of BM dye by adsorption on Cs and CNC/ZnO NPs

The researchers shifted towards natural biopolymers and waste materials as economical alternative adsorbents[337]. Various types of adsorbents such as chitosan, cellulose, cotton, fly ash, clay, biomass, and sludge were applied in the adsorption process for removals of dyes [338-344].

In this work, functionalized cellulose (Cs) and cellulose/zinc oxide nanocomposite (CNC/ZnO NPs) derived from peanut and pea shells, an abundant, inexpensive and unexploited plant material, has been used as adsorbents for removing MB dye from aqueous solution by adsorption technique.

We studied the effects of various parameters influencing the adsorption capacity, that affect the adsorption process in wastewater treatment such as adsorbent dose, initial dye concentration, contact time, initial pH dye solution, and temperature under the aspects of thermodynamic study, adsorption isotherms, and adsorption kinetics. When an adsorption process reaches equilibrium, it means the active sites of the adsorbent are saturated with adsorbate molecules and no further adsorption can take place.

After a specific time, the samples were withdrawn and centrifuged, and the concentration of dyes in liquid phase was determined with UV visible spectrophotometer at 663 nm. To calculate the amount of adsorption capacity at equilibrium (Qe mg/g) was calculated using **Equation (II.5)** and the adsorption

efficiency removal of dyes (R%) was evaluated using **Equation (II.6)**, and adsorption isotherms were determined.

5. Evaluation the antimicrobial activities of CNCs and CNC /ZnO NPs

Globally, bacteria, yeast, and molds are the common types of microorganisms pathogenic and responsible for the spoilage of a considerable number of food products [345]. Foodborne disease is another pervasive food safety problem caused by the consumption of contaminated food products, which has been a significant safety concern to public health [346, 347].

Microorganisms are available naturally in the surrounding environment [348]. These microorganisms can survive under adverse conditions used in food preservation such as low temperature, modified atmosphere packaging, and vacuum packaging, as well as resist conventional pasteurization [349-352]. Therefore, new eco-friendly methodologies are required to reduce the growth of pathogenic bacteria and prolong the shelf-life of food products, without using chemical preservatives.

This work aims to evaluate the antimicrobial activities of the nanocomposite synthesis CNC/ZnO NPs by two methods from peanut shells and pea shells, on some pathogenic bacteria and fungi. Agar well diffusion method has been used to determine the antimicrobial activities against Gram-positive bacteria (*Staphylococcus aureus*), Gram-negative bacteria (*Escherichia coli* and *Klebsiella pneumonia*), and one fungus (*Candida albicans*).

5.1. Biological material

For investigated the antibacterial activity of the nanocomposites CNC/ZnO NPs, We used one reference yeast strain *Candida albicans* ATCC 10231 and three strains of bacteria including one Gram-positive namely *Staphylococcus aureus* ATCC 25923, and two Gram-negative strains, namely *Escherichia coli* ATCC 25922 and *Klebsiella pneumonia*ATCC 70603. The bacterial strains obtained from El-Medjed Laboratory, El-Oued, Algeria. The antibiotic *Lévofloxacine* was used as a positive control were used for evaluating antimicrobial activity, were chosen based on their clinical and pharmacological importance[353].

5.2. Preparation of bacterial culture suspension (inocula)

Before carrying out the antibacterial tests, two consecutive subcultures are carried out for each strain first, for bacteria the strains are revived in a nutrient broth (BN), and incubated at 37°C for 24 hours, second subculture is carried out on solid medium (nutrient agar) is inoculated in streaks on a box containing the nutrient agar medium (GN). The bacterial strains are inoculated into the Mueller-Hinton sterile (M.H) agar plates and incubated at 37°C for 24 hours. The bacterial strains were stored at 4°C in the nutrient agar slant to have bacterial cells in their exponential phase of growth. (fasting culture).

Whereas the Candida albicans strain is revived in a nutrient broth and incubated at 30° C. for 24 hours then cultured on a petrie dish containing Sabouraud dextrose agar. It is then incubated at 30°C for 72 hours and stored at 4°C.

According to the [354], from a few well-isolated and perfectly identical colonies were taken from the bacterial and fungique cultures, then they put and dispersed in volum of 10 ml saline solution (NaCl 0.9%) from physiological water and well homogenized to have the dilution 10^{-1}.

5.3. Preparation of synthetic compounds for microbiological assay

A stock solution of 20mg of each synthesized compounds from peanut shells and pea shells (CNCs and CNC/ZnO NPs) dissolved in 1 mL of dimethyl sulfoxide (DMSO) as solvent was prepared (knowing that the samples are insoluble substances, so the solubility in the solvent was very low).The study of the antibacterial and antifungal activities against the reference strains is carried out by different and complementary techniques. In this work we have used the well diffusion method (WD) on agar.

Agar welldiffusion method

Agar well diffusion method is widely used to evaluate the antimicrobial activity of plants or microbial extracts [355, 356]. This experiment was carried out according to the method described by [357-360] with a slight modification.

a) Seeding

The seeding is carried out according to the technique of [354], Similarly to the procedure used in disk-diffusion method well diffusion method (WD) is a diffusion method similar to disc diffusion.

Mueller-Hinton agar (MHA) was heated to 55°C, then, aseptically poured the super cooled M.H agar culture medium into Petri dishes at a rate of 15 to 20 ml per dish (4mm thick) the dishes are dried at room temperature on the bench (**Figure III. 10**). A volume of the bacterial inoculum was uniformly spread using sterile cotton swab on over the entire a sterile Petri dish MH agar (**Figure III. 11**). Then, a hole with a diameter of 6 mm (20 mm apart from one another) is punched aseptically with a sterile cork borer or a tip. Then, the dispersed a volume 50 µL solution of samples of CNCs and CNC/ZnO NPs (from peanut and pea shells) were poured at 20mg/L concentration is introduced into the well. Then, agar plates are incubated under suitable conditions depending upon the test microorganism. Also were used DMSO as negative control in order to check the growth of the different strains; and in parallel, the antibiotic *Lévofloxacine* was used as a positive control. Finally, the plates were incubated at 37°C for 24 hours under aerobic conditions. The experiment is repeated three times for each HE and for each bacterial species.

b) Reading

To highlight the presence or absence of the effect of antibiotics on the strains tested and the sensitivities of the microorganism species to the samples. The antimicrobial agent diffuses in the agar medium and inhibits the growth of the microbial strain tested **(Figure III. 12**), the reading is done by measuring the diameter of the zone of inhibition around the well (including the diameter of well) using a caliper or a ruler in (mm) after 24 hours of in incubation at 37°C [361].

The results are expressed by the diameter of the zone of inhibition or in the form of mean ± mean standard deviation and values <6 mm were considered as not active against microorganisms

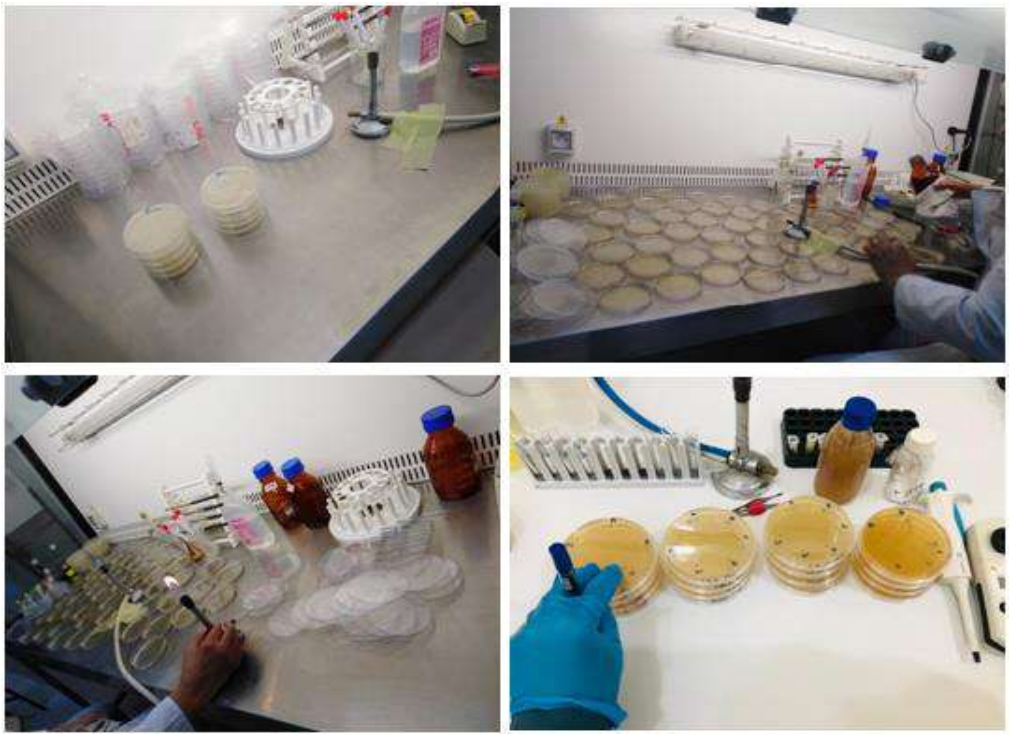

Figure III. 10:*The preparation of Mueller-Hinton agar of the agar well diffusion method.*

Figure III. 11:*Diffusion and expansion the bacterial inoculumon over Mueller-Hinton agar the entire into Petri dishes.*

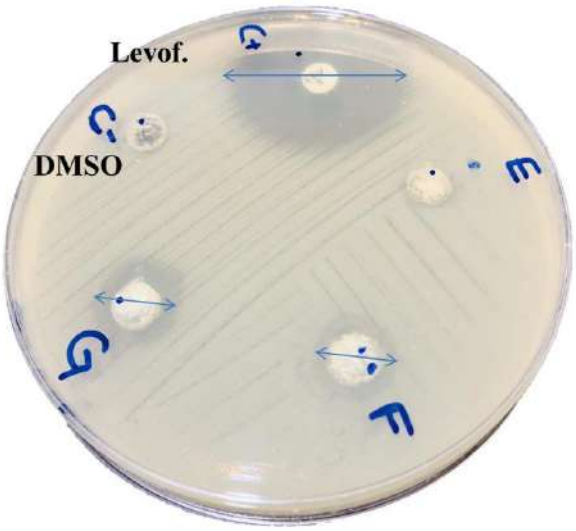

Figure III. 12:*Measurement of the diameter of the inhibition zone for the well diffusion method.*

CHAPTER FOUR:

RESULTS AND DISCUSION

1. Characterization of CNC/ZnO NPs:

The chemical compositions of the bleached pulps were determined using the known standard methods (Browning, 1967) for calculeted the cellulose extraction percentage in all the steps and were as follows in **Table IV.1.**

Table IV. 1: *The cellulose extraction percentage from peanut and pea shells after all the different steps.*

(%)	Hot Water	HCl	NaOH	$NaClO_2$	Cellulose (Cs)
Peanut shells	**2.21**	**14.50**	**30.87**	**20.61**	**31.81**
Pea shells	**4.94**	**8.86**	**40.5**	**16.89**	**28.81**

1.1. X-ray diffraction (XRD)

Figure IV. 1 and Figure IV. 2 show the X-ray diffraction pattern of the cellulose (Cs), cellulose nanocrystal (CNCs), and cellulose/zinc oxide nanoparticles (CNC/ZnO NPs) samples, prepared from peanut shells and pea shells along with that of the crude samples.

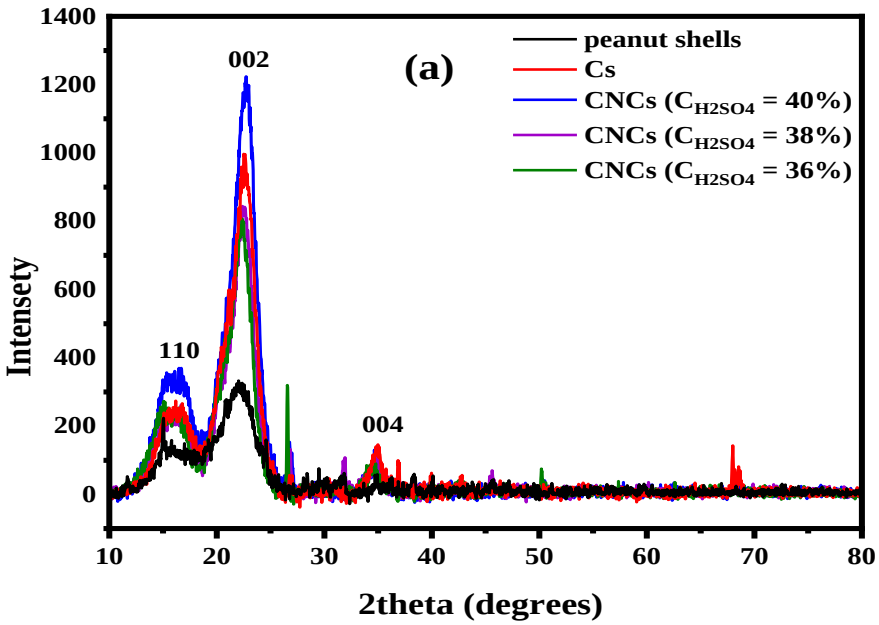

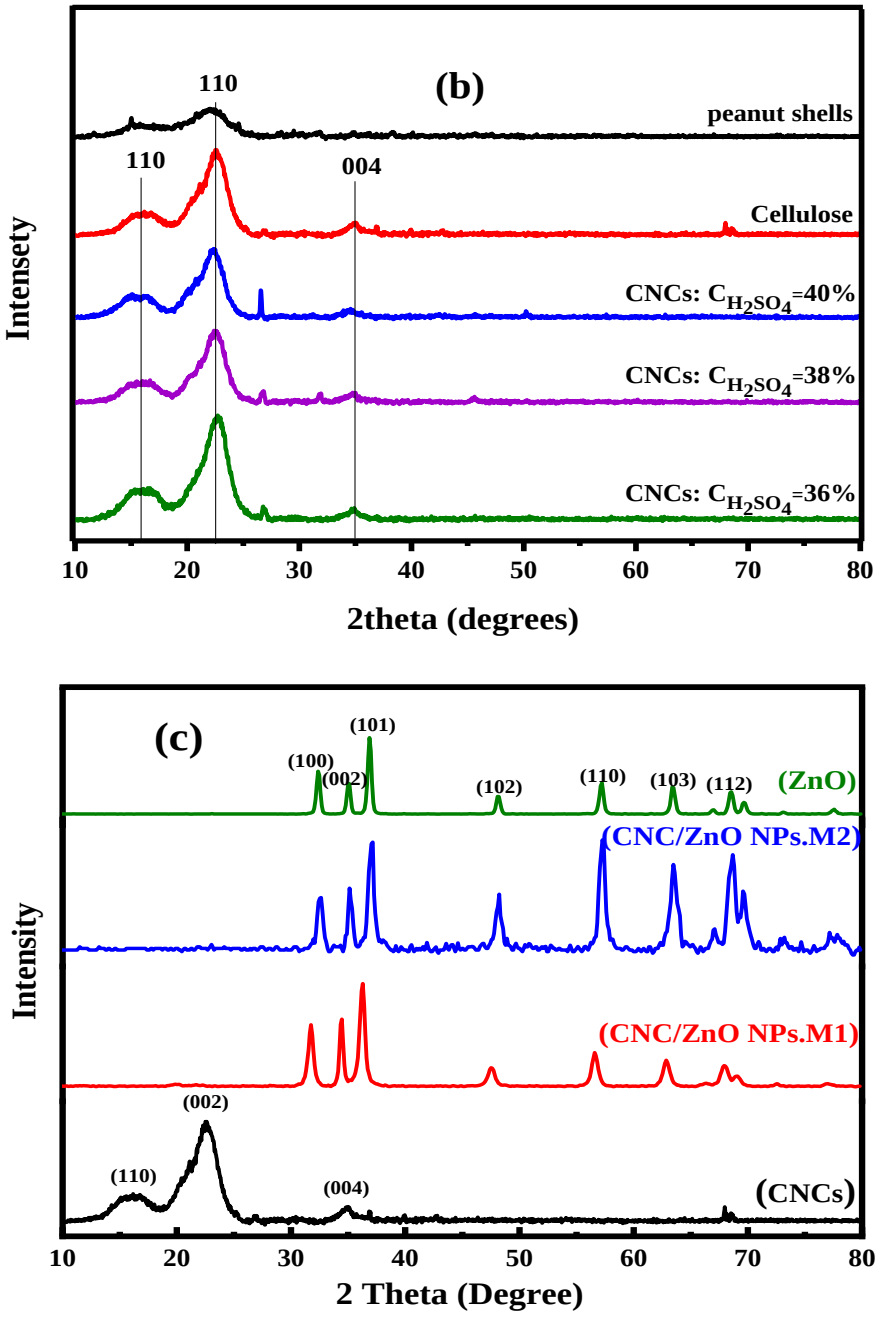

Figure IV. 1: *X ray diffraction patterns of all the samples extracted from peanut shells (a-b) for CNCs and (c) for CNC/ZnO NPs.*

As shown in **Figure IV. 1(a-b),** the monoclinic structure of all samples of the Cs and CNCs extracted from peanut shells have a typical crystal lattice for cellulose (Nelson & O'Connor, 1964), are determined through the diffraction peaks corresponding to the surface lattice planes (101), (002), and (040) are observed at 2θ values = (15.89°, 22.53°, 34.95°) of the Cs and CNCs [362-365].

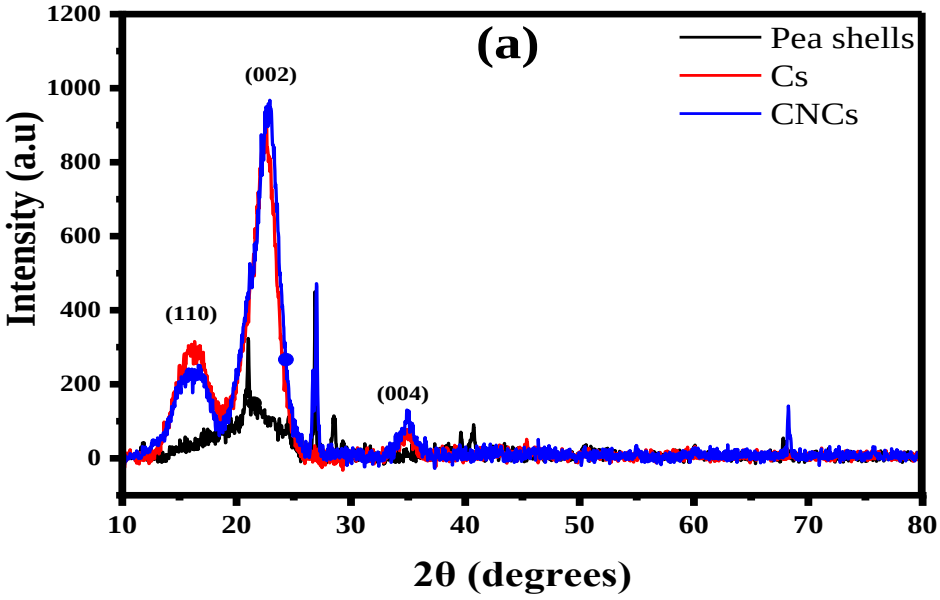
(a)
Pea shells
Cs
CNCs
(002)
(110)
(004)
Intensity (a.u)
2θ (degrees)

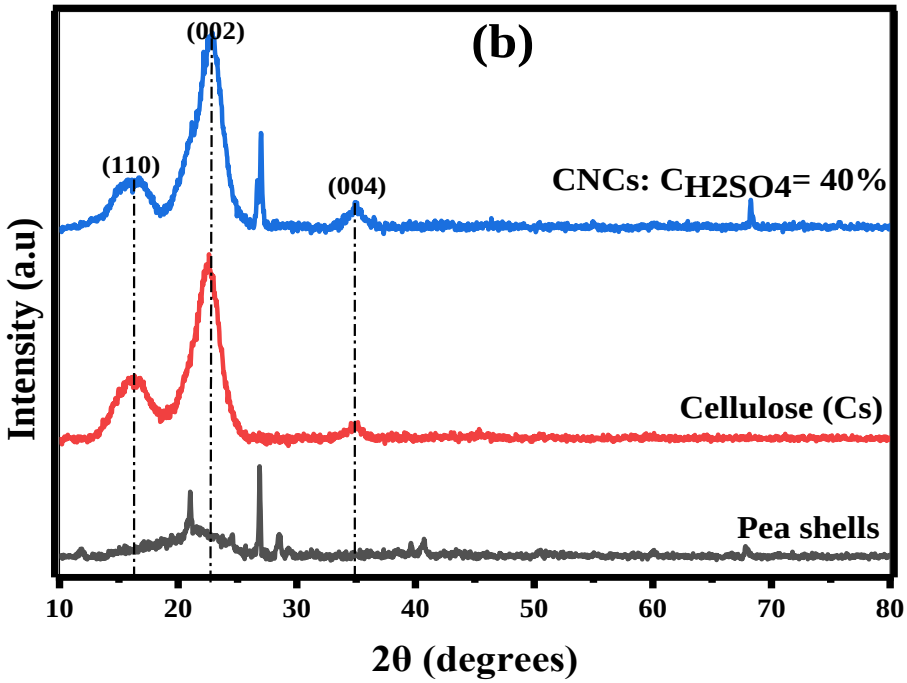
(b)
(002)
(110)
(004)
CNCs: C$_{H2SO4}$= 40%
Cellulose (Cs)
Pea shells
Intensity (a.u)
2θ (degrees)

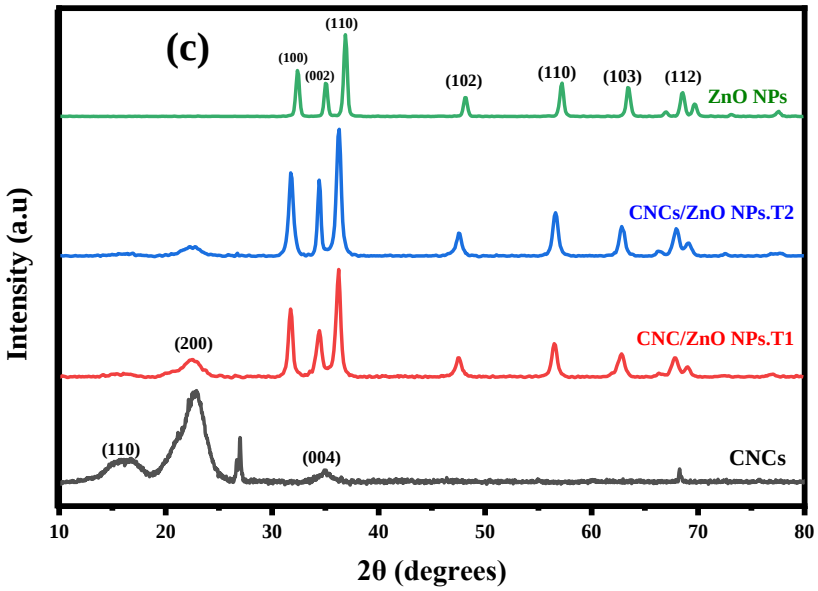

Figure IV. 2: X ray diffraction patterns of all the samples extracted from pea shells (a-b) for CNCs and (c) for CNC/ZnO NPs.

Figure IV. 2(a-b) shows The results shown the XRD data of the crude sample Cs and CNCs extracted from pea shells, where we notice the emergence of crystalline peaks at 2θ = (16.87°, 22.85, 35.04°) and 2θ = (17.05°, 22.85°, 34.93°) of the Cs and CNCs, respectively. They express the crystalline levels of each (110), (200), and (004) of the series and are the characteristics of the typical cellulose structure of cello-cello[366, 367]. The initial network-level peak (110) indicates the presence of amorphous components of Cs and CNCs [57-60]. We can be seen that the main sharp crystalline peaks for CNCs formed at about 2θ = 22° of the (002) lattice plane [368-371]. The peak appears at 2θ = 34° of the (004) lattice plane, which is due to the amorphous part of cellulose and CNCs [76, 362, 365, 372].

This result combined with standard XRD data (COD ID 4114994) [221] shows that cellulose exists in the allotropic form of cellulose I [373]. Cellulose has a structure consisting of two regions arranged alternately, the crystalline region has a structure orderly, rigid, and loosely structured amorphous regions.

The hydrolysis process to create CNCs with HCl and H_2SO_4 does not change the crystal structure of cellulose, but only helps to cut off the amorphous regions and retain the crystalline regions. The highest density of CNCs was in the samples treated with 40% for H_2SO_4 solution concentration, where we find that the increase in the intensity value of all other peaks is small between the radiations of the Cs and CNCs

in both samples. This observation indicated that the first cellulose structure after alkaline treatment and bleaching using chlorine water and the acid hydrolysis treatment, in particular, gave it a nanocrystalline structure since the first stage of cellulose extraction as the second acid hydrolysis treatment to obtain CNCs did not change the position and intensity of these peaks [374].

Figure IV. 1(c) and **Figure IV. 2(c)** show the XRD pattern of CNC/ZnO NPs samples synthesized from CNCs with ZnO NPs from peanut shells and pea shells which were synthesized by two different methods. The diffraction peaks are 2θ = (31.8°, 34.47°, 36.29°, 47.59°, 56.64°, 62.92°, 66.45°, 68.02°, and 69.16°) and 2θ = (31.74°, 34.43°, 36.24°, 47.53°, 56.51°, 62.84°, 66.32°, 67.84°, and 69.04°) corresponding to (100), (002), (101), (102), (110), (103), (200), (112), (201) crystal planes from (CNC/ZnO NPs.M1; CNC/ZnO NPs.M2) synthesized from CNCs of peanut shells and (CNC/ZnO NPs.P1; CNC/ZnO NPs.P2) synthesized from CNCs of pea shells, respectively. All diffraction positions and relative intensity peaks are correctly set using JCPDS file card 0361451 and are a good fit to the hexagonal ZnO wurtzite structure in previously reported work [369].

This result is similar to previously published results [375, 376] and is consistent with the wurtzite hexagonal lattice of ZnO, indicating that ZnO NPs have been successfully synthesized on CNCs. In addition, the high-intensity diffraction peaks show that the synthesized ZnO has a good crystalline structure and also indicate that the presence of ZnO NPs crystals does not change the crystal structure of CNCs.

Table IV. 2: *Crystallization Index (CrI) and Crystal Size (CrS) of all sample from peanut shells and pea shells:*

Samples		Cs	CNCs (36%)	CNCs (38%)	CNCs (40%)	CNC/ZnO NPs (M1-T1)	CNC/ZnO NPs (M2-T2)
Peanut shells	CrI (%)	72.52	69.714	68.757	77.957	/	/
	CrS (nm)	9.21	11.82	11.90	8.88	20.14	27.31
Pea shells	CrI (%)	69.82	/	/	73.381	78.38	72.27
	CrS (nm)	12.29	/	/	12.28	19.64	19.99

Also, from XRD diffractograms we determined the crystallinity index (CrI) and crystal average size (CrS). The calculated CrI and CrS of the different samples from peanut shells and pea shells.

All CNCs samples had similar CrI values with slightly lower values for Cs. Generally, the second acid treatment (H_2SO_4 solution) with different concentrations of CH2SO4 = 36%, 38%, and 40% from the peanut shells samples, this treatment had an effect on the CrI of the prepared CNCs. According to **Table IV. 2**, the CrI ratio values for the (Cs and CNCs) are (72.52 %, 77.95%) and (69.82 %, and 73.38%) of the peanut shells and pea shells, respectively.

the acid treatment does not change the crystal structure of cellulose but only helps to cut off the amorphous regions and retain the crystalline regions. Therefore, the crystal content CrI [377], calculated by the Segal formula according to **Equation (III. 3)** of the CNCs samples is higher than that of Cs and the higher value of CrI for the CNCs after acid treatment with concentration C_{H2SO4} = 40% from the peanut shells samples regardless of the kind of source used pea shells or peanut shells.

The reason for this is due to the reduction of cellulose chains after the removal of amorphous components such as hemicellulose, pectin, lignin, and impurities in the fibers, and the reduction of hydrophobicity after treatment [368, 378]. Therefore, the concentration of H_2SO_4 solution is 40% was approved for the preparation of CNC/ZnO NPs.

In this study, the mean crystal sizes (CrS) of Cs, CNCs, and CNC/ZnO NPs structures synthesized by two different methods were calculated from the XRD data using the Debye-Scherrer formula according to **Equation (III. 2)**

The CrS of Cs, CNCs, CNC/ZnO NPs.M1, and CNC/ZnO NPs.M2 varied from peanut shells were 9.21 nm, 8.88 nm, 20.14 nm, and 27.31 nm, respectively. The CrS of Cs, CNCs, CNC/ZnO NPs.T1, and CNC/ZnO NPs.T2 from pea shells was 12.29 nm, 12.28 nm, 19.64 nm, and 19.99 nm, respectively.

The samples of Cs and CNCs from peanut shells had the smallest CrS followed by the pea shells, but in the nanocomposite of CNC/ZnO NPs, the samples from pea shells had the smallest CrS followed by the peanut shells in the different synthesis methods used in this study.

This observation indicated that the first cellulose structure after alkaline treatment and bleaching using chlorine water and the acid hydrolysis treatment, in particular, gave it a nanocrystalline structure since the first stage of cellulose

extraction as the second acid hydrolysis treatment to obtain CNCs did not change the position and intensity of these peaks **Figure IV. 1(c)** and **Figure IV. 2(c).**Here mild acid-alkali conditions were used for the fractioning process of biomass (peanut shells and pea shells). The alkaline treatment in cellulose extraction leads to the formation of crystals, which in turn leads to the disorder of fibrous crystals, which are considered amorphous because they are not part of the crystals. Swelling of the structure due to penetration of the cellulose fibers by NaOH, resulting in an increase in crystal size [370]. While the acid treatment of HCl during the extraction of cellulose and by H_2SO_4 during the preparation of CNCs reduces the size of the crystals, this approach ensures the minimum degradation of valuable substances contained in biomass such as pectic and hemicellulosic polysaccharides. Also, a low-temperature process was chosen contrary to high-temperature hydrothermal processes in the preparation of CNCs by the second acid treatment with H_2SO_4 solution. The polysaccharides are weakly bonded among each other and are packed in less structured tissue compared with peanut shells biomass. Hence, the low temperature is sufficient enough to improve and miniaturization of cellulose crystal size which makes beneficial changes as it increases the specific surface area and water absorption capacity of bio-fibers, depending on their crystal size, as increasing crystal size can enhance the resistance to moisture absorption and chemical reactions of the fibers [374].

The different properties of each method used to synthesize the CNC/ZnO NPs, lead to a different degree of stabilization of $Zn(OH)_2$ NPs against agglomeration of CNCs. This leads to the formation of ZnO NPs on the CNCs with the observed variation in its density (confirmed by DREX), Crystallite Size, and final shape of CNCs/ZnO NPs formed. These characteristic peaks of pure ZnO observed in the XRD patterns confirm the formation and growth of ZnO NPs in CNC. Furthermore, XRD analysis also revealed that all recorded peak intensity distributions confirm the hexagonal writing structure of ZnO [370, 371]. Although the positions of the different ZnO peaks were similar for the two different methods, the width of the peaks decreased and the intensity of the peaks gradually increased by increasing ZnO content, indicating an increase in crystal size and crystallinity [76].

It can be seen that the reflection peaks are broadened in the samples synthesized by the first method, indicating that the particle size in the first method is reduced and has more ZnO NPs**.** Can be observed in all the corresponding CNCs peaks with low intensities, especially in the first method, which may be due to forms

the thick layer from ZnO NPs as a coating for CNCs (confirmed by SEM images), which results from difficulty determining the value of the CrI.

1.2. Fourier Transform Infrared Spectroscopy (FTIR)

The samples extracted from the peanut shells and pea shells were diagnosed through many main steps, namely the raw samples for peanut and pea shells, cellulose (Cs), cellulose nanocrystals (CNCs), and the nanocomposites CNC/ZnO NPs it were synthesised by two different methods.

The first and most important observation in infrared analysis is that all samples share almost the same chemical bonds. By (shape), arrangement and comparison in reading, we notice the appearance of certain peaks or an improvement in their sharpness with a decrease in the intensity of the peaks which express the non-cellulosic materials which appeared in the spectrum of the raw material and disappearance from the other asThese FTIR spectra matched well with each other while functional groups analysis and bonding type conformations directly suggest the similar chemical structure.

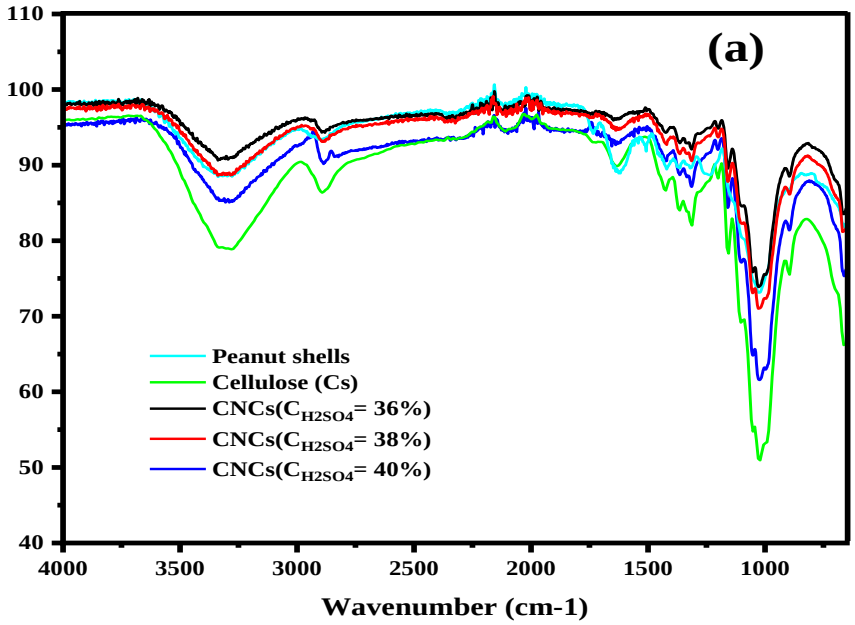

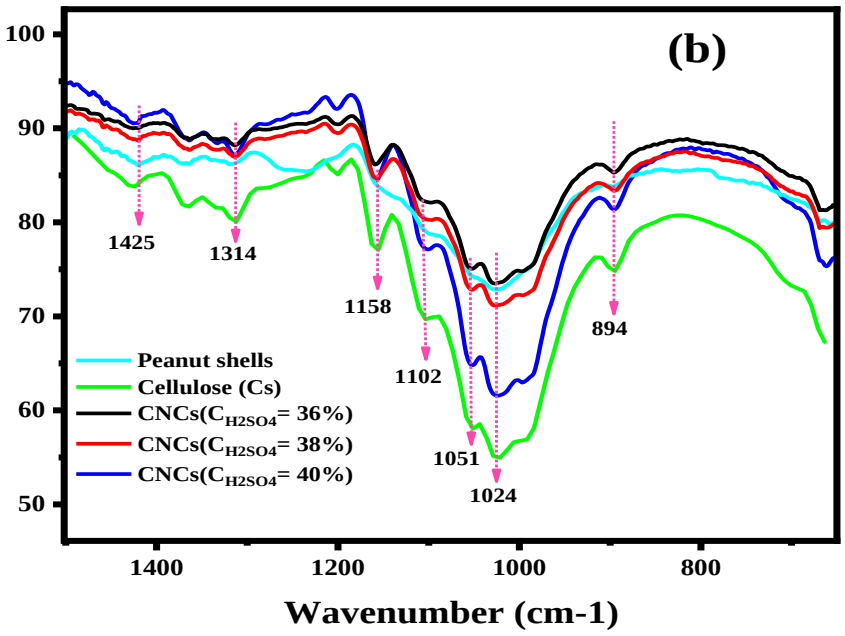
(b)
100
90
80
70
60
50
1425
1314
1158
1102
1051
1024
894
Peanut shells
Cellulose (Cs)
CNCs(C$_{H2SO4}$= 36%)
CNCs(C$_{H2SO4}$= 38%)
CNCs(C$_{H2SO4}$= 40%)
1400
1200
1000
800
Wavenumber (cm-1)

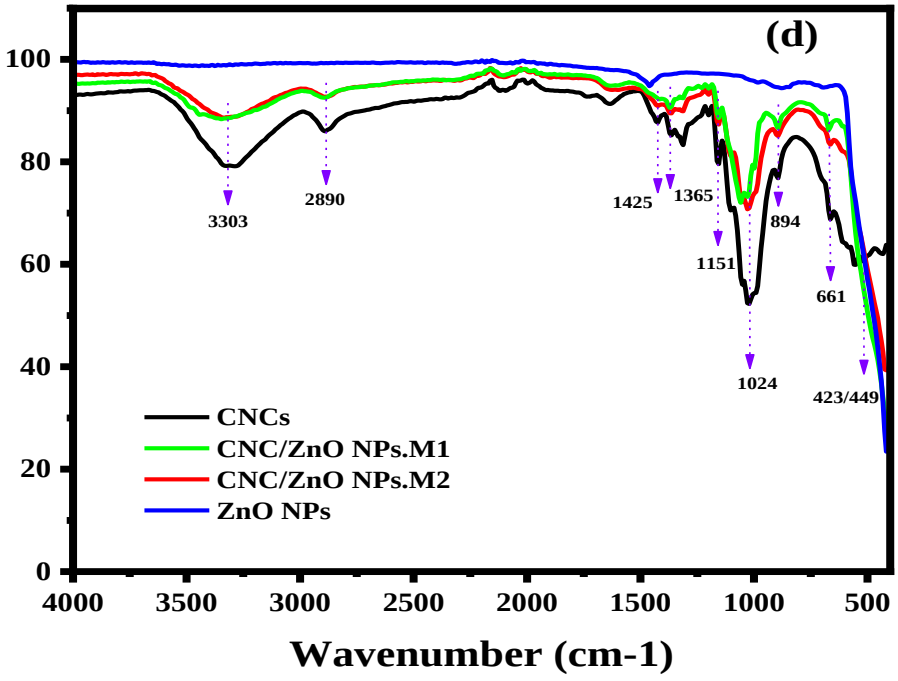
(d)
100
80
60
40
20
0
3303
2890
1425
1365
1151
1024
894
661
423/449
CNCs
CNC/ZnO NPs.M1
CNC/ZnO NPs.M2
ZnO NPs
4000
3500
3000
2500
2000
1500
1000
500
Wavenumber (cm-1)

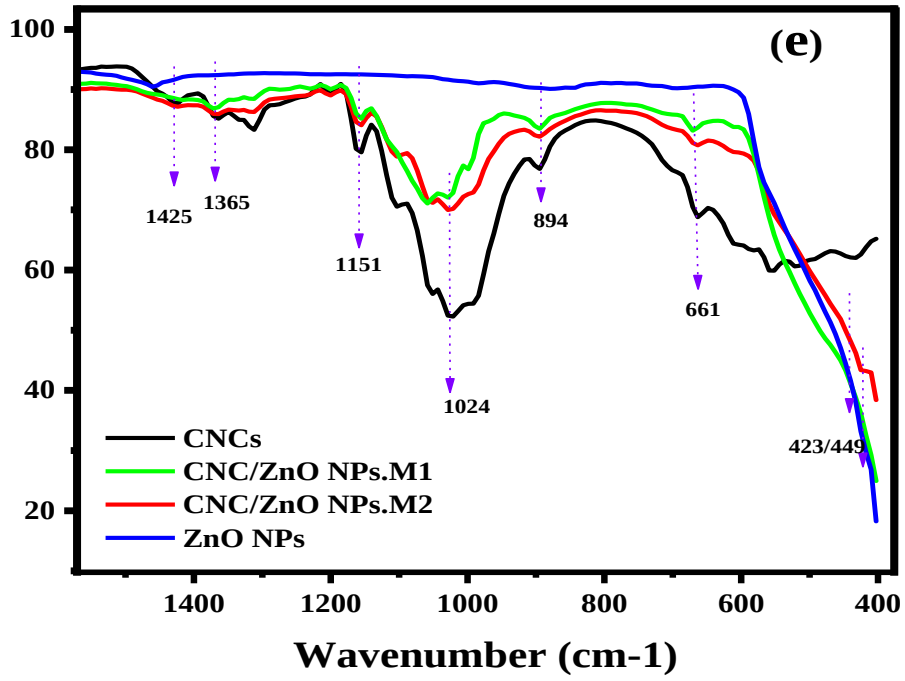

Figure IV. 3: FT-IR spectra of fabricated CNCs(a,b, and c) and CNC//ZnO NPs (d-e) from peanut shells.

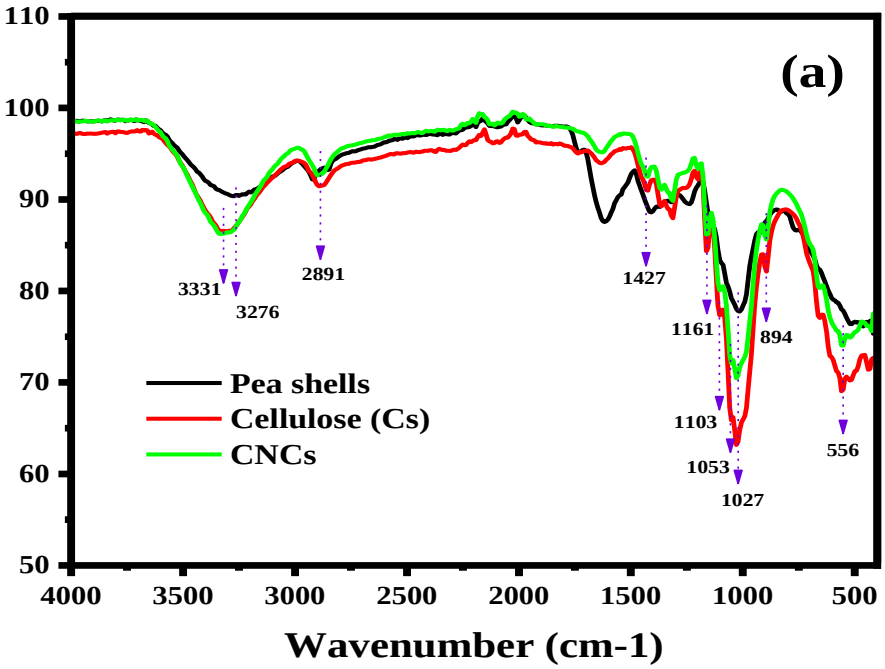

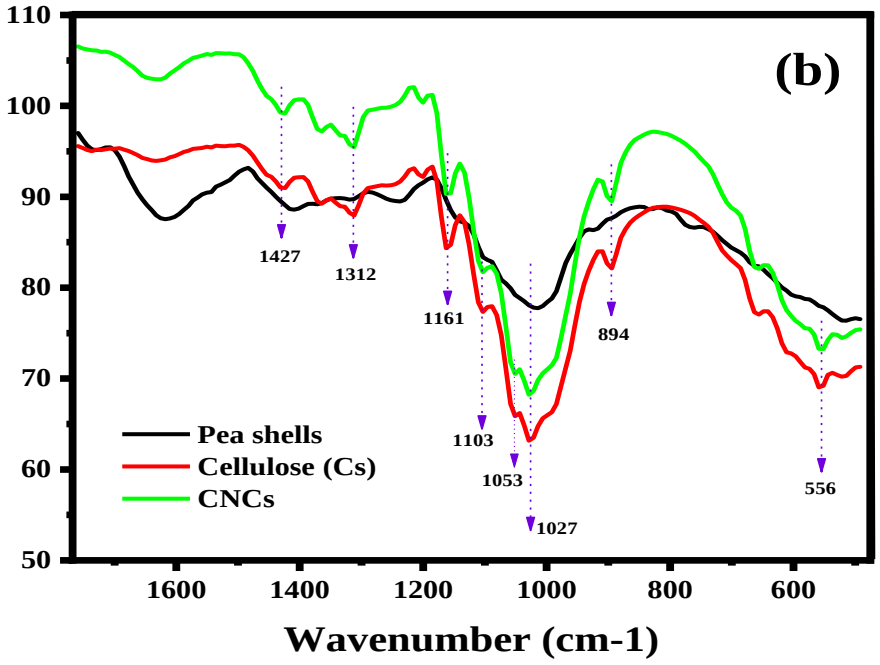
(b)
Pea shells
Cellulose (Cs)
CNCs
1427
1312
1161
1103
1053
1027
894
556
Wavenumber (cm-1)

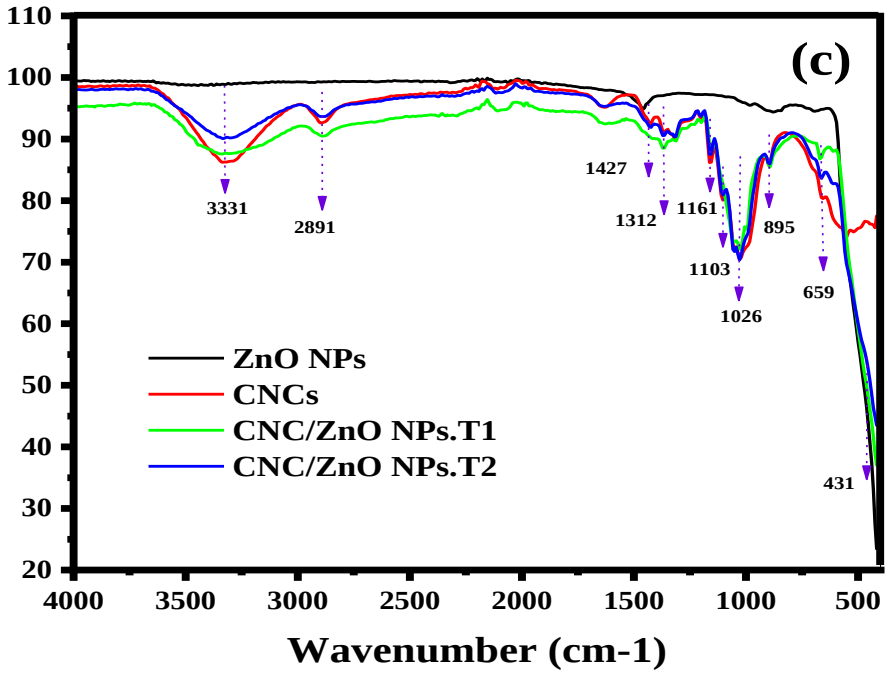
(c)
ZnO NPs
CNCs
CNC/ZnO NPs.T1
CNC/ZnO NPs.T2
3331
2891
1427
1312
1161
1103
1026
895
659
431
Wavenumber (cm-1)

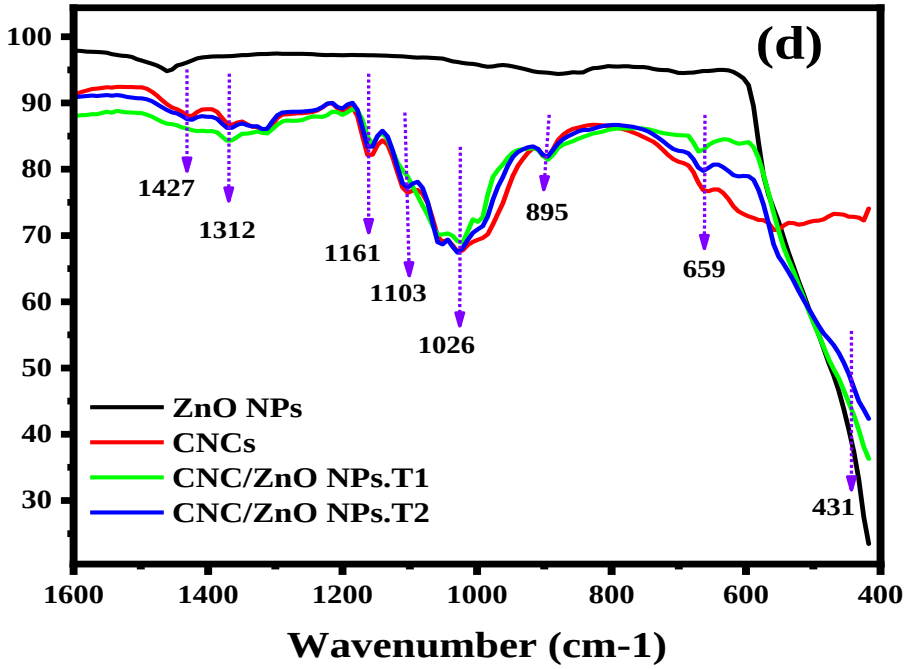

Figure IV. 4: *FT-IR spectra of fabricated CNCs (a-b) and CNC//ZnO NPs (d-e) from pea shells.*

most of the bands appeared characteristic of Cs in all the spectra of CNCs and CNC/ZnO NPs clearly with little change in their intensities and frequencies, including the strong bands between 3331cm^{-1} and 3283 cm^{-1} in Cs and in all the nanomaterial spectra CNCs and CNC/ZnO NPs, it is caused by the stretching vibrations of the –OH groups (from absorbed H_2O, secondary –OH groups, and intermolecular and intermolecular H bonds) [379].

As displayed in **Figure IV. 3** and **Figure IV. 4,**The bands at 2891–2890 cm^{-1}are linked to the aliphatic moieties and assigned to –CH and νas CH_2. Furthermore, also observed the acetyl group's C–H bending at approximately 1370 cm^{-1} [379, 380].

The absorption peak at 1731cm^{-1} we find in the crude sample only and disappears in Cs and CNCs originates from the acetyl and ester groups in hemicellulose, or carboxylic acid groups in the ferulic and p-coumaric components of lignin. The existence of this peak shoulder was also reported in other works with wheat straw, rice husks and soy hulls [154, 381, 382]. where the absence of this peak indicates Successive chemical treatments remove most of the lignin and hemicellulose from the nanofiberswith the purification process.

The C–O–C from the glucosidic units and β (1→4) glucosidic linkage of cellulose displayed their characteristic bands at 1161–1158 cm^{-1} and 1053–1051 cm^{-1}, respectively. remains unaltered, revealing that it does not participate in the reaction and that only the –OH groups are acetylated [383]. This means that the raw material has undergone a chemical treatment which modifies its chemical functions by the appearance of peaks expressing the increase in the proportion of cellulosic components after removal of non-cellulosic materials [384].

The crystalline cellulose phase is associated with the peak at approximately 1420—1430 cm^{-1}, while the amorphous component of cellulose is assigned to the band at 897 cm^{-1} [383].

For CNCs, the appearance of the characteristic band at a wave number of 1202/1200 cm^{-1} and 659 cm^{-1}, indicating the existence of S=O stretching from sulfate groups in the sulfate CNCs through the esterification of hydroxyl groups during the sulfuric acid hydrolysis of Cs [385, 386].

The FT-IR spectrum of the CNCs has absorption tips similar to cellulose (**Figure IV. 3(a-b)** and **Figure IV. 4(a-b)**) but with lower intensity. The reason is the cellulose structure of CNCs samples was preserved after the acid hydrolysis of Cs and the functional groups are located in a rigid crystalline structure, which reduces the ability of the bond to vibrate when absorbed by IR radiation.mples until it completely decays into the spectra of Cs and CNCs.

For the CNC/ZnO NPs of all samples (**Figure IV. 3(d-e)** and **Figure IV. 4(c-d)**) the existence of cellulose was determined through exhibit typical characteristic peaks of cellulose, including the bands around 3331/3303 cm^{-1} and 1367/1365 cm^{-1}, which characterize the stretching and bending vibrations of the hydroxyl groups O–H [387, 388].

2891/2890 cm^{-1}, 1427/1425 cm^{-1}, 1061/1058 cm^{-1} and 1633/1629cm^{-1}, attributed to the C–H stretching, H-C-H bending, C–O stretching vibrations and OH group oscillations of adsorbed water molecules on the sample , respectively [362, 389-391].

In the nanoparticules CNC/ZnO NPs spectras, the characteristic peaks of O–H stretching vibrations were shifted towards higher wave number (i.e. from 3276 cm^{-1} in the shells to 3331 cm^{-1} in the Cs, CNCs, and CNC/ZnO NPs) this is due to the strong interaction between the oxygen atoms of the carboxyl groups on the CNC surface with ZnO gives strong evidence of the metal oxides-polymer bonding (Zinc

oxide-Cellulose) through the COO linkage indicating formation of hydrogen bonds between CNCs and ZnO [392].

This inference is also supported by the appearance of new bands in the CNC/ZnO NPs attributed to ν (M–O) at 431 and 423 cm^{-1} which were assigned to the stretching vibration of the Zn–O bonds. for CNC/ZnO NPs for pea shells and CNC/ZnO NPs for peanut shells, respectively [20, 320, 393, 394].

Thus, these results of the FTIR spectrum confirmed the successful preparation of CNC/ZnO NPs from the peanut and pea shells by two different methods, that created ZnO NPs mounted on CNCs support through electrostatic interaction of COOH groups on CNCs and ZnO surfaces.

Table IV. 3:*The Important IR Peaks of all the samples (shells, Cs, CNCs, and CNC/ZnO NPs).*

Assignment	Wavenumber (cm^{-1})		
	Cs and CNCs	CNC/ZnO NPs M1 and T1	CNC/ZnO NPs M2 and T2
-OH(covalentbond,hydrogenbonding)	3331/ 3303	3331/ 3303	3331/ 3303
-CH	2891	2891	2891
C=O stretchingof theacetyl group	–	1740	1740
H_2Oabsorbed(absorbedwaterhydrogen-bonded))	1633/ 1629	1633/1629	1633/1629
-CH_2((symmetric)atC-6;crystallineregion)	1430	1430	1425
C–HbendingvibrationofCH_3intheacetylgroup)	–	1369	1365
-CH2(waggingatC-6)Or-COHinaplaneatC-2andC-3	1320	1319	1322
-COHinaplaneatC-6	1253	–	–
C–Ostretchingoftheacetylgroup	–	1222	1215
-CO,-OH(C-O-Catβ-glycosidiclinkage)	1160	1168	1164
γ-ringinplane	1103	1122	1125
C-O(c-o-cofthecellulosebackbone)	1052	1037	1040
-COatC-6	1029	952	1010
-CH2(C-O-Catβ-glycosidiclinkage;amorphousregion)	898	899	902

1.3. UV–visible Spectroscopy (UV-Vis)

UV-Vis absorption spectroscopy plays a very important role in examining the optical properties of nanoparticles [68]. Significant absorbances were seen for the CNC/ZnO NPs solutions in the UV light range of 300 to 400 nm.

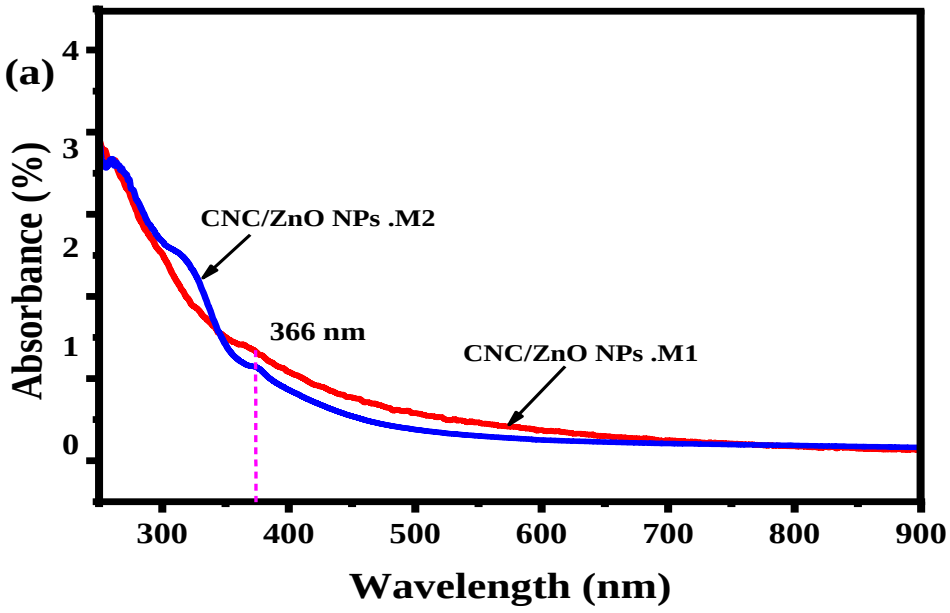
(a)
Absorbance (%)
0
1
2
3
4
CNC/ZnO NPs .M2
366 nm
CNC/ZnO NPs .M1
300
400
500
600
700
800
900
Wavelength (nm)

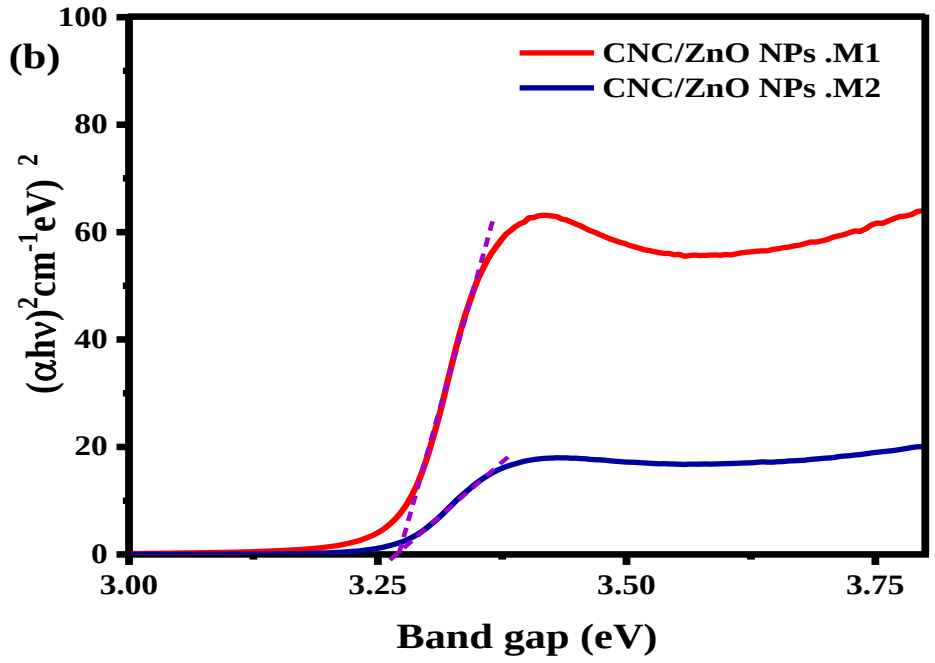
(b)
CNC/ZnO NPs .M1
CNC/ZnO NPs .M2
(αhν)²cm⁻¹eV)²
0
20
40
60
80
100
3.00
3.25
3.50
3.75
Band gap (eV)

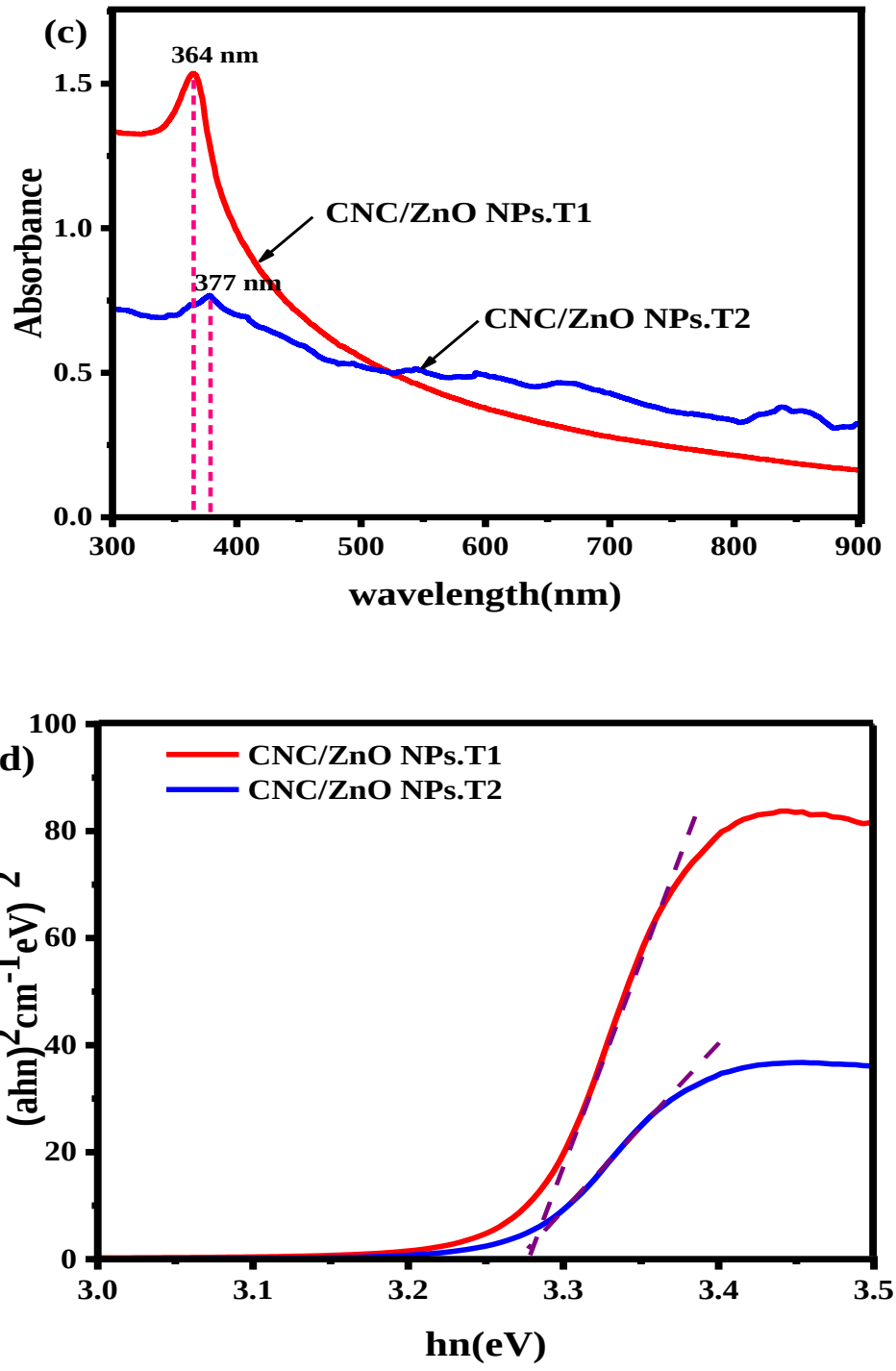

Figure IV. 5*:* **(a-c)***UV–Vis absorption spectrum,* **(b-d)** *Plots of* $(\alpha h\nu)^2$ *versus hv of CNC/ZnO NPs from two methods (M1, M2 from peanut shells) and (T1, T2 from pea shells.*

Figure IV. 5(a) shows the absorption peak at 366 nm for the CNC/ZnO NPs.M1 and CNC/ZnO NPs.M2 synthesized from peanut shells for the first and second methods, respectively. **Figure IV. 5(c)** shows two absorption peaks at 364 nm

and 377 for CNC/ZnO NPs.T1 and CNC/ZnO NPs.T2 synthesized of the first method and second method from pea shells, respectively, which may be an indicator of CNC/ZnO NPs formation.

This peak confirms the synthesis of pure ZnO NPs in the CNCs and the successful use of peanut shells and pea shells to obtain CNC/ZnO NPs by two methods, Furthermore, it has been reported that the peak position of the UV-Vis spectrum correlates with nanoparticle size and color changes with decreasing nanoparticle crystal size [395].

The bandgap energy is calculated based on the numerical derivative of the optical absorption coefficient using the Tauc relationship between the optical absorption coefficient (α), the photon energy (hv), the constant (A), and the direct bandgap energy (eg). **Figure IV. 5 (b-d)** was found to have a band gap energy value of 3.27 eV and 3.66 eV for the ZnO NPs synthesized from peanut shells and pea shells, respectively, which is in correlation with the previously reported value [396]. For example, differences in different ratios may be due to differences in methods used and average crystal size.

1.4. Scanning electron microscopy (SEM-EDS)

In order to observe the difference in microstructure of the samples before and after extraction, it was examined under a scanning electron microscope SEM.

Figure IV. 6 and **Figure IV. 7** shows SEM graphs of the different samples (Cs, CNCs, and CNC/ZnO NPs) extracted from peanut shells and pea shells. We can clearly see a big difference between the structure of the raw sample and the structure of Cs and CNCs extracted after going through all the stages of the treatment.

It is also noted in **Figure IV. 6 (b)** and **Figure IV. 7(g)** that the texture of the cellulose fibers is excellent, as it comes in the form of fibers without the presence of damaged or irregular areas after what was in the form of plaques in the raw sample.

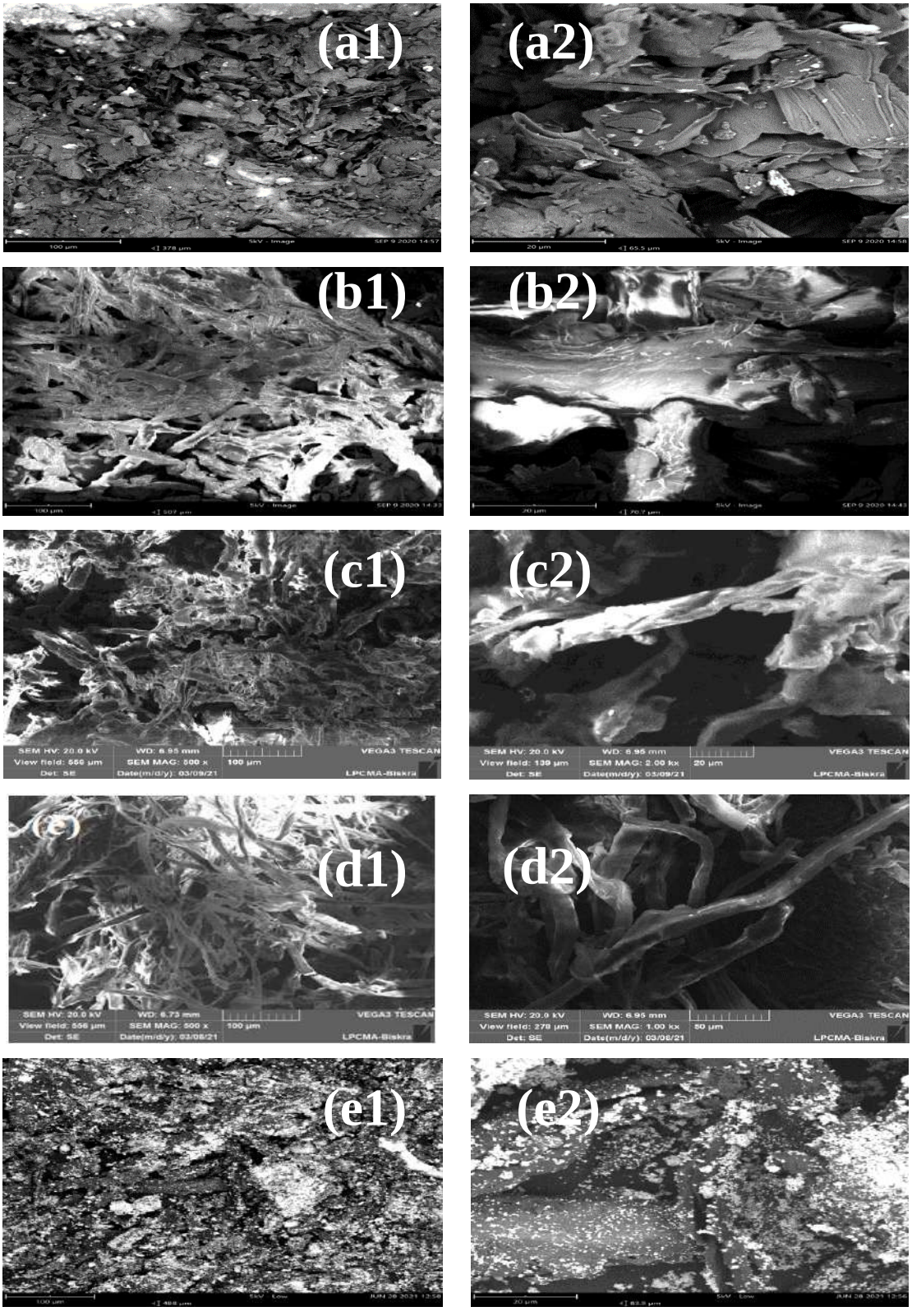

Figure IV. 6*: SEM image:* (a1-a2) *of shells,* (b1-b2) *of Cs,* (c1-c2) *of CNCs,* (d1-d2) *of CNC/ZnO NPs.M1, and* (e1-e2) *of CNC/ZnO NPs.M2 from peanut shells.*

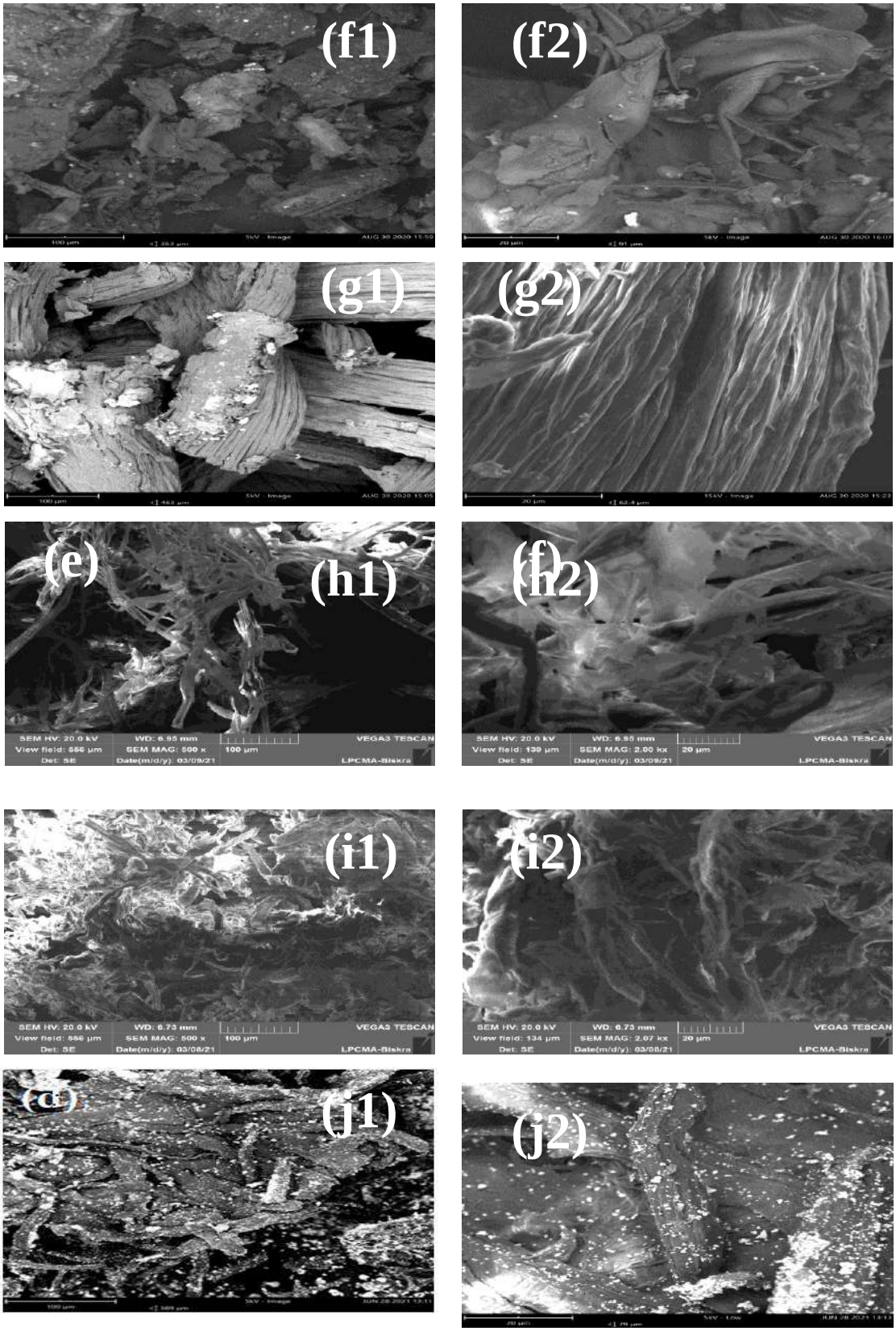

Figure IV. 7*: SEM image:* (a1-a2) *of shells,* (b1-b2) *of Cs,* (c1-c2) *of CNCs,* (d1-d2) *of CNC/ZnO NPs.T1, and* (e1-e2)*of CNC/ZnO NPs.T2 from pea shells.*

The surface of the cellulose fiber displays defibrillation of the fibrils into individual fibrils of different sizes, but they are close size. Their smooth and flexible characteristics also indicate that they are free from noncellulosic rigid components such as hemocellulose, lignin, and other inorganic contaminants.

No significant differences were observed between all samples of Cs and CNCs prepared using different kind of source found (peanut and pea shells). In the synthesis of CNCs, shortening of cellulose fibers by treatment with the acid hydrolysis (H_2SO_4) occurred and CNCs formed. Through the **Figure IV. 6 (c)** and **Figure IV. 7(h)** the morphology of CNCs is rods-like or needle-like due to chemical influence during synthesis due to the disintegration the cellulose (Cs) amorphous part by hydronium ions attack and then resulted the cellulose nanocrystals(CNCs) [181]. The extended hydrolysis time for 4 h promoted more isolated individual crystallites, this was owing to further weakened hydrogen bonding between cellulose molecular chains [397]. In addition, both Cs and CNCs showed homogeneous dispersion behavior, which related to the good stability of the colloidal suspension [398].

There is also a decrease in the dimensions of the Cs and CNCs compared to the raw sample, this proves that the percentage of crystallized Cs and CNCs is high and this is confirmed by the XRD, but were we observed the presence of some strands of cellulosic microcrystals in the different CNCs samples prepared and quite the opposite, the presence of some strands of cellulosic nanocrystals in the different Cs samples prepared. This indicates that the sample particles are not all of uniform size.

Figure IV. 6 (d-e) and **Figure IV. 7(i-j)** summarize the formation process of ZnO in CNCs network by two different methods.

In the first method for preparing the nanocomposite CNC/ZnO NPs, we synthesized ZnO on CNCs while the CNCs were in a dissolved state. For a better understanding of cellulose dissolution in the solvent, We chose the mixture of NaOH/urea solution used for cellulose dissolution, because the cellulose treated in deionized water exhibited the original fibrous shape due to the insolubility of cellulose in deionized water (deionized water was a solvent).

Given the fact that cellulose, as a linear chain of ringed glucose molecules, was linked by β(1−4) glycosidic bonds showing a flat ribbon-like conformation and deionized water failed to break intramolecular hydrogen bonds between the adjoining ring molecules, the linear configuration of the cellulose chain was intact [398].

while the morphology of cellulose from the NaOH/urea solution was a colorless liquid mixture which indicates that the cellulose fibers have melted. The explanation for that could be that cellulose molecules would aggregate to hide the hydrophobic glucopyranoside's ring planes.

Interestingly, the regenerated product after adding $ZnCl_2$ solution to the transparent mixture (cellulose/urea / NaOH) appeared in the form of cellulose nanocrystals **Figure IV. 6 (d)** and **Figure IV. 7(i)**. Moreover, a light-colored layer was observed on the surface of the treated CNCs [399], which means that the addition of $ZnCl_2$ to the system and the availability of more -OH ions resulting from NaOH led to the replacement of −Cl by −OH. After the removal of the ions Cl, Na, and excess Zn^{2+} in the solution to balance the charge of Zn^{2+} ions fixed on the CNC surface, which leads to the formation of $Zn(OH)_2$[21].

Where the electron-rich oxygen of the polar hydroxyl in the cellulosic molecular chain interacted with Zn^{2+} ions in solution through electrostatic force to form cellulose/zinc oxid complexes, disrupting intramolecular hydrogen bonds and cellulose.

Thus, it has already achieved the formation of zinc oxide in the form of a layer encapsulated by the CNCs.

For comparison purposes, ZnO nanoparticles were also prepared both in the presence of CNCs with the second method, $ZnCl_2$ solution was used to obtained a Zn^{2+} ions for synthesis ZnO precursor on the CNCs. This solution system was able to hydrolyze nano-sized CNCs [400]. Thus CNCs underwent hydrolysis in $ZnCl_2$ solution, this led to the liberation of zinc ions in the aqueous solution. After that, NaOH solution was added in to the system. When the solution became basic

First, the electron-rich oxygen from polar hydroxyls in cellulose molecular chain interacted with Zn^{2+} ions in the solution through electrostatic force to form Zn/cellulose complexes, resulting in the disruption of inter and intramolecular hydrogen bonds of cellulose. Then, the −OH replaced −Cl to counter balance the charge of Zn^{2+} ions immobilized on CNCs surface, leading to the formation of $Zn(OH)_2$[21]. Perhaps Zn^{2+} ions were still surrounded by some −Cl ions. When they transformed to ZnO crystals, which may result in new ZnO nuclei on CNCs surface and thus formation of flower-like ZnO clusters [401]. which after the precipitation process between CNCs and Zn^{2+} ions, water separation follows by drying to form ZnO molecules during the hydrothermal reaction. During the reaction, the mixture

was milky or light yellow, implying that no dissolution of cellulose occurred, as a result, the growth of ZnO crystals on the CNCs surface increases the surface area.

Compared to Cs, CNCs had more surface hydroxyl groups, which provide more active sites for the growth of ZnO nanoparticles, enabling their stable fixation in the 3D network structure and avoiding their agglomeration [402].

Besides that, other CNC/ZnO NPs synthesis conditions, such as reaction temperature and time could have impact on the ZnO morphology[403]. It is also worthy to note that the $ZnCl_2$ supernatant is recyclable and reusable after the reaction.

The number of hydroxyl groups on the cellulose surface had a significant effect on growth of ZnO [404]. While the number of free hydroxyl groups on cellulose was directly related to the size of cellulose, the smaller the size of the CNC/ZnO NPs particles, the fewer the number of hydroxide groups, that is, almost all of them are attached to zinc ions, and the larger the size of the resulting CNC/ZnO NPs particles, the greater the number of free hydroxyl groups on the surface The increased surface area provides more binding sites for the precursor ZnO. The electrostatic interactions between CNCs and ZnO particles promoted the uniform dispersion and nucleation growth of ZnO on the CNCs matrix.

The form of CNC/ZnO NPs for second methods, It should be emphasized that in all the reaction conditions, rod-like CNCs could still be observed from the SEM images and the ZnO NPs evenly dispersed in the self-assembled CNCs 3D network. The ZnO particles are well dispersed on the CNCs surface flower-like with a narrow size distribution formed. Each flower-like cluster consisted of several rough-surface conical-shape “petals” that connected and stacked together (**Figure IV. 6 (e)** and **Figure IV. 7(j)**).

To evaluate the chemical composition of shells, Cs, CNCs, and CNC/ZnO NPs. EDS was recorded arbitrarily from the samples surfaces. In EDS spectrum in **Figure IV. 8 (a, f)** are showed numerous well-defined peaks were evident related to elements chemicals C, O, N, Na, Mg, k, Cl, and S in from peanut shells and pea shells.

EDS spectra in the **Figure IV. 8 (b,g)** of Cs samples and **Figure IV. 8 (c, h)** of CNCs samples showed the peaks of carbon and oxygen elements, which clearly support the chemical composition of classic cellulose.

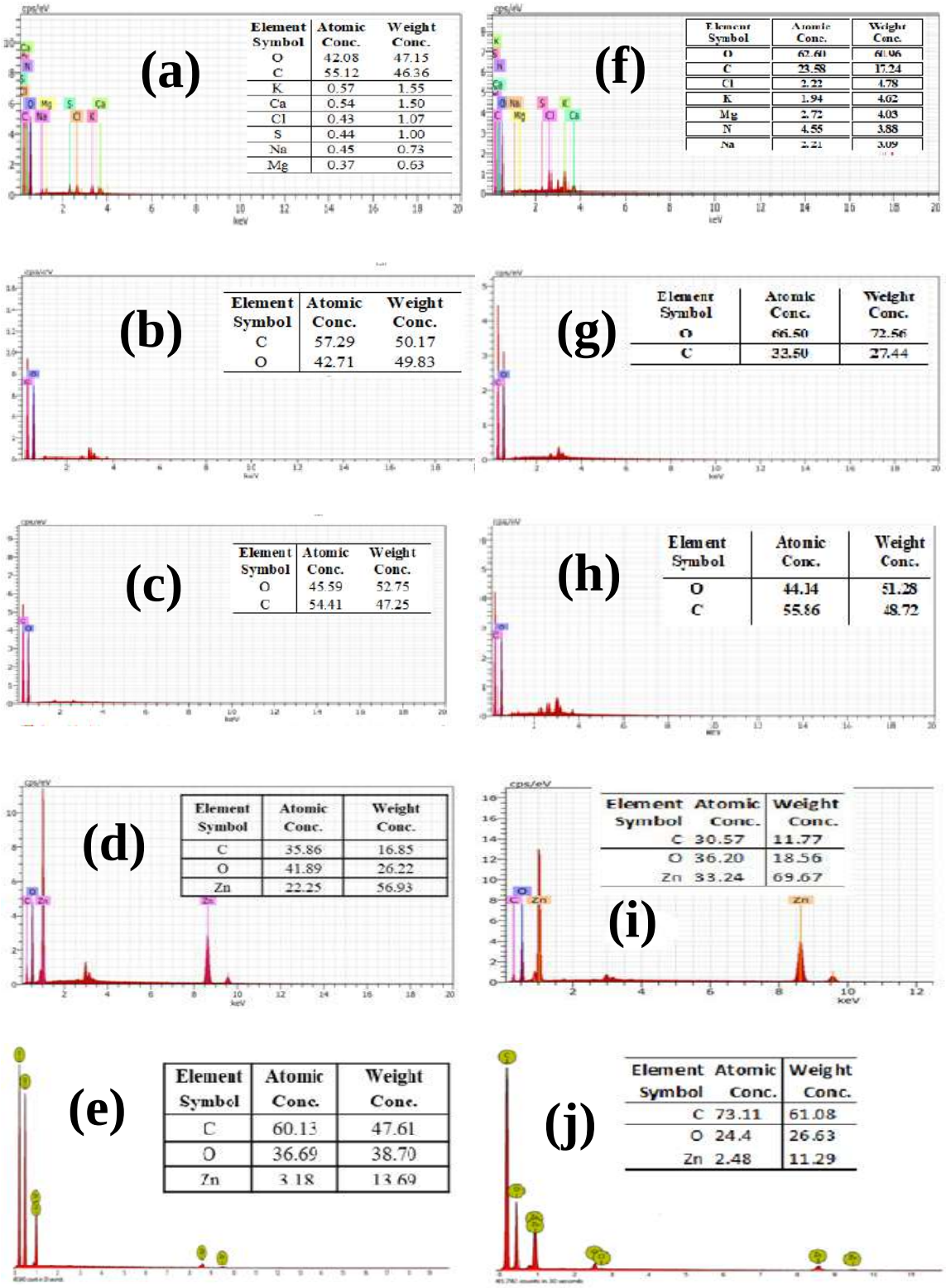

Figure IV. 8*: EDAX: (a, b, c, d, and e) of (Shells, Cs, CNCs, CNC/ZnO NPs.M1, and CNC/ZnO NPs.M2) from peanut shells and : (f, g, h, i, and j) of (Shells, Cs, CNCs, CNC/ZnO NPs.T1, and CNC/ZnO NPs.T2) from pea shells.*

Also, the obtained results confirmed that the acid hydrolysis for long time (4 hours) didn't change the elemental composition of cellulose nanocrystals and no other peak related to impurities was detected in the spectrum which further confirms the purity of the Cs and CNCs, supporting the statement as analyzed by FTIR results.

However, a slight difference was observed in the percentages for carbon and oxygen, which changed from Cs with 21.87% C and 78.13% O to CNCs with 54.41% C and 45.59% O from peanut shells. Also, the samples from pea shells,witch changed from Cs with 33.5% C and 66.5% O to CNCs with 55.86% C and 44.14% O, respectively resulting from the removal of amorphous residues [405, 406].

Figure IV. 17 (d, e, h, and j) showed the composition analysis and their corresponding distribution maps using EDX spectroscopy of the prepared bio-nanocomposites ZnO/CNC NPs samples by two different methods from peanut and pea shells, the existence of all three elements, C, O, and Zn. These elements characterize the presence of two components ZnO and CNCs in the sample. The recognition of Zn peaks in the EDX spectra indicates the successful intercalation of the ZnO NPs with the CNCs. Otherwise, the bands of C and O are ascribed to the binding energies of the CNCs.

Similarly, the EDX mapping of the prepared ZnO NPs shows the uniform distribution of Zn atoms along with C and O throughout the CNCs polymer matrix. As can be seen as a high percentage of Zn in the samples of the first method compared to its percentage in the samples of the second method, with 56.93% and 13.69% to the first and second method, respectively from peanut shells, and from pea shells with 69.67% and 11.29% to a first and second method, respectively. This confirms the fact that Zn is distributed in a constant manner on the entire surface of CNCs in the first method, while it was observed as white dots in the form of flowers-like scattered randomly on the surface of CNCs in the second method.

2. Study of removal of BM dye by adsorption on Cs and CNC/ZnO NPs (Adsorption study)

2.1. Factors Experimental Influencing the Adsorption Process

2.1.1. Effect of mass influence

The effect of the dosage or mass of the sorbent on the sorption of MB dye by cellulose (Cs) and cellulose/zinc oxide nanocomposite (CNC/ZnO NPs) was investigated by varying the amount the mass of the sorbent from 20mg to 100 mg in the test solution in the pH of solution at contact periods of 30 min at a speed of 500 rpm while maintaining the initial MB concentration and the volume of the solution are 100 ppm 50 mL respectively.

According to **Figures (IV. 9)** and **(IV.10)** show the effect of the mass of the sorbent on the adsorption efficiencies and the adsorbed capacity of the MB dye.

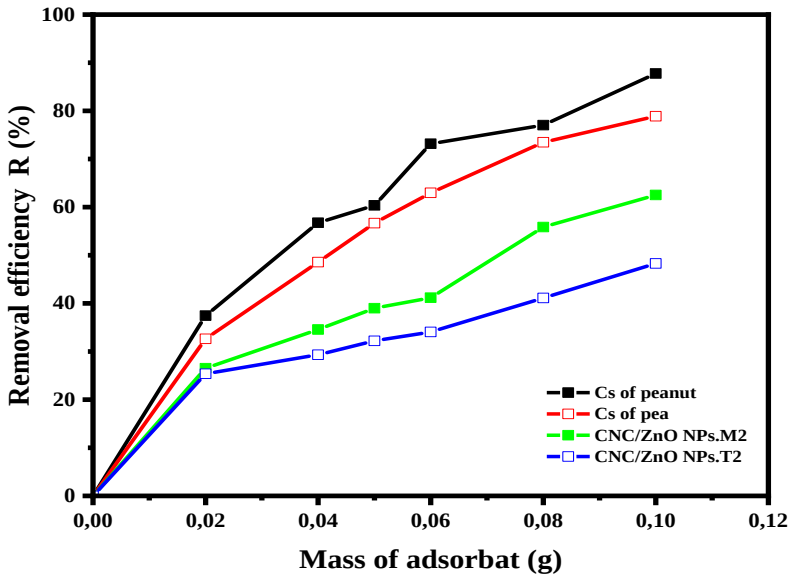

***Figure IV.9**: Effect of adsorbent mass on the percentage removal for removal of MB dye at: (m=(0.02 to 0.1) g, V= 50 ml, C_0= 100 ppm, pH= 7, T= 25±2 °C, and t= 30 min).*

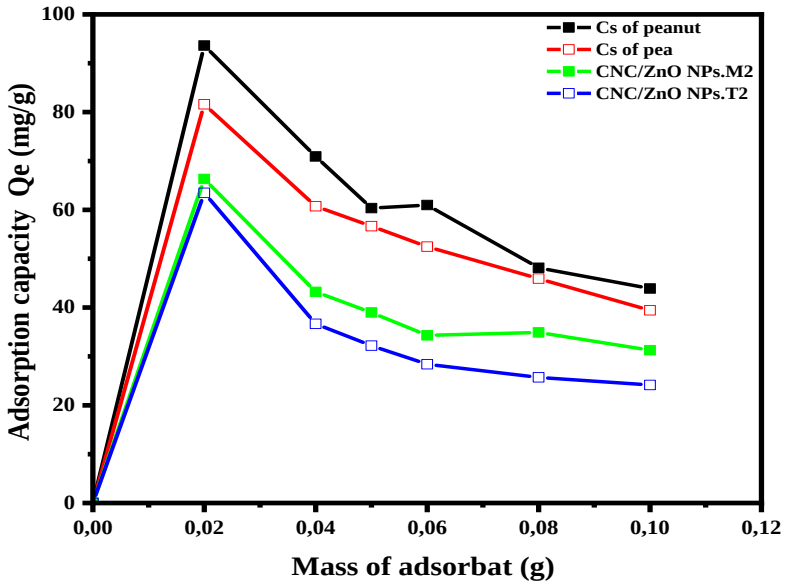

Figure IV.10: *Effect of adsorbent mass on the adsorption capacity for removal of MB dye at:(m= (0.02 to 0.1) g, V= 50 ml, C_0 100 ppm, pH=7, T= 25±2 °C, and t= 30 min).*

The **Figures (V. 1)** and**(V.2)** reveal that:

- the increase in the adsorbent dosage of each sample of Cs and CNC/ZnO NPs leads to an decreased in adsorption efficiency and a decrease in the adsorption capacity per unit mass of sorbent and a decrease in the concentration of the dye in solution, i.e. better elimination of the pollutant.
- When the adsorbent dosage of the sorbent increases from 20 mg to 100 mg the adsorption capacity decreases from 93.63 to 43.88 mg/g and 81.60 to 39.43 mg/g from Cs of peanut shells and pea shells, respectively and from 66.32 to 31.25 mg/g and 63.46 to 24.14 mg/g from CNC/ZnO NPs of peanut shells and pea shells, respectively. But the percentage of removal increases from 37.68 to 76.4 % and 32.64 to 87.87 % from Cs of peanut shells and pea shells, respectively and from 26.53 to 62.51 % and 25.38 to 48.29 % from CNC/ZnO NPs of peanut shells and pea shells, respectively. This can be attributed to the increased surface area available and the increased number of active sites on the surface of the material used.
- for high masses of sorbent, there is a very rapid surface sorption and, consequently, a decrease in the time required to reach equilibrium. When the mass of the sorbent increases the equilibrium time decreases .

- For sorbent masses greater than or equal to 80 mg, the percentage removed of dye remains constant.

At a low level of adsorbent dosage, the adsorption sites were fully available for MB adsorption, resulting in a higher capacity. When the adsorbent dose increases, the particles agglomerate, affecting the surface area. As a result, active adsorbent sites become saturated, triggering a low adsorption capacity of a high adsorbent dose composite [407].

2.1.2. Effect of contact time

In order to determine the time required for the occurrence of contact, we prepared 9 samples, each sample containing 50 ml from a solution of MB dye at an initial concentration of 100 ppm, an adsorbent dosage of 60 mg for Cs and CNC/ZnO NPs from peanut shells and 80 mg for Cs and CNC/ZnO NPs from pea shells. these samples were subjected to agitation process for different contact times of 05 to 75 min at pH of the MB solution (pH= 7), and at room temperature (25±2 °C).

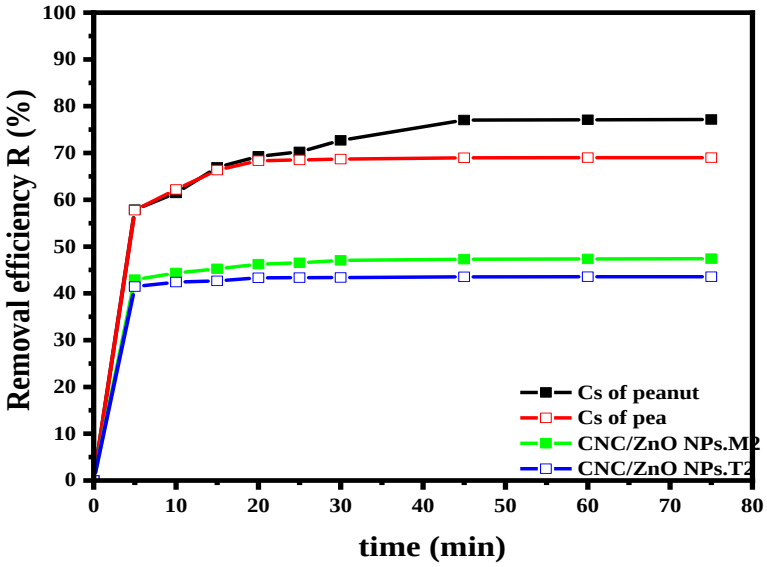

***Figure IV.11**: Effect of contact time on the percentage removal for removal of MB dye at: (V= 50 ml, C_0 100 ppm, pH=7, T= 25±2 °C, and t= (05 to 75) min).*

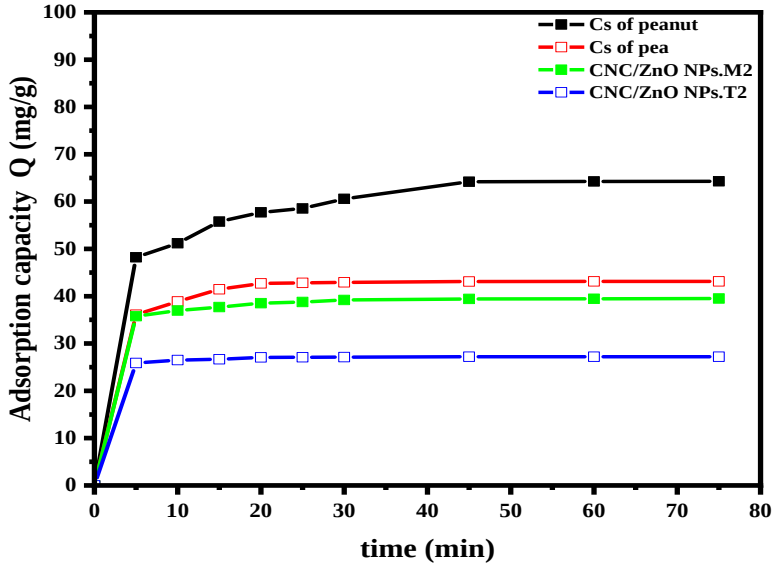

***Figure IV.12**: Effect of of contact time on the adsorption capacity for removal of MB dye at: (V= 50 ml, C_0 100 ppm, pH=7, T= 25±2 °C, and t= (05 to 75) min).*

The adsorption capacity **(Figure IV.12)** increases with increasing contact time (05 to 75 min) from 61.91to 69.01mg/g and 42.02 to 45.48 mg/g from Cs of peanut shells and pea shells, respectively and from 35.77to 39.5 mg/g and 25.89 to 27.22 mg/g from CNC/ZnO NPs of peanut shells and pea shells, respectively. But the percentage of removal **(Figure V.11)** increases from 72 to 80.26 % and 65.16 to 70.53 % from Cs of peanut shells and pea shells, respectively and from 42.92 to 47.4 % and 41.43 to 43.55 % from CNC/ZnO NPs of peanut shells and pea shells, respectively.

The adsorption rate appears rapid at the initial period of the contact time and gradually decreases with time until equilibrium. Maximum adsorption was achieved at 45 minutes time interval and no significant increase found by further increase in time.

The initial faster rate was due to accumulation of MB on surfaces of the adsorbents which is a rapid step [408].

Initially, excess of vacant places are available on the surface of sorbent, and uptake of BM dye was more, so there was continuous increase in adsorption capacity by increasing time slot from zero to 45 minutes. But, further increase could not cause sufficient change in adsorption of BM dye as vacant spaces are already filled, and equilibrium is achieved [409]. An optimum contact time to occupy the active site over

the adsorbent and adsorbate led to saturation; hence, the adsorption capacity will not increase [410].

2.1.3. Effect of initial concentration

The effect of the concentration of MB dye on the adsorption rate was studied by preparing 9 samples of MB dye and of different initial concentrations was varied in range of 05 to 300 ppm. Each sample containing 50 ml from a solution at pH solution (pH= 07), contact time for 05 to 75 min, and adsorbent dosage for Cs and CNC/ZnO NPs are 60 mg and 80 mg from samples of peanut shells and pea shells, respectively. Equilibrium attained when the concentration of the final solution remained the same with increasing adsorption timeat room temperature 25 °C.

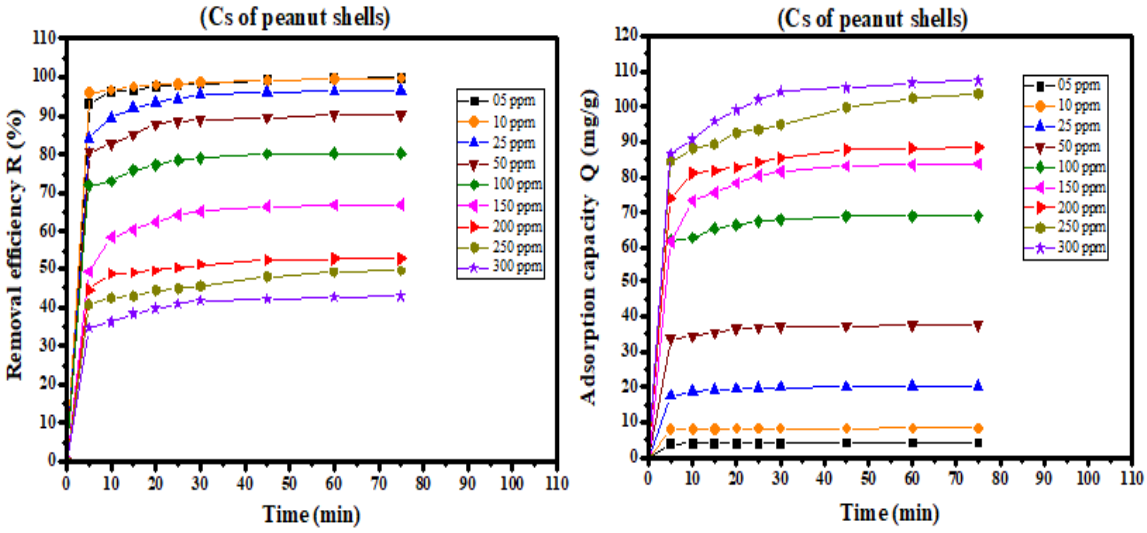

***Figure IV.13**: Effect of initial concentration on the percentage removal and adsorption capacity for removal of MB dye from Cs of peanut shells at: (m= 0.06 g, V= 50 ml, C_0=(05 to300) ppm, pH=7, T= 25±2 °C, and t= (05 to 75) min).*

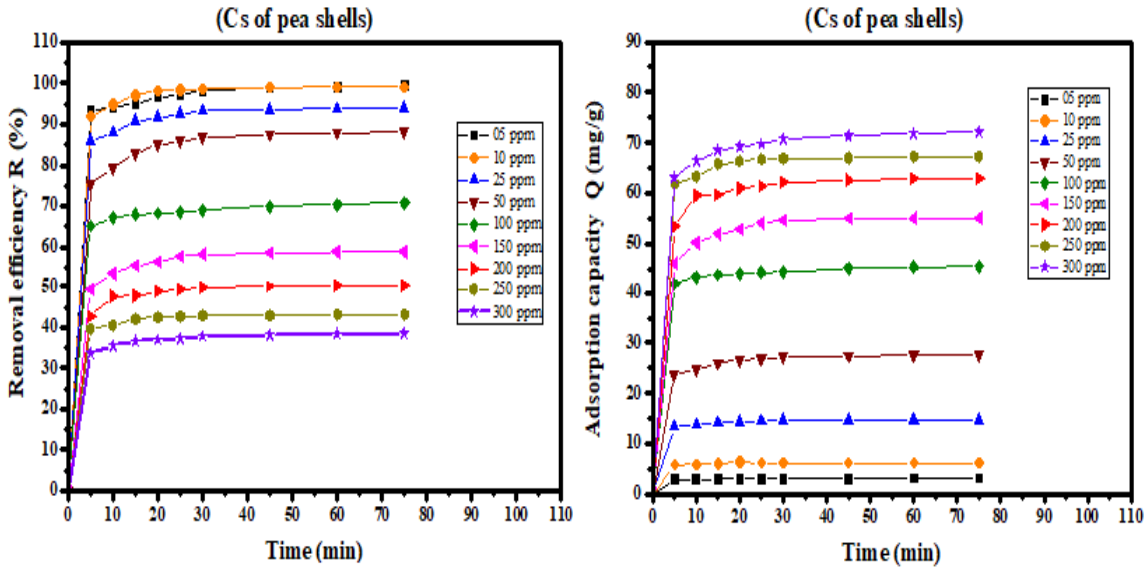

Figure IV.14: *Effect of initial concentration on the percentage removal and adsorption capacity for removal of MB dye from Cs of pea shells at: (m= 0.08 g, V= 50 ml, C_0=(05 to300) ppm, pH=7, T= 25±2 °C, and t= (05 to 75) min).*

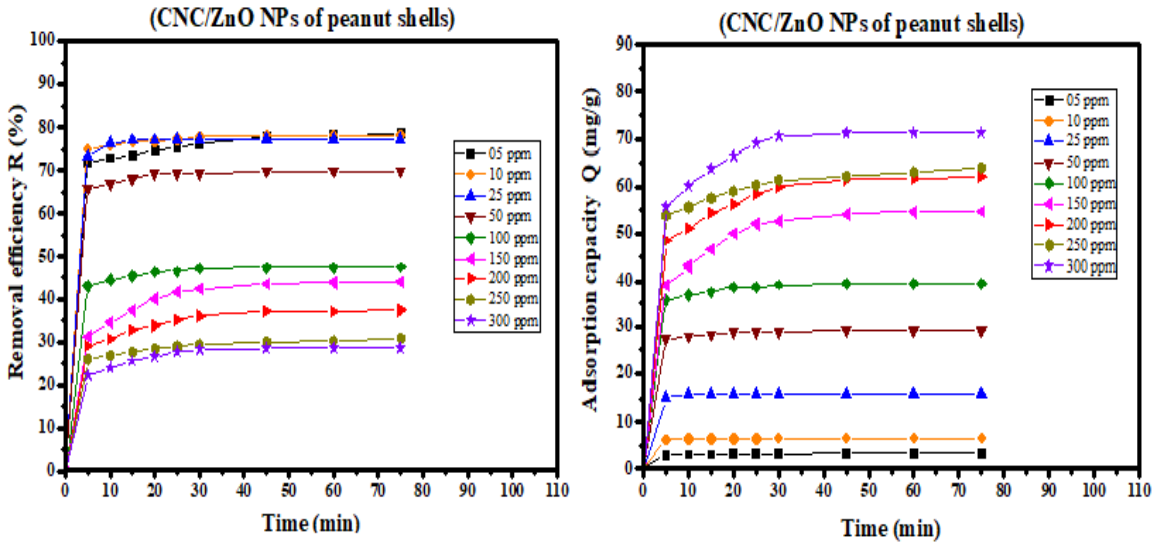

Figure IV.15: *Effect of initial concentration on the percentage removal and adsorption capacity for removal of MB dye from CNC/ZnO NPs.M2 of peanut shells at: (m= 0.06 g, V= 50 ml, C_0=(05 to300) ppm, pH=7, T= 25±2 °C, and t= (05 to 75) min).*

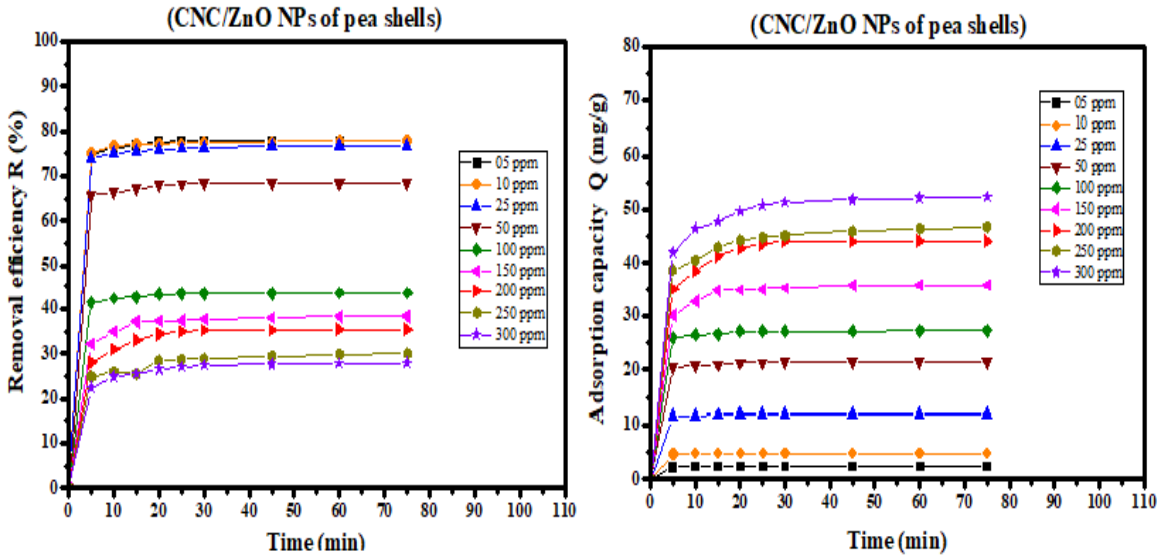

***Figure V.16**: Effect of initial concentration on the percentage removal and adsorption capacity for removal of MB dye from CNC/ZnO NPs.T2 of pea shells at: (m= 0.08 g, V= 50 ml, C_0=(05 to300) ppm, pH=7, T= 25±2 °C, and t= (05 to 75) min).*

That is shown in **Figure (IV.13)** to **(Figure IV.16)**, at initial concentration 300 ppm with 75 min contact time, all the samples gave the highest adsorption capacity of 107.33 mg/g and 71.26 from Cs and CNC/ZnO NPs of peanut shells, respectively. From the pea shells samples, it was found highest adsorption capacity of 72.1 mg/g to 52.4 mg/g from Cs and CNC/ZnO NPs, respectively.

According to **(Figure IV.13)** to **(Figure IV.16),** rapid increase in adsorption capacity was observed initially. In fact, we can see that the MB dye fixation curves on Cs and CNC/ZnO NPs, can be divided into two parts: the first part of the kinetics corresponding to a very short phase, where the fixation of MB dye is very fast, it is carried out in the first minutes of adsorption and a second phase of medium speed where the quantity adsorbed evolves more slowly and the adsorption rate is relatively low. As vacant spaces were available on the surface of sorbent. So, Increasing initial concentration of MB dye also raised adsorption to the construction of sorbate sorbate associations that provides the driving force to overcome the resistance to the mass transfer owing to increased adsorption of sorbate on available sites [411].

Adsorbent readily occupies these adsorption sites, and adsorption capacity has positive influence of concentration in this range. Further increase in concentration from 150 to 300 ppm has no significant effect on adsorption phenomenon. The latter is well represented by a saturation level. This phenomenon can be explained by the

existence of a first step of adsorption of MB dye on easily accessible sites probably located on the external surfaces of the solid supports, followed by a molecular diffusion of the dyes towards the adsorption sites. less accessible such as interfoliar spaces of solids, or within organic matter before reaching an adsorption equilibrium where all sites become occupied.

The rapid fixation is explained by the great affinity of the supports for the retention of MB dye and by a better diffusion of the substrate through the pores of these adsorbents. These results obtained are similar to the results of the adsorption of dyes on different adsorbents such as: aerobic granules [412], kaolinite [413], and other adsorbents [414, 415]. Also report that accommodation for sorbate decreases as concentration is very high due to unavailability of resident sites [416].

We can conclusion, the initial dye concentration factor significantly impacts the proportion of dye removal. Based on the linear relationship between dye concentration and accessible binding sites on an adsorbent surface. Then, it decreases slightly when the concentration increases because, , more dye can bind on the usable adsorbent surface, and then, the saturation of the surface active site makes it constant. As the dye concentration rises, the driving force for mass transfer rises, resulting in increased MB adsorption. Increased MB concentration results in more dye molecules, resulting in saturation and a reduction in adsorption capacity [417].

2.1.4. Effect of pH

The mechanism interaction between the dyes and the various adsorbents used change according to the pH of the solution [418, 419]. In this context, the effect of pH on the adsorption of MB has been studied over a wide range pH = (2 and 10), we prepared 9 samples, each sample containing 50 ml from a solution of MB dye at an initial concentration of 100 ppm, an adsorbent dosage of 60 mg for Cs and CNC/ZnO NPs from peanut shells and 80 mg for Cs and CNC/ZnO NPs from pea shells. these samples were subjected to agitation process for different contact times of 05 to 75 min at room temperature (25 °C).The pH of the solution was adjusted to the desired values by the addition of H_2SO_4 (0.02 M) or NaOH (0.02 M).

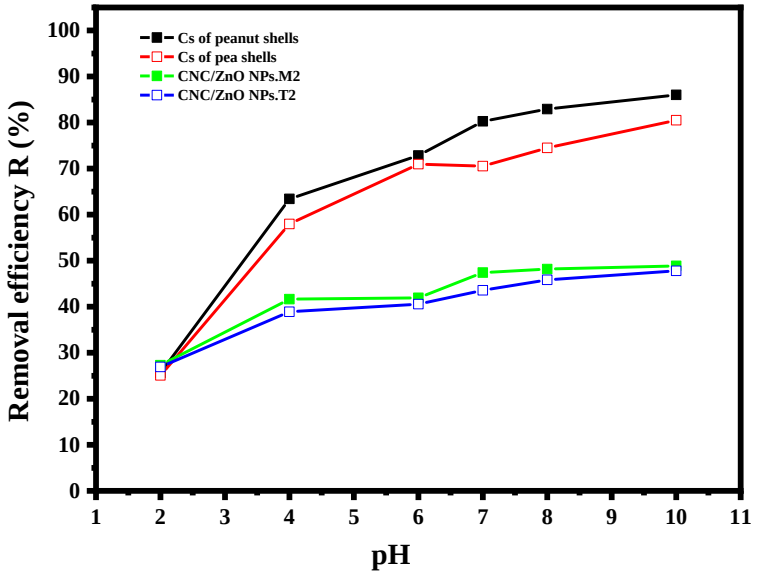

***Figure IV.17**: Effect of pH on the percentage removal for removal of MB dye at: (V= 50ml, C_0 100 ppm, pH= (2 to 10), T= 25±2 °C, and t= (05 to 75) min).*

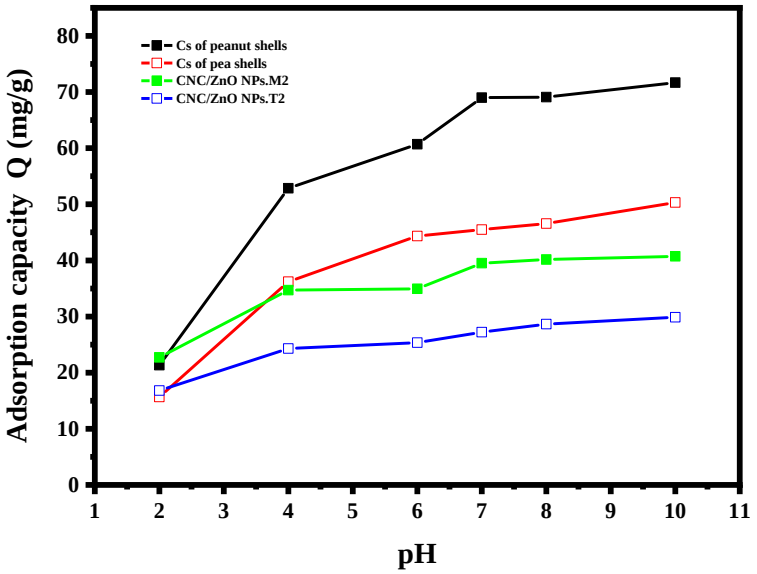

***Figure IV.18**: Effect of pH on the adsorption capacity for removal of MB dye at: (V= 50ml, C_0 100 ppm, pH= (2 to 10), T= 25±2 °C, and t= (05 to 75) min).*

Figure IV.17 showed that at lower pH values, removal of the BM dye was low but increased with increasing pH to optimal values of 10 in all the samples raw and modified (Cs and CNC/ZnO NPs) with 75 min contact time gave the highest

adsorption capacity of 71.68 mg/g and 40.88 from Cs and CNC/ZnO NPs of peanut shells, respectively. While in the samples from the pea shells, it was obtained an highest adsorption capacity of 50.31 mg/g to 29.87 mg/g from Cs and CNC/ZnO NPs, respectively.

- **Neutral and basic medium (pH > 6):**

In this region, The surface of adsorbent becomes positively charged at lower pH due to protonation of hydroxyl ions present in Cs and CNC/ZnO NPs;the adsorption capacity of the BM dye on both Cs and CNC/ZnO NPs adsorbents increases significantly with an increase in pH in the basic medium.

On the other hand, At a higher pH level, more binding sites are free and there is less competition between the H+ ions and the cationic MB dye[420]. Moreover, all O–H groups are free and increasing in number. Thus, it was observed that the reaction at higher pH can render a strong electrostatic attraction against MB. These results concluded that MB dye adsorption on Cs and CNC/ZnO NPs dependent the pH of the solution. Similar results were attained and disclosed by other researchers[421, 422].

- **Acidic medium (pH < 6):**

The adsorption capacity of the BM dye decreases with decreasing pH, the surface of adsorbent becomes positively charged due to protonation of hydroxyl ions present in Cs and CNC/ZnO NPs.Furthermore, as the solution pH decreases, more H^+ ions are encountered with the positively charged MB and covering the active sites of the Cs and CNC/ZnO NPs surface. This decrease can be explained by a noticeably strong electrostatic repulsion efect between the negative charge of the solid and the cationic form of the BM dye, which occupies the active sites[423].

For all the samples, the optimum pH range was found to be from 6 to 10, within which Cs and CNC/ZnO NPs show the best adsorption behavior. When the pH is increased between 7 and 10, there is a slight influence and a slight increase in the adsorption capacity of the BM dye. Moreover, this behavior confirms the high stability of Cs and CNC/ZnO NPs, highlighting the advantage of using these materials in adsorption over a wide pH range. Furthermore, the samples attract positive ions over a wide range of pH, except for the acidic medium (pH <6), where a decrease in the adsorption capacity for acidic pH values is observed.

2.1.5. Effect of temperature

In this context, the effect of temperature on the adsorption of MB has been studied over a wide range T= (25, 40, and 55) ±2 °C, we prepared 03 samples, each sample containing 50 ml from a solution of MB dye at an initial concentration of 100 ppm, an adsorbent dosage of 60 mg for Cs and CNC/ZnO NPs from peanut shells and 80 mg for Cs and CNC/ZnO NPs from pea shells. these samples were subjected to agitation process for maximum time 75 min at pH solution.

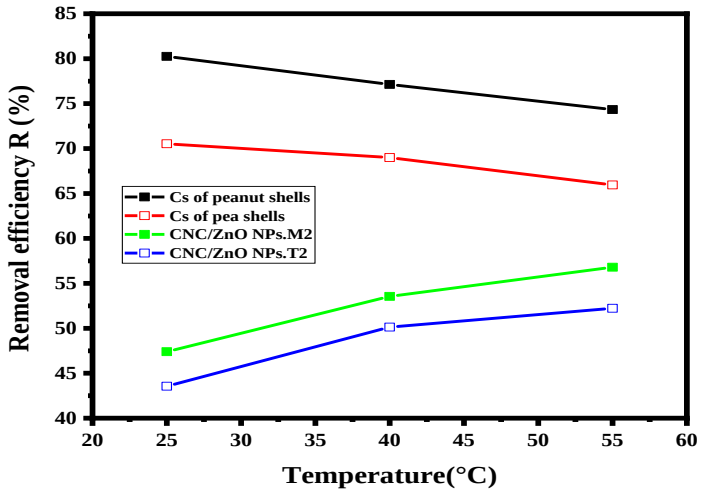

Figure IV.19: *Effect of temperature on the percentage removal for removal of MB dye at: (V= 50ml, C_0 100 ppm, pH= 7, T= (25, 40, and 55) ±2 °C, and t= 75 min).*

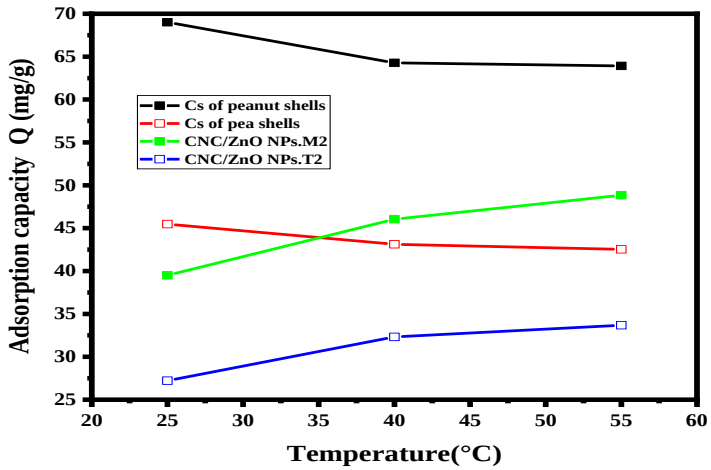

Figure IV.20: *Effect of temperature on the adsorption capacity for removal of MB dye at: (V= 50ml, C_0 100 ppm, pH= 7, T= (25, 40, and 55) ±2 °C, and t= 75 min).*

According to **Figure IV.19** and **Figure IV.20**, for Cs, when the temperature increases from 25 to 55 °C, we note a decrease in the adsorption capacity from peanut shells decreases from 69.01 to 63.92 mg/g, andshow the percentage of removal decreases from 80.26 to 74.34%, respectively. Similarly, the adsorption capacity of Cs derived from pea shells decreases from 45.48 to 42.53 mg/g, and the percentage of removal decreases from 70.53 to 65.95%, respectively. A decrease in temperature leads to a decrease in the stability of the bonds between the active sites of the substance and the BM dye molecule. With regard to Cs synthesized from peanut shells and pea shells, an exothermic thermal phenomenon appears. From these findings, it can be observed that an increase in the temperature of the solution leads to a decrease in adsorption capacity. This can be explained by the exothermic nature of the sorption process and the weakening of bonds between the dye and the active sites of the sorbent at higher temperatures.

The experimental results obtained for CNC/ZnO NPs showed that the adsorption capacity of BM dye increased with the temperature rise from 25 to 55 °C.

According to **Figure IV.19** and **Figure IV.20**, for CNC/ZnO NPs derived from peanut shells, the adsorption capacity increased from 39.5 to 48.84 mg/g,, respectively while the percentage of removal increased from 47.4 to 56.80%. Similarly, for CNC/ZnO NPs derived from pea shells, the adsorption capacity increased from 27.22 to 33.68 mg/g, and the percentage of removal increased from 43.55 to 52.22 %, respectively.

The increase in temperature enhances the movement of BM dye ions, facilitating their penetration into the internal structure of CNC/ZnO NPs. This leads to an increase in intraparticle diffusion and the creation of more adsorption sites, resulting in better fixation and enhancing the adsorption phenomenon[424].

The temperature parameterization has a positive effect on this process by providing a strong energy contribution, thereby overcoming the repulsion forces at the interfaces of the liquid and solid media. This trend suggests that the adsorption process in CNC/ZnO NPs follows an endothermic adsorption process[425].

Therefore, it is noteworthy that the role of temperature plays an important part in the kinetics of dye retention[426].

2.2. Adsorption Kinetics

In order to investigate the adsorption kinetics of MB dye, We used in this study, the kinetic laws of the pseudo-first-order model and the pseudo-second-order. The adsorption rate constants of MB dye on the different adsorbents, for the pseudo-first and pseudo-second-order model, are determined graphically by plotting ln(Qe-Qt) as a function of time for the determination of the rate constant (K1) and t/Qt as a function of time for determining the second rate constant (K2). The linear form of the first-order kinetic and the pseudo-secondorder kinetic model is expressed from **Equations (II. 2)** and **(II. 4)** (in chapter III), respectively. For a linear form, a computer-based procedure was used in Microsoft Excel 2010 using the solver add-in method .

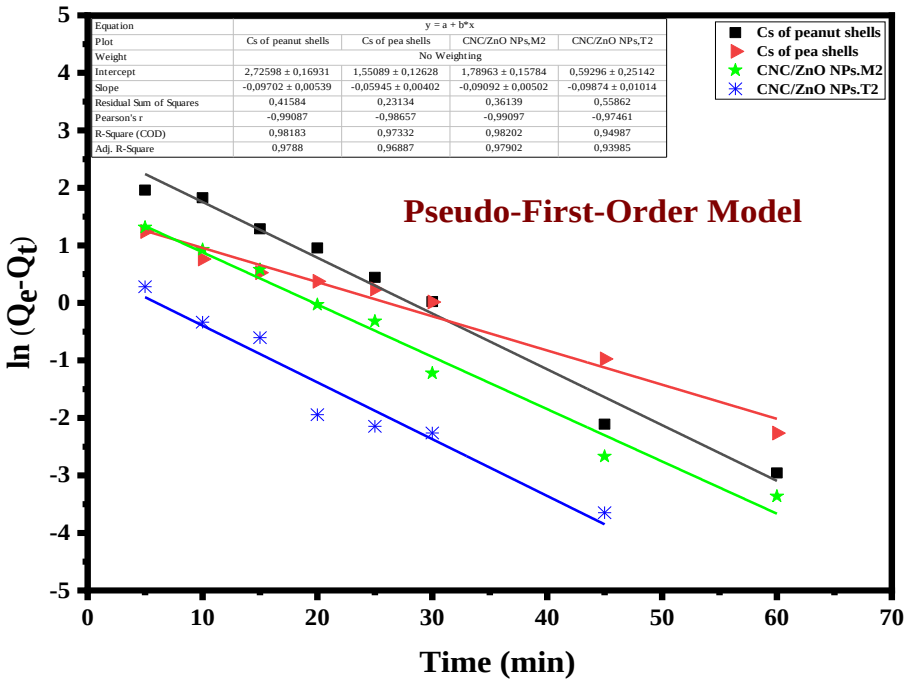

Figure IV.21: *The pseudo-first-order kinetic of MB dye adsorption on Cs and CNC/ZnO NPsfrom peanut shells and pea shells at: (V= 50 ml, C0 100 ppm, pH=7, T= 25±2 °C, and t= (05 to 75) min).*

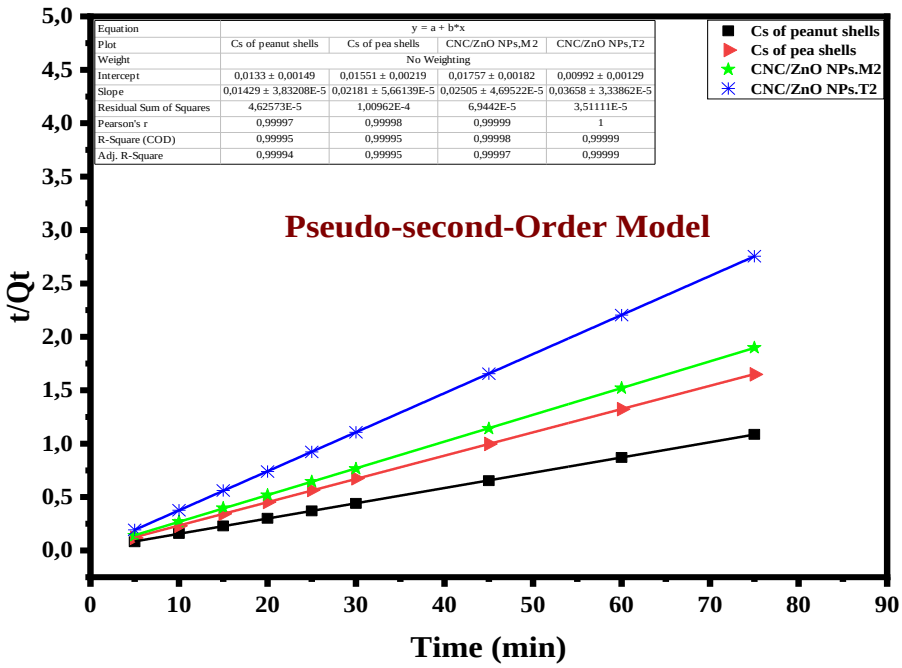

Figure IV.22: *The pseudo-second-order kinetic of MB dye adsorption on Cs and CNC/ZnO NPs from peanut shells and pea shells at: (C0 100 ppm, pH=7, T= 25±2 °C, and t= (05 to 75) min).*

Table IV.4:*Estimated kinetic models parameters for MB adsorption on Cs and CNC/ZnO NPs from peanut shells and pea shells at: (C0=100 ppm, pH= 7, T= 25°C).*

Adsorption isotherm (T= 25C)	Parameter (C_i=100ppm)	Samples: Cs of peanut shells	Cs of pea shells	CNC/ZnO NPs.M2	CNC/ZnO NPs.T2
	Qe exp(mg/g)	**69.0174**	**45.4838**	**39.49956**	**27.2196**
Pseudo-First-Order	**Qe cal (mg/g)**	15.271	4.71567	5.98723	1.80933
	K_1 (1/min)	-0.00162	-0.00099	-0.00152	-0.00165
	R^2	0.9788	0.96887	0.97902	0.99799
Pseudo-Second-Order	**Qe cal (mg/g)**	**69.979**	**45.8505**	**39.920**	**27.3373**
	K_2(g/mg.min)	0.01535	0.030669	0.03571	0.134888
	R^2	**0.9999**	**0.99995**	**1**	**1**

According to the results of the modeling, **Table(IV.4)** and **Figures (IV.21** and **IV.22)**shows that the model which presents the highest correlation factor is that of the pseudo-second-order model. The values of the quantity adsorbed at equilibrium found in this model are very close to those of the quantities adsorbed experimentally with a large correlation coefficient R^2 such that (R^2 =1) for all the adsorbents, it can therefore be deduced that the model of pseudo-second-order is the one that best describes the adsorption process of methylene blue on all the samples of Cs and CNC/ZnO NPs adsorbents.

The pseudo-second-order model is based on the phenomenon of binding molecules to the solid phase until saturation, with chemisorption being the determining step of adsorption. On the other hand, the pseudo-first-order model is only valid for the first minutes. A similar phenomenon is observed in the adsorption of MB dye [427-429].

2.3. Adsorption Isotherm

The Cs and CNC/ZnO NPs adsorbents adsorption properties were investigated by submerging the sample in MB at different concentrations from 05 to 300 mg/l. The Langmuir, Freundlich, and Temkin models were applied to explain the equilibrium adsorption isotherm. Since this information can connect the adsorbate and absorbent, the surface and adsorbate might adhere via chemisorption or physisorption.

The Langmuir isotherm model describes the information for the adsorption of MB dye onto the surface of Cs and CNC/ZnO NPs adsorbent homogeneously, and the BM dye molecule formed a monolayer at the adsorption sites. The Freundlich isotherm model predicts that nonideal multilayer adsorption occurs on the adsorbent's uneven surface and that the adsorbent's surface is heterogeneous.

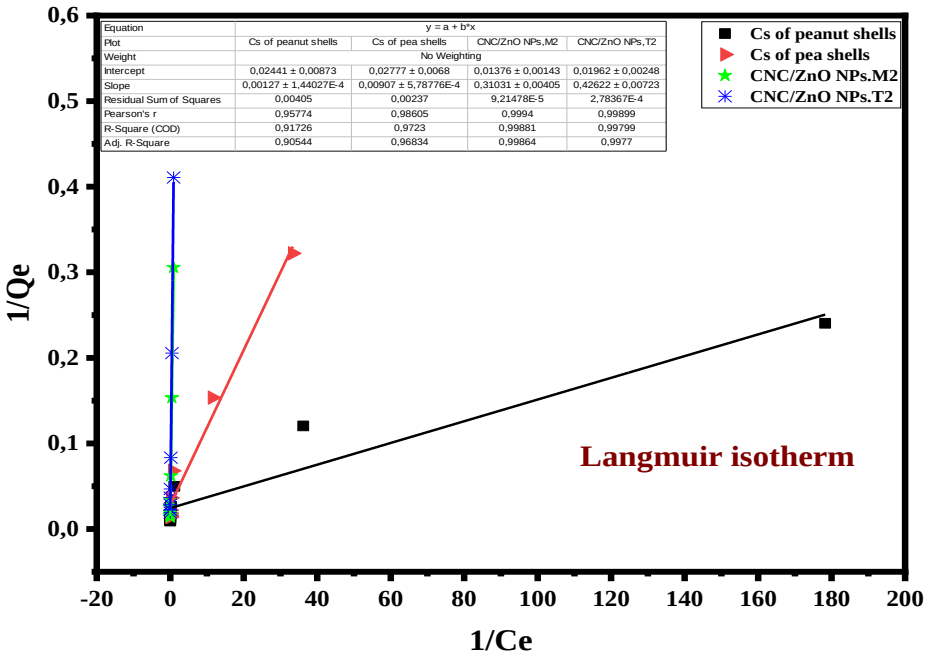

Figure IV.23: *The Langmuir isotherm of MB dye adsorption on Cs and CNC/ZnO NPs from peanut shells and pea shells at: (C0=(05 to 300) ppm, pH=7, T=* 25±2 *°C, and t= (05 to 75) min).*

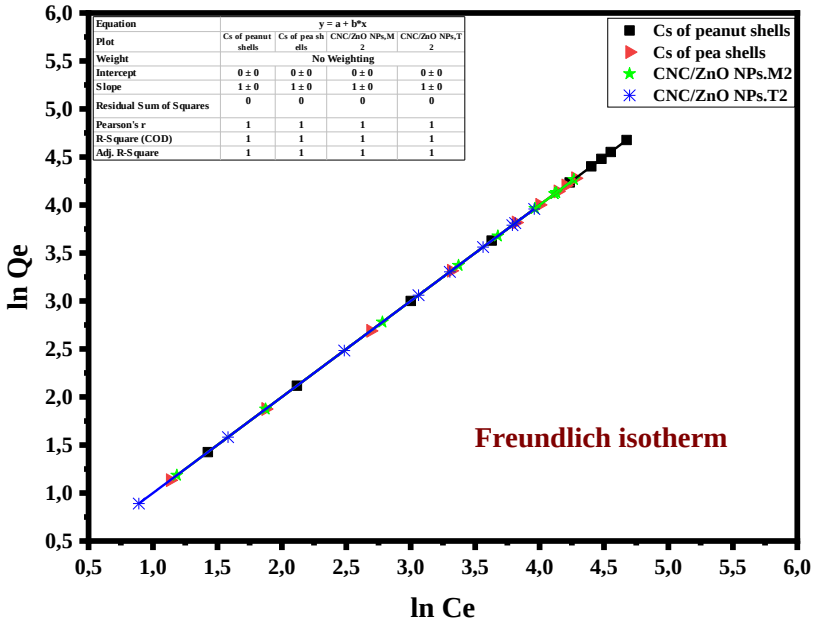

Figure IV.24: *The Freundlich isotherm of MB dye adsorption on Cs and CNC/ZnO NPs from peanut shells and pea shells at: (C0=(05 to 300) ppm, pH=7, T=* 25±2 *°C, and t= (05 to 75) min).*

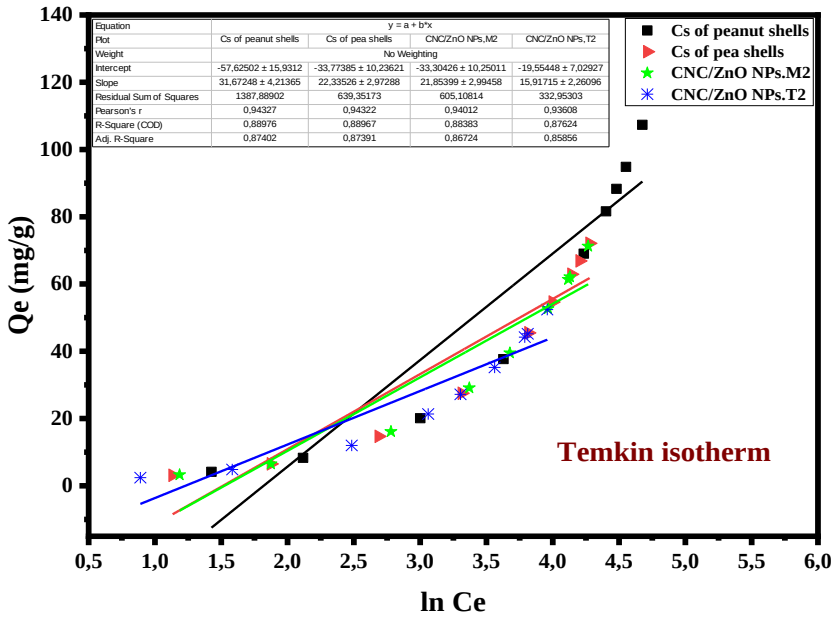

Figure IV.25: *The Temkin isotherm of MB dye adsorption on Cs and CNC/ZnO NPsfrom peanut shells and pea shells at: (C0=(05 to 300) ppm, pH=7, T= 25±2 °C, and t= (05 to 75) min).*

Table IV.5:*Estimated isotherm models parameters for MB adsorption on Cs and CNC/ZnO NPs from peanut shells and pea shells at: (C0=(05 to 300) ppm, pH=7, T= 25±2 °C, and t= (05 to 75) min).*

Adsorption isotherm (T= 25C)	Parameter	Samples: Cs of peanut shells	Cs of pea shells	CNC/ZnO NPs.M2	CNC/ZnO NPs.T2
Langmuir isotherm	**Qmax (mg/g)**	40.9668	36.01008	72.6744186	50.968
	KL (L/mg)	19.2204	3.06174	0.04434275	0.046
	RL	0.00052	0.00356	0.18402	0.17847
	R^2	0.91726	0.9723	0.91726	0.99799
Freundlich isotherm	**Kf (mg/g)(L/mg)$^{1/n}$**	0	0	0	0
	1/n	1	1	1	1
	R^2	**1**	**1**	**1**	**1**
Temkin isotherm	**KT (L/mg)**	0.162122	0.22044	0.2178509	0.29272
	BT (J/mol)	31.67248	22.33526	21.85399	15.9172
	R^2	0.88976	0.88967	0.88383	0.87624

Form 1 of the Langmuir equation The linearization of the Langmuir model **Equation (II. 8)** By plotting 1/Qe as a function of 1/Ce, we obtain a straight line with a slope of 1/KLQmax and an ordinate at the origin of 1/Qmax The modeling of the experimental results of the sorption isotherms of BM by Cs and CNC/ZnO NPs are presented on the **Figure IV.23** and the parameters obtained are grouped in **Table IV.5**.

For Freundlich's model, by plotting ln Qe as a function of ln Ce, if the variation of Qe as a function of ln Ce is linear, we must obtain a straight line with a slope equal to 1/n and ordinate at the origin equal to ln kF. The modeling of the sorption isotherms of methylene blue by the Freundlich relation **Equation (II. 11)**is presented in **Figure IV.24**. The model parameters, as well as the correlation coefficients, are given in **Table V.2**.

For the Temkin model, By plotting Qe as a function of ln Ce, we obtain a straight line with slope RT/BT and ordinate at the origin equal to RT/BT ln AT. The results of the modeling of the sorption isotherms by the Temkin relation **Equation (II. 13)** is presented in **Figure IV.25**. Temkin parameters and correlation coefficients are given in **Table IV.5**.

- The results provided by the linear transform of the Freundlich model show that the form of this equation gives an excellent fit of the experimental data because the correlation coefficients obtained are very good (R =1) [307].
- In all cases, the correlation coefficients (K) obtained by form 1 of the Langmuir equation are superior to those determined by the Freundlich and Temkin relationship with all samples of Cs and CNC/ZnO NPs.
- By the Freundlich model, the linear regression is very good, with the averages of the error percentages calculated by the Freundlich model being higher than those given by the Langmuir and Temkin model in all the samples of Cs and CNC/ ZnO NPs.
- The values of n are equal to 1 ($1 \geq n \geq 0$). This means that the sorption of BM by Cs and CNC/ZnO NPs is favorable.

We can therefore conclude that the Freundlich equation gives a better adjustment of the experimental data compared to the different forms of the Langmuir model and that of Temkin.

2.4. Adsorption thermodynamics

The adsorption process was determined by determining the thermodynamic functions at different working temperatures(25°C, 40°C, and 55°C). The standard change for Gibb's free energy ΔG◦ (kJ/mol), enthalpy ΔH◦ (kJ/mol), and entropy ΔS◦ (kJ/mol K) were calculated using the following **equations (II. 16)** and **(II. 17)**, respectively[430] for MB dye adsorption onto the Cs and CNC/ZnONPs from peanut shells and pea shells. The values of ΔH° and ΔS° can be calculated from the slope and intercept of the plot of ln KC versus 1/T, All of the thermodinamics parameters are presented in **Table IV.6**.

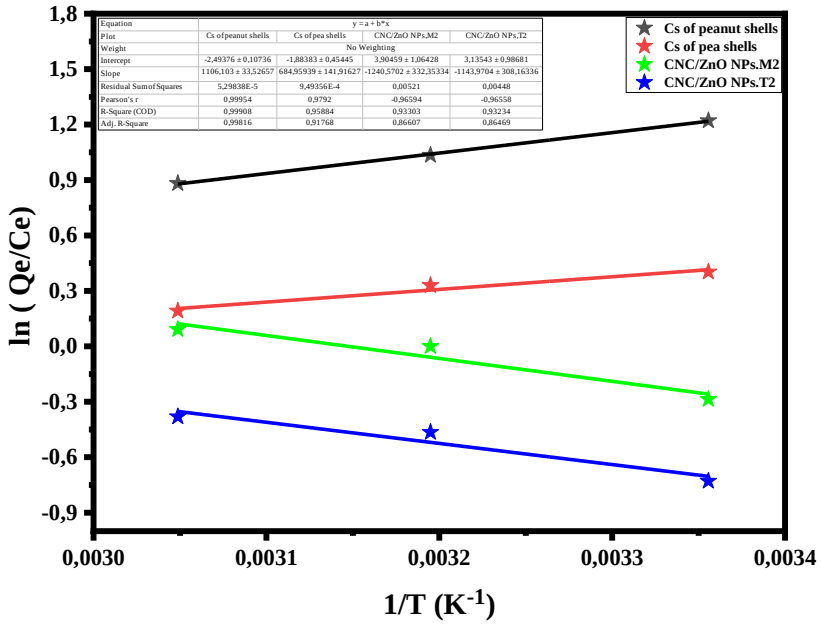

Figure IV.26: *The Thermodynamics isotherm of MB dye adsorption on Cs and CNC/ZnO NPs from peanut shells and pea shells at :(C0=(100 ppm, pH=7, T=* 25±2 *°C, and t= (05 to 75) min).*

Table IV.6: *Estimated Thermodynamics models parameters for MB adsorption on Cs and CNC/ZnO NPs from peanut shells and pea shells at: (C0=(100 ppm, pH=7, T=* 25±2 *°C, and t= (05 to 75) min*).

	ΔH° (kJ/mol)	ΔS° (J/molK)	ΔG° (kJ/mol)			R^2
			25°C	40°C	55°C	
Cs of peanut shells	-9.196	-20.733	-3.024	-2.691	-2.404	0.999
Cs of pea shells	-5.694	-15.662	-0.997	-0.858	-0.521	0.958
CNC/ZnONPs.M2	10.314	32.462	0.709	-0.084	-0.0518	0.933
CNC/ZnONPs.T2	9.511	26.068	1.807	1.098	1.155	0.932

In the thermodynamic parameter for the CNC/ZnO NPs for peanut and pea shells, ΔG° has given the adsorption processes information. From **Table IV.6**, the ΔG° exhibited decreasing values with an increase in temperature, this can be led to the adsorption of MB as a degree of spontaneous process and thermodynamically more favorable. In addition, the values of ΔG° were less than 60 KJ/mol confirming the adsorption of MB dye on the CNC/ZnO NPs for peanut shells and pea shells was physical sorption processes[431]. The value of ΔS° was found to be positive to establish the increased randomness in the solid/liquid interface interaction during the adsorption process. The positive values of ΔH° point out that the more interaction of the CNC/ZnO NPs for peanut shells and pea shells with MB dye [432]. The obtained results are confirming the adsorption process is endothermic.

In conclusion, about the Cs of peanut shells and pea shells, the value of ΔG° is negative at all the temperatures studied, which indicates the favorability and spontaneity of adsorption process[433].

Increasing the temperature does not favor the adsorption of this dye. The adsorption phenomenon is exothermic, due to the negative value of the enthalpy ΔH°, physisorption can be considered the predominant type of adsorption because ΔH°< 40 kJ/mol [434]. The negative value of ΔS° indicates that during adsorption on this material, there is a decrease in disorder at the interface of the solid/solution system caused by the dimensions of the adsorbate molecule[435].

3. Evaluation the antimicrobial activities of CNCs and CNC /ZnO NPs

Pathogenic bacteria and fungi cause a broad range of diseases in both humans and animals. Extensive research and sophisticated scientific approach have become inevitable for the establishment of new therapeutic values to overcome microbial resistance and the nonselective and unsystemic use of antibiotics. In the study, the well diffusion method (WD) on agar was used to study the antimicrobial activities of CNCs and CNC/ZnO NPs extracted from peanut shells and pea shells against both the Gram-positive bacteria (*Staphylococcus aureus*), Gram-negative bacteria (*Escherichia coli* and *Klebsiella pneumonia*), and one fungus (*Candida albicans*).

Furthermore, the effect of the diffirent synthesis methods used in this study on antimicrobial activity was investigated by measuring the inhibition zone of samples different synthesis methods of CNCs and CNC/ZnO NPs.

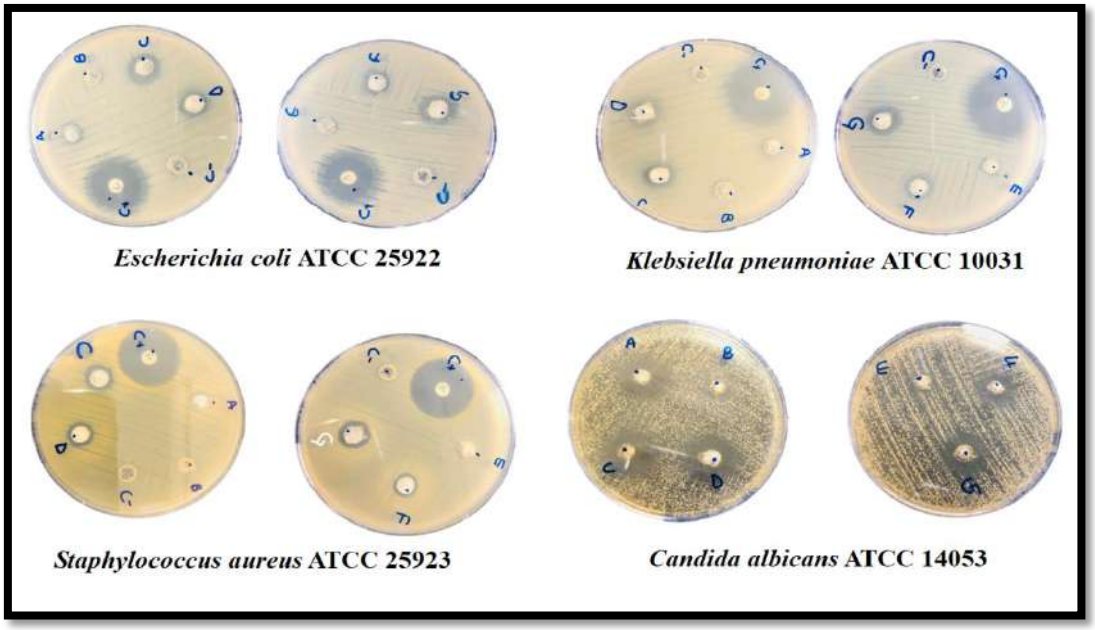

***Figure IV.27** : The antimicrobial activities of CNCs and CNC/ZnO NPs extracted from peanut shells and pea shells against both the bacteria and one fungus.*

A: ZnO NPs, (**B**: CNCs, **C**: CNC/ZnO NPs.M1, **D**: CNC/ZnO NPs.M2) from peanut shells, (**E**: CNCs , **F**: CNC/ZnO NPs.T1 , **G**: CNC/ZnO NPs.T1) from pea shells, $\mathbf{C}^{+}$: Positif control (Antibiotic *Lévofloxacine*), and $\mathbf{C}^{-}$: negative control (DMSO).

In general, all tested strains showed dose-dependent inhibition susceptibility to low concentration samples as a result of their insolubility in DMSO with bacterial and fungal strains found to be the most sensitive. The inhibition zones shown in the **Table (IV. 7**).

Table IV. 7: *The inhibition zones for the different samples of CNCs and CNC/ZnO NPs from peanut shells and pea shells*

Activity:		Antibacterial			Antifungal
bacterial strains:		***Escherichia coli ATCC 25922***	***Klebsiella pneumonia* ATCC 10031**	***Staphylococcus aureus* ATCC 25923**	***Candida albicans* ATCC 14053**
ZnO NPs		7.16 ± 0.235	7.16 ± 0.235	6.83 ± 0.235	14.33 ± 0.471
CNCs	Peanut shells	7± 0.00	6.83 ± 0.235	7.16 ± 0.235	8.16 ± 0.235
	Pea shells	7± 0.00	6.33 ± 0.471	6.33 ± 0.471	/
CNC/ZnO NPs (First method)	Peanut shells	10.33 ± 0.471	11.33 ± 0.471	11 ± 0.00	16.66 ± 0.471
	Pea shells	9.66 ± 0.471	10.66 ± 0.471	11 ± 0.00	15.66 ± 0.471
CNC/ZnO NPs (Second method)	Peanut shells	11.33 ± 0.471	11 ± 0.00	9.33 ± 0.471	19.66 ± 0.471
	Pea shells	12.83+0.235	12+00	12.83+0.235	18.33+0.471
Levofloxacin		29.33 ± 0.471	22.66 ± 0.471	27.66 ± 0.471	/
DMSO		/	/	/	/

The obtained results showed that CNCs hybridized with ZnO NPs prepared by both methods has a positive reaction and close sensitivity against all three tested gram (-) and gram (+) strains, as the results of both samples are close and have almost the same intensity of effect (ranging from 9 to 12 mm). About the antifungal activity, it showed a strong sensitivity against *Candida albicans*, as the sample prepared by the

second method (between 19 mm and 18 mm) showed a higher inhibition than the sample prepared by the first method (between 17 mm and 15 mm).

This confirms that CNC/ZnO NPs extracted from plant waste (peanut and pea shells) have antibacterial and antifungal properties. Whereas, the antibiotic used in general represented a strong inhibition of all tested bacterial strains except for *Candida albicans*. Although this inhibition varies from one strain to another, it remains superior to studied samples.

The obtained results showed that CNCs hybridized with ZnO NPs prepared by both methods has a positive reaction and close sensitivity against all three tested gram (-) and gram (+) strains, as the results of both samples are close and have almost the same intensity of effect (ranging from 9 to 11 mm and 9 to 12 mm from peanut and pea shells, respectively). About the antifungal activity, it showed a strong sensitivity against Candida albicans, as the sample prepared by the second method showed a higher inhibition (19 mm and 18 mm from peanut and pea shells, respectively) than the sample prepared by the first method (17 mm and 15 mm from peanut and pea shells respectively).

This confirms that CNC/ZnO NPs extracted from plant waste (peanut and pea shells) have antibacterial and antifungal properties. Whereas, the antibiotic used in general represented a strong inhibition of all tested bacterial strains except for *Candida albicans*. Although this inhibition varies from one strain to another, it remains superior to studied samples.

From these results, the addition of ZnO NPs was proven to be able to increase the ability of CNCs to inhibit bacteria by 3 to 4 mm in the IZ, and to inhibit fungi by 8.5 mm and 11.5 mm in the IZ in CNC/ZnO NPs. On the other hand, the addition of ZnO NPs more percentage to CNCs did not show an increment in the area of inhibition. This could be due to the limited ability of ZnO NPs to bind CNCs. Based on the chemical structure of CNCs and ZnO NPs, the bonds that occurred in the biocomposite are strong hydrogen bonds between the hydroxyl group of ZnO NPs dissolved in water and the hydroxyl group of CNCs. From the dissolution difficulty of CNCs and ZnO NPs, can be not bound all CNCs by ZnO NPs [436].

The search for natural additives, especially economical additives, has increased dramatically in recent years as consumers become increasingly concerned about foods containing such artificial additives. Therefore, it is necessary and beneficial to develop natural products with antibacterial activity [437].

Based on the significant antibacterial and antifungal activity, and in addition to its distinctive physical and chemical properties for CNC/ZnO NPs for example very weak solubility in water and DMSO solution. We can be used CNCs, CNC/ZnO-NPs as an effective antimicrobial material either in pristine form or in combination or carrier for antibiotics.

Padmavathy et al [438], ZnO NPs also have an abrasive surface roughness that impairs the antibacterial process and destroys the bacterial membrane of both Grampositive and Gram-negative bacteria. Jones et alinvestigated the antibacterial activity of ZnO, TiO_2, CuO, CeO_2, Al_2O_3, and MgO against the bacteriumStaphylococcus aureusand compared their antibacterial activities. The ZnO NPs among them and showed significant growth inhibition [439].

According Candan et al [440], the effect of water-soluble substances is weaker than that of water-insoluble substances. This may indicate that water-insoluble compound molecules can insert themselves into and disrupt bacterial cell membranes.

Yamamoto et al, investigated the ability of Escherichia coli and Staphylococcus aureus to control bacteria cultured in an infusion medium to the influence of ZnO NPs size. It was found that the antibacterial activity increased with decreasing particle size. Regarding our antifungal activity results, they are interesting. Therefore, it is necessary and beneficial to develop natural products with antibacterial activity [441].

The biocomposite CNC/ZnO NPs.M2 was chosen to be the most optimum sample with the optical and morphological properties with anti-microbial activities tested. Regarding our antifungal activity results, they are interesting. Therefore, further studies on the preparation conditions of this compound are required to pave the way for the development of potential new drugs for the treatment of drug-resistant opportunistic fungal infections.

The antibacterial mechanisms of CNC/ZnO NPs

Antimicrobials are defined as substances used to destroy microorganisms or prevent their growth and include antibiotics and other antibacterial and antifungal agents. The biocomposite mixture is thought to be able to inhibit microbes by several mechanisms.

The first mechanism suggests that CNC/ZnO NPs enable the formation of reactive oxygen species (ROS) such as hydroxyl ions and hydrogen peroxide, which causes oxidative stress and damages the cell membrane and DNA, leading to bacterial death [439, 442].

The second mechanism by the dissolution of CNC/ZnO NPs into zinc ions, which is known to inhibit several bacterial cells activities by destroying the structure of cell walls and denaturing proteins, interfering with enzymeand amino acid metabolisms causing bacterial death [395, 443, 444].

The third mechanism propose that CNC/ZnO NPs interact directly with cell membrane through electrostatic forces, which damages the membrane plasma, and causes intracellular content leaks[437, 445, 446].

This happends because the process of inhibiting the growth of microorganisms is generally caused by several things including the presence of disruptive compounds on the cell walls, causing increased cell membrane permeability resulting in loss of cell components, inactivity of enzymes in cells, and the process of destruction or damage to genetic material [447, 448].

Conclusion

Cellulose, which is found in abundance on Earth, is the primary building block of plant cell walls. Its chemical properties allow for modification, making it useful in a wide range of applications. The originality of this work is the good results that were found based on the recycling of plant waste represented in peanut shells and pea shells. In this work, CNCs were extracted from peanut shells by acid treatment method using different concentrations of H_2SO_4 solution (36%, 38%, and 40%) as a shape, size, and crystallinity index.

The particle size of CNCs from different C_{H2SO4} = (36%, 38%, and 40%) are 11.82 nm, 11.90 nm, and 8.88 nm, and the crystallinity index is 69.71%, 68.75%, and 77.95%, respectively. Also, with acid treatment method was used to obtain CNCs from pea shells by using an H_2SO_4 solution (concentration = 40%) as a shape, size, and crystallinity index. The particle size of CNCs is 12.28nm, and the crystallinity index is 73.38%.

Then, the CNC/ZnO NPs compound was prepared by two different techniques. In the first stage, we relied on the first technique of dissolving cellulose in a basic

solution, while in the second technique, we used cellulose crystals directly without dissolving them. In the second stage, ZnO NPs were prepared by sol-gel synthesis method on the CNCs. The particle size of CNC/ZnO NPs from the first method and second methods is 20.14 nm and 27.31 nm, and the band gap energies are 3.66 eV and 3.66 eV, respectively from peanut shells. Also, from pea shells, the particle size of CNC/ZnO NPs from the first technique and second technique from pea shells is 19.64 nm and 19.99 nm, and the band gap energies are 3.27 eV and 3.27 eV, respectively.

The Cs and CNC/ZnO NPs prepared by second methods extracted from peanut shells and pea shells were tested in removing methyl blue dye by adsorption process. Various variables were studied (mass, contact time, initial concentration, pH, and temperature).

From the obtained results, an unexpected opposite result was shown that Cs alone were more efficient than the CNC/ZnO NPs in removing BM dye.Upon adsorption of positive MB dye, the adsorption results obtained by cellulose were better than cellulose modified with zinc oxide. The equilibration time is almost identical for all kinetics performed between 5 to 75 minutes for all studied concentrations. An increase in the mass, initial concentration, and pH of dye leads to an increase in the amount adsorbed on the surface of the different adsorbents.

The higher the temperature, the more positive effect (increased adsorption capacity) on the CNC/ZnO NPs but on the pure Cs is the negative effect (decreased adsorption capacity).The maximum adsorption capacity (Qmax) of BM dye for Cs and CNC/ZnO NPs extracted from peanut shells are 69.01 and 39.5 mg/g, respectively. For Cs and CNC/ZnO NPs extracted from pea shells are 45.48 and 27.22 mg/g, respectively.

Adsorption kinetics The adsorption process takes place in two steps: a very fast first phase of less than 30 minutes duration and a second phase of equilibrium after 30 minutes. These kinetics have been modeled by several models, the model that best describes experimental results is the pseudo-second-order model.

The antimicrobial activities of biosynthesized CNC/ZnO NPs synthesized by two different methods from peanut shells and pea shells were tested using the well diffusion method.

all samples of CNC/ZnO NPs have shown significant antibacterial activity against both gram-positive and gram-negative bacteria and fungi. However, the activity was strongly influenced by the method used for the synthesis of CNC/ZnO NPs; higher antimicrobial activities were obtained in samples synthesized by the first method.

References

1. Carmen, Z. and S. Daniela, *Textile organic dyes-characteristics, polluting effects and separation/elimination procedures from industrial effluents-a critical overview*. Vol. 3. 2012: IntechOpen Rijeka.
2. Mu, B., et al., *A water/cottonseed oil bath with controllable dye sorption for high dyeing quality and minimum discharges.* Journal of cleaner production, 2019. **236**: p. 117566.
3. Feng, J., B. Xing, and H. Chen, *Catalytic ozonation of humic acid in water with modified activated carbon: Enhancement and restoration of the activity of an activated carbon catalyst.* Journal of environmental management, 2019. **237**: p. 114-118.
4. Maleki, S.S., K. Mohammadi, and K.-s. Ji, *Characterization of cellulose synthesis in plant cells.* The Scientific World Journal, 2016. **2016**.
5. Adel, A.M., et al., *Influence of cellulose polymorphism on tunable mechanical and barrier properties of chitosan/oxidized nanocellulose bio-composites.* Egyptian Journal of Chemistry, 2017. **60**(4): p. 639-652.
6. Klemm, D., et al., *Nanocelluloses: a new family of nature-based materials.* Angewandte Chemie International Edition, 2011. **50**(24): p. 5438-5466.
7. Salem, S.S., et al., *A comprehensive review of nanomaterials: Types, synthesis, characterization, and applications.* Biointerface Res. Appl. Chem, 2022. **13**(1): p. 41.
8. Salem, S.S. and A. Fouda, *Green synthesis of metallic nanoparticles and their prospective biotechnological applications: an overview.* Biological trace element research, 2021. **199**: p. 344-370.
9. He, X., et al., *Cellulose and cellulose derivatives: Different colloidal states and food-related applications.* Carbohydrate Polymers, 2021. **255**: p. 117334.
10. Huang, C., et al., *A comprehensive investigation on cellulose nanocrystals with different crystal structures from cotton via an efficient route.* Carbohydrate Polymers, 2022. **276**: p. 118766.
11. Shaghaleh, H., X. Xu, and S. Wang, *Current progress in production of biopolymeric materials based on cellulose, cellulose nanofibers, and cellulose derivatives.* RSC advances, 2018. **8**(2): p. 825-842.
12. Zhao, J., et al., *Room temperature preparation of cellulose nanocrystals with high yield via a new ZnCl2 solvent system.* Carbohydrate Polymers, 2022. **278**: p. 118946.
13. Elfeky, A.S., et al., *Multifunctional cellulose nanocrystal/metal oxide hybrid, photo-degradation, antibacterial and larvicidal activities.* Carbohydrate polymers, 2020. **230**: p. 115711.
14. Abu-Elghait, M., et al., *Ecofriendly novel synthesis of tertiary composite based on cellulose and myco-synthesized selenium nanoparticles: Characterization, antibiofilm and biocompatibility.* International Journal of Biological Macromolecules, 2021. **175**: p. 294-303.
15. Al-Shemy, M.T., A. El-Shafie, and A. Alaneny, *Facile in-situ synthesis of nanocrystalline celluloses-silver bio-nanocomposite for chitosan based active packaging.* Egyptian Journal of Chemistry, 2022.
16. Król, A., et al., *Zinc oxide nanoparticles: Synthesis, antiseptic activity and toxicity mechanism.* Advances in colloid and interface science, 2017. **249**: p. 37-52.

17. Wu, J. and D. Xue, *Progress of science and technology of ZnO as advanced material.* Science of Advanced Materials, 2011. **3**(2): p. 127-149.
18. Wasim, M., et al., *An overview of Zn/ZnO modified cellulosic nanocomposites and their potential applications.* Journal of Polymer Research, 2021. **28**(9): p. 338.
19. Li, H., et al., *Preparation and characterization of carboxymethyl cellulose-based composite films reinforced by cellulose nanocrystals derived from pea hull waste for food packaging applications.* International Journal of Biological Macromolecules, 2020. **164**: p. 4104-4112.
20. Shi, C., et al., *Construction of Ag–ZnO/cellulose nanocomposites via tunable cellulose size for improving photocatalytic performance.* Journal of Cleaner Production, 2021. **288**: p. 125089.
21. Lim, Z., et al., *A facile approach towards ZnO nanorods conductive textile for room temperature multifunctional sensors.* Sensors and Actuators B: Chemical, 2010. **151**(1): p. 121-126.
22. Ramsden, J., *Essentials of nanotechnology*. 2008: BookBoon.
23. Borm, P.J., et al., *The potential risks of nanomaterials: a review carried out for ECETOC.* Particle and fibre toxicology, 2006. **3**: p. 1-35.
24. Show, P.L., W.S. Chai, and T.C. Ling, *Microalgae for Environmental Biotechnology: Smart Manufacturing and Industry 4.0 Applications*. 2022: CRC Press.
25. O'Malley, S.M., *Computational methods for contrast-enhanced intravascular ultrasound sequence analysis*. 2007: University of Houston.
26. Baig, N., I. Kammakakam, and W. Falath, *Nanomaterials: A review of synthesis methods, properties, recent progress, and challenges.* Materials Advances, 2021. **2**(6): p. 1821-1871.
27. Janssen, M.H., et al., *Evaluation of the performance of immobilized penicillin G acylase using active-site titration.* Biotechnology and bioengineering, 2002. **78**(4): p. 425-432.
28. Sheldon, R.A., *Enzyme immobilization: the quest for optimum performance.* Advanced Synthesis & Catalysis, 2007. **349**(8-9): p. 1289-1307.
29. NANOMATERIAUX, L., *Effets sur la santé de l'homme et sur l'environnement*. 2006, Afsset July.
30. Seshan, K., *Handbook of thin film deposition techniques principles, methods, equipment and applications, second editon*. 2002: CRC Press.
31. Robbie, K., et al., *Designed Nanoparticles*. 2007, unpublished.
32. BOUAFIA, A., *Optimisation de biosynthèse des nanoparticules d'oxyde de fer par l'utilisation de différents extraits des plantes et évaluation de leur activité biologique*. 2022, Universty of Eloued جامعة الشهيد حمه لخضر.
33. Yan, K., T. Lafleur, and J. Liao, *Facile synthesis of palladium nanoparticles supported on multi-walled carbon nanotube for efficient hydrogenation of biomass-derived levulinic acid.* Journal of nanoparticle research, 2013. **15**: p. 1-7.
34. Ostiguy, C., et al., *Les nanoparticules de synthèse-Connaissances actuelles sur les risques et les mesures de prévention en SST-2e édition.* 2010.
35. Ealia, S.A.M. and M. Saravanakumar. *A review on the classification, characterisation, synthesis of nanoparticles and their application*. in *IOP conference series: materials science and engineering*. 2017. IOP Publishing.
36. Singh, A.K., *Engineered nanoparticles: structure, properties and mechanisms of toxicity*. 2015: Academic Press.

37. Salavati-Niasari, M., F. Davar, and N. Mir, *Synthesis and characterization of metallic copper nanoparticles via thermal decomposition.* Polyhedron, 2008. **27**(17): p. 3514-3518.
38. Tai, C.Y., et al., *Synthesis of magnesium hydroxide and oxide nanoparticles using a spinning disk reactor.* Industrial & engineering chemistry research, 2007. **46**(17): p. 5536-5541.
39. Aitken, R.J., et al., *Manufacture and use of nanomaterials: current status in the UK and global trends.* Occupational medicine, 2006. **56**(5): p. 300-306.
40. Kroto, H.W., et al., *C60: Buckminsterfullerene.* nature, 1985. **318**(6042): p. 162-163.
41. Sano, N., et al., *Synthesis of carbon'onions' in water.* Nature, 2001. **414**(6863): p. 506-507.
42. Chandra, S., et al., *Synthesis, functionalization and bioimaging applications of highly fluorescent carbon nanoparticles.* Nanoscale, 2011. **3**(4): p. 1533-1540.
43. Ramesh, S., *Sol-Gel Synthesis and Characterization of Ag.* 2013.
44. Mann, S., et al., *Sol− gel synthesis of organized matter.* Chemistry of materials, 1997. **9**(11): p. 2300-2310.
45. Dazzazi, A., *Synthèse et caractérisation de nanoparticules d'oxydes métalliques par voie organométallique: vers des applications biomédicales*. 2013, Toulouse 3.
46. Bhaviripudi, S., et al., *CVD synthesis of single-walled carbon nanotubes from gold nanoparticle catalysts.* Journal of the American Chemical Society, 2007. **129**(6): p. 1516-1517.
47. Adachi, M., S. Tsukui, and K. Okuyama, *Nanoparticle synthesis by ionizing source gas in chemical vapor deposition.* Japanese journal of applied physics, 2003. **42**(1A): p. L77.
48. Kuppusamy, P., et al., *Biosynthesis of metallic nanoparticles using plant derivatives and their new avenues in pharmacological applications–An updated report.* Saudi Pharmaceutical Journal, 2016. **24**(4): p. 473-484.
49. حليلو, سهيلة, and بريبش, *Mise en oeuvre et valorisation de nanoparticules d'oxyde de fer obtenu par méthode verte.* 2021.
50. Hasan, S., *A review on nanoparticles: their synthesis and types.* Res. J. Recent Sci, 2015. **2277**: p. 2502.
51. Kammler, H.K., L. Mädler, and S.E. Pratsinis, *Flame synthesis of nanoparticles.* Chemical Engineering & Technology: Industrial Chemistry-Plant Equipment-Process Engineering-Biotechnology, 2001. **24**(6): p. 583-596.
52. D'Amato, R., et al., *Synthesis of ceramic nanoparticles by laser pyrolysis: from research to applications.* Journal of analytical and applied pyrolysis, 2013. **104**: p. 461-469.
53. Mohammadi, S., A. Harvey, and K.V. Boodhoo, *Synthesis of TiO2 nanoparticles in a spinning disc reactor.* Chemical Engineering Journal, 2014. **258**: p. 171-184.
54. Amendola, V. and M. Meneghetti, *Laser ablation synthesis in solution and size manipulation of noble metal nanoparticles.* Physical chemistry chemical physics, 2009. **11**(20): p. 3805-3821.
55. Shah, P. and A. Gavrin, *Synthesis of nanoparticles using high-pressure sputtering for magnetic domain imaging.* Journal of magnetism and magnetic materials, 2006. **301**(1): p. 118-123.

56. Khan, Y., et al., *Classification, synthetic, and characterization approaches to nanoparticles, and their applications in various fields of nanotechnology: a review.* Catalysts, 2022. **12**(11): p. 1386.
57. Lugscheider, E., et al., *Magnetron-sputtered hard material coatings on thermoplastic polymers for clean room applications.* Surface and Coatings Technology, 1998. **108**: p. 398-402.
58. Yadav, T.P., R.M. Yadav, and D.P. Singh, *Mechanical milling: a top down approach for the synthesis of nanomaterials and nanocomposites.* Nanoscience and Nanotechnology, 2012. **2**(3): p. 22-48.
59. Pimpin, A. and W. Srituravanich, *Review on micro-and nanolithography techniques and their applications.* Engineering Journal, 2012. **16**(1): p. 37-56.
60. Hulteen, J.C., et al., *Nanosphere lithography: size-tunable silver nanoparticle and surface cluster arrays.* The Journal of Physical Chemistry B, 1999. **103**(19): p. 3854-3863.
61. Buffet, P.-E., *Évaluation du risque environnemental des nanoparticules métalliques: biodisponibilité et risque potentiel pour deux espèces clés des écosystèmes estuariens*. 2012, Nantes.
62. Li, W., *Elaboration par un procédé de précipitation de nanoparticules aux propriétés contrôlées: application à la magnétite*. 2011, Institut National Polytechnique de Lorraine.
63. Bhagyaraj, S.M. and O.S. Oluwafemi, *Nanotechnology: the science of the invisible*, in *Synthesis of inorganic nanomaterials*. 2018, Elsevier. p. 1-18.
64. Khan, I., K. Saeed, and I. Khan, *Review nanoparticles: properties, applications and toxicities.* Arab J Chem, 2019. **12**(2): p. 908-931.
65. Huang, C., et al., *Effect of structure: A new insight into nanoparticle assemblies from inanimate to animate.* Science advances, 2020. **6**(20): p. eaba1321.
66. Reghunadhan, A., N. Kalarikkal, and S. Thomas, *Mechanical property analysis of nanomaterials*, in *Characterization of Nanomaterials*. 2018, Elsevier. p. 191-212.
67. Fernández-García, M. and J. Rodriguez, *Metal Oxide Nanoparticles, Encycl. Inorg.* Bioinorg. Chem, 2011: p. 1-11.
68. Ivanova, A., *Nanoporous metal oxides templated by nanocrystalline cellulose: synthesis and applications in photovoltaics and photocatalysis*. 2015, München, Ludwig-Maximilians-Universität, Diss., 2015.
69. Xie, Y., et al., *Antibacterial activity and mechanism of action of zinc oxide nanoparticles against Campylobacter jejuni.* Applied and environmental microbiology, 2011. **77**(7): p. 2325-2331.
70. Martin, P.M., et al., *Piezoelectric films for 100-MHz ultrasonic transducers.* Thin Solid Films, 2000. **379**(1-2): p. 253-258.
71. Brown, H.E., *Zinc oxide rediscovered*. 1957: New Jersey Zinc Company.
72. Wyckoff, R., *Crystal Structures, Vol. 1, Interscience Publ.* Inc., New York, 1963.
73. Kim, N.H. and H.W. Kim, *Room temperature growth of zinc oxide films on Si substrates by the RF magnetron sputtering.* Materials Letters, 2004. **58**(6): p. 938-943.
74. Desgreniers, S., *High-density phases of ZnO: Structural and compressive parameters.* Physical Review B, 1998. **58**(21): p. 14102.

75. Muthukumar, P., et al., *Structural and optical properties of zno nano particles grown on copper substrate by electrodeposition method.* Dig J Nanomater Biostruct, 2013. **8**: p. 1455-1459.
76. Mahamuni, P.P., et al., *Synthesis and characterization of zinc oxide nanoparticles by using polyol chemistry for their antimicrobial and antibiofilm activity.* Biochemistry and biophysics reports, 2019. **17**: p. 71-80.
77. Klingshirn, C.F., et al., *Zinc oxide: from fundamental properties towards novel applications.* 2010.
78. Bowker, M., et al., *The mechanism of methanol synthesis on copper/zinc oxide/alumina catalysts.* Journal of Catalysis, 1988. **109**(2): p. 263-273.
79. Saji, K., N. Joshy, and M. Jayaraj, *Optical emission spectroscopic studies on laser ablated zinc oxide plasma.* Journal of applied physics, 2006. **100**(4): p. 043302.
80. Donnay, J.D.H., *Crystal Data: Inorganic compounds*. Vol. 2. 1973: National Bureau of Standards.
81. Chen, S., et al., *YM lu, JY Zhang, DZ Shen, XW Fa.* Journal of Crystal Growth, 2002. **240**: p. 467-472.
82. Perrin, J., et al., *A-Si: H deposition from SiH4 and Si2H6 RF-discharges: Pressure and temperature dependence of film growth in relation to α-γ discharge transition.* Japanese journal of applied physics, 1988. **27**(11R): p. 2041.
83. Michel, H.-J., et al., *Adsorbates and their effects on gas sensing properties of sputtered SnO2 films.* Applied surface science, 1998. **126**(1-2): p. 57-64.
84. Rastogi, A., et al., *Biological synthesis of nanoparticles: An environmentally benign approach*, in *Fundamentals of Nanoparticles*. 2018, Elsevier. p. 571-604.
85. Nicolosi, A., *Effet de l'exposition périnatale aux nanoparticules d'oxyde de zinc sur l'activité des réseaux de neurones moteurs impliqués dans les fonctions respiratoire et locomotrice*. 2017, Université de Bordeaux.
86. Shaltouki, P., et al., *Synthesis and characterization of nanoparticles propolis using beeswax.* Iranian Journal of Chemistry and Chemical Engineering, 2019. **38**(2): p. 9-19.
87. Zhang, Y., et al., *Biomedical applications of zinc oxide nanomaterials.* Current molecular medicine, 2013. **13**(10): p. 1633-1645.
88. Dadi, R., *Synthèse de nanoparticules d 'oxydes métalliques et leur activité antibactérienne*. 2019, Université Paris-Nord-Paris XIII.
89. Abd El Megid, A.D., et al., *Biochemical role of zinc oxide and propolis nanoparticles in protection rabbits against coccidiosis.* Benha veterinary medical journal, 2018. **34**(1): p. 314-328.
90. Lee, H., S.B.A. Hamid, and S. Zain, *Conversion of lignocellulosic biomass to nanocellulose: structure and chemical process.* The Scientific World Journal, 2014. **2014**.
91. Burhenne, L., et al., *The effect of the biomass components lignin, cellulose and hemicellulose on TGA and fixed bed pyrolysis.* Journal of Analytical and Applied Pyrolysis, 2013. **101**: p. 177-184.
92. Demirbaş, A., *Estimating of structural composition of wood and non-wood biomass samples.* Energy Sources, 2005. **27**(8): p. 761-767.
93. Li, X., et al., *Determination of hemicellulose, cellulose and lignin in moso bamboo by near infrared spectroscopy.* Scientific reports, 2015. **5**(1): p. 1-11.

94. Zabed, H., et al., *Fuel ethanol production from lignocellulosic biomass: an overview on feedstocks and technological approaches.* Renewable and sustainable energy reviews, 2016. **66**: p. 751-774.
95. Scheller, H.V. and P. Ulvskov, *Hemicelluloses.* Annual review of plant biology, 2010. **61**: p. 263-289.
96. Sella Kapu, N. and H.L. Trajano, *Review of hemicellulose hydrolysis in softwoods and bamboo.* Biofuels, Bioproducts and Biorefining, 2014. **8**(6): p. 857-870.
97. Gírio, F.M., et al., *Hemicelluloses for fuel ethanol: a review.* Bioresource technology, 2010. **101**(13): p. 4775-4800.
98. Azadi, P., et al., *Liquid fuels, hydrogen and chemicals from lignin: A critical review.* Renewable and Sustainable Energy Reviews, 2013. **21**: p. 506-523.
99. Wang, H., M. Tucker, and Y. Ji, *Recent development in chemical depolymerization of lignin: a review.* J. Appl. Chem, 2013. **2013**(9).
100. Isikgor, F.H. and C.R. Becer, *Lignocellulosic biomass: a sustainable platform for the production of bio-based chemicals and polymers.* Polymer Chemistry, 2015. **6**(25): p. 4497-4559.
101. Liu, W.-J., H. Jiang, and H.-Q. Yu, *Thermochemical conversion of lignin to functional materials: a review and future directions.* Green Chemistry, 2015. **17**(11): p. 4888-4907.
102. Olivera, S., et al., *Potential applications of cellulose and chitosan nanoparticles/composites in wastewater treatment: A review.* Carbohydrate polymers, 2016. **153**: p. 600-618.
103. Maiti, S., et al., *Preparation and characterization of nano-cellulose with new shape from different precursor.* Carbohydrate polymers, 2013. **98**(1): p. 562-567.
104. Si, J., et al., *Biomimetic composite scaffolds based on mineralization of hydroxyapatite on electrospun poly (ε-caprolactone)/nanocellulose fibers.* Carbohydrate polymers, 2016. **143**: p. 270-278.
105. Khalil, H.A., A. Bhat, and A.I. Yusra, *Green composites from sustainable cellulose nanofibrils: A review.* Carbohydrate polymers, 2012. **87**(2): p. 963-979.
106. Isogai, A., *Wood nanocelluloses: fundamentals and applications as new bio-based nanomaterials.* Journal of wood science, 2013. **59**: p. 449-459.
107. Nechyporchuk, O., M.N. Belgacem, and J. Bras, *Production of cellulose nanofibrils: A review of recent advances.* Industrial Crops and Products, 2016. **93**: p. 2-25.
108. Park, Y., W. Doherty, and P.J. Halley, *Developing lignin-based resin coatings and composites.* Industrial crops and products, 2008. **27**(2): p. 163-167.
109. Mahmoud, M.E., et al., *Solid–solid crosslinking of carboxymethyl cellulose nanolayer on titanium oxide nanoparticles as a novel biocomposite for efficient removal of toxic heavy metals from water.* International journal of biological macromolecules, 2017. **105**: p. 1269-1278.
110. Ioelovich, M., *Cellulose as a nanostructured polymer: a short review.* BioResources, 2008. **3**(4): p. 1403-1418.
111. Yahya, M., et al., *Reuse of selected lignocellulosic and processed biomasses as sustainable sources for the fabrication of nanocellulose via Ni (II)-catalyzed hydrolysis approach: a comparative study.* Journal of Polymers and the Environment, 2018. **26**: p. 2825-2844.

112. Hokkanen, S., A. Bhatnagar, and M. Sillanpää, *A review on modification methods to cellulose-based adsorbents to improve adsorption capacity.* Water research, 2016. **91**: p. 156-173.
113. Kumar, R., R.K. Sharma, and A.P. Singh, *Cellulose based grafted biosorbents-Journey from lignocellulose biomass to toxic metal ions sorption applications-A review.* Journal of Molecular Liquids, 2017. **232**: p. 62-93.
114. Postek, M.T., et al., *Ionizing radiation processing and its potential in advancing biorefining and nanocellulose composite materials manufacturing.* Radiation Physics and Chemistry, 2018. **143**: p. 47-52.
115. Marett, J., A. Aning, and E.J. Foster, *The isolation of cellulose nanocrystals from pistachio shells via acid hydrolysis.* Industrial Crops and Products, 2017. **109**: p. 869-874.
116. Abdelhamid, H.N. and A.P. Mathew, *Cellulose-based materials for water remediation: adsorption, catalysis, and antifouling.* Frontiers in Chemical Engineering, 2021: p. 74.
117. Bacakova, L., et al., *Versatile application of nanocellulose: From industry to skin tissue engineering and wound healing.* Nanomaterials, 2019. **9**(2): p. 164.
118. Phanthong, P., et al., *Nanocellulose: Extraction and application.* Carbon Resources Conversion, 2018. **1**(1): p. 32-43.
119. Mondal, S., *Preparation, properties and applications of nanocellulosic materials.* Carbohydrate polymers, 2017. **163**: p. 301-316.
120. Lavoine, N., et al., *Microfibrillated cellulose–Its barrier properties and applications in cellulosic materials: A review.* Carbohydrate polymers, 2012. **90**(2): p. 735-764.
121. Moon, R.J., et al., *Cellulose nanomaterials review: structure, properties and nanocomposites.* Chemical Society Reviews, 2011. **40**(7): p. 3941-3994.
122. Habibi, Y., L.A. Lucia, and O.J. Rojas, *Cellulose nanocrystals: chemistry, self-assembly, and applications.* Chemical reviews, 2010. **110**(6): p. 3479-3500.
123. Jonas, R. and L.F. Farah, *Production and application of microbial cellulose.* Polymer degradation and stability, 1998. **59**(1-3): p. 101-106.
124. Dufresne, A., *Comparing the mechanical properties of high performances polymer nanocomposites from biological sources.* Journal of Nanoscience and Nanotechnology, 2006. **6**(2): p. 322-330.
125. Wang, X., et al., *Fabrication and characterization of nano-cellulose aerogels via supercritical CO2 drying technology.* Materials Letters, 2016. **183**: p. 179-182.
126. Tang, Y., et al., *Extraction of cellulose nano-crystals from old corrugated container fiber using phosphoric acid and enzymatic hydrolysis followed by sonication.* Carbohydrate polymers, 2015. **125**: p. 360-366.
127. Abitbol, T., et al., *Nanocellulose, a tiny fiber with huge applications.* Current opinion in biotechnology, 2016. **39**: p. 76-88.
128. Jiang, F. and Y.-L. Hsieh, *Chemically and mechanically isolated nanocellulose and their self-assembled structures.* Carbohydrate polymers, 2013. **95**(1): p. 32-40.
129. Tonoli, G., et al., *Cellulose micro/nanofibres from Eucalyptus kraft pulp: preparation and properties.* Carbohydrate polymers, 2012. **89**(1): p. 80-88.
130. Guzman, J.T., et al., *Chemically extracted nanocellulose from sisal fibres by a simple and industrially relevant process.* Cellulose, 2017. **24**(1): p. 107-118.

131. Sirviö, J.A., et al., *Bisphosphonate nanocellulose in the removal of vanadium (V) from water.* Cellulose, 2016. **23**: p. 689-697.
132. Lin, N. and A. Dufresne, *Nanocellulose in biomedicine: Current status and future prospect.* European Polymer Journal, 2014. **59**: p. 302-325.
133. Shamskar, K.R., H. Heidari, and A. Rashidi, *Preparation and evaluation of nanocrystalline cellulose aerogels from raw cotton and cotton stalk.* Industrial Crops and Products, 2016. **93**: p. 203-211.
134. Meng, F., et al., *Extraction and characterization of cellulose nanofibers and nanocrystals from liquefied banana pseudo-stem residue.* Composites Part B: Engineering, 2019. **160**: p. 341-347.
135. Yang, X., et al., *Effects of preparation methods on the morphology and properties of nanocellulose (NC) extracted from corn husk.* Industrial Crops and Products, 2017. **109**: p. 241-247.
136. Rajinipriya, M., et al., *Importance of agricultural and industrial waste in the field of nanocellulose and recent industrial developments of wood based nanocellulose: a review.* ACS Sustainable Chemistry & Engineering, 2018. **6**(3): p. 2807-2828.
137. Dilamian, M. and B. Noroozi, *A combined homogenization-high intensity ultrasonication process for individualizaion of cellulose micro-nano fibers from rice straw.* Cellulose, 2019. **26**: p. 5831-5849.
138. Li, M., et al., *Preparation and characterization of cellulose nanofibers from de-pectinated sugar beet pulp.* Carbohydrate Polymers, 2014. **102**: p. 136-143.
139. Desmaisons, J., et al., *A new quality index for benchmarking of different cellulose nanofibrils.* Carbohydrate Polymers, 2017. **174**: p. 318-329.
140. Klemm, D., et al., *Cellulose: fascinating biopolymer and sustainable raw material.* Angewandte chemie international edition, 2005. **44**(22): p. 3358-3393.
141. Huang, Y., et al., *Recent advances in bacterial cellulose.* Cellulose, 2014. **21**: p. 1-30.
142. Panaitescu, D.M., et al., *Structural and morphological characterization of bacterial cellulose nano-reinforcements prepared by mechanical route.* Materials & Design, 2016. **110**: p. 790-801.
143. Lin, S.-P., et al., *Biosynthesis, production and applications of bacterial cellulose.* Cellulose, 2013. **20**(5): p. 2191-2219.
144. Jozala, A.F., et al., *Bacterial nanocellulose production and application: a 10-year overview.* Applied microbiology and biotechnology, 2016. **100**: p. 2063-2072.
145. Castro, C., et al., *Structural characterization of bacterial cellulose produced by Gluconacetobacter swingsii sp. from Colombian agroindustrial wastes.* Carbohydrate Polymers, 2011. **84**(1): p. 96-102.
146. Iguchi, M., S. Yamanaka, and A. Budhiono, *Bacterial cellulose—a masterpiece of nature's arts.* Journal of materials science, 2000. **35**(2): p. 261-270.
147. Kiziltas, E.E., et al., *Preparation and characterization of transparent PMMA–cellulose-based nanocomposites.* Carbohydrate polymers, 2015. **127**: p. 381-389.
148. Zhang, Z.-Y., et al., *A biocompatible bacterial cellulose/tannic acid composite with antibacterial and anti-biofilm activities for biomedical applications.* Materials Science and Engineering: C, 2020. **106**: p. 110249.

149. Zhang, X., et al., *Preparation and characterization of cellulose nanofiber/zinc oxide composite films.* Journal of Biobased Materials and Bioenergy, 2020. **14**(2): p. 203-208.
150. Berglund, L.A. and T. Peijs, *Cellulose biocomposites—from bulk moldings to nanostructured systems.* MRS bulletin, 2010. **35**(3): p. 201-207.
151. Chinga-Carrasco, G., *Cellulose fibres, nanofibrils and microfibrils: The morphological sequence of MFC components from a plant physiology and fibre technology point of view.* Nanoscale research letters, 2011. **6**(1): p. 1-7.
152. Li, Q.Q., *Nanocellulose: Preparation, characterization, supramolecular modeling, and its life cycle assessment*. 2012, Virginia Tech.
153. Farooq, A., et al., *Structure and properties of high quality natural cellulose nano fibrils from a novel material Ficus natalensis barkcloth.* Journal of Industrial Textiles, 2021. **51**(4): p. 664-680.
154. Alemdar, A. and M. Sain, *Isolation and characterization of nanofibers from agricultural residues–Wheat straw and soy hulls.* Bioresource technology, 2008. **99**(6): p. 1664-1671.
155. Wang, B. and M. Sain, *The effect of chemically coated nanofiber reinforcement on biopolymer based nanocomposites.* BioResources, 2007. **2**(3): p. 371-388.
156. Oun, A.A. and J.-W. Rhim, *Characterization of nanocelluloses isolated from Ushar (Calotropis procera) seed fiber: Effect of isolation method.* Materials Letters, 2016. **168**: p. 146-150.
157. Osong, S.H., S. Norgren, and P. Engstrand, *Processing of wood-based microfibrillated cellulose and nanofibrillated cellulose, and applications relating to papermaking: a review.* Cellulose, 2016. **23**: p. 93-123.
158. Wang, B. and M. Sain, *Dispersion of soybean stock-based nanofiber in a plastic matrix.* Polymer International, 2007. **56**(4): p. 538-546.
159. Chen, H., et al., *A review on the pretreatment of lignocellulose for high-value chemicals.* Fuel Processing Technology, 2017. **160**: p. 196-206.
160. Yue, Y., et al., *Cellulose fibers isolated from energycane bagasse using alkaline and sodium chlorite treatments: Structural, chemical and thermal properties.* Industrial Crops and Products, 2015. **76**: p. 355-363.
161. Zheng, H., *Production of fibrillated cellulose materials-Effects of pretreatments and refining strategy on pulp properties*. 2014.
162. Siqueira, G., et al., *Morphological investigation of nanoparticles obtained from combined mechanical shearing, and enzymatic and acid hydrolysis of sisal fibers.* Cellulose, 2010. **17**: p. 1147-1158.
163. Penttilä, P.A., et al., *Small-angle scattering study of structural changes in the microfibril network of nanocellulose during enzymatic hydrolysis.* Cellulose, 2013. **20**: p. 1031-1040.
164. Wahlström, R. and A. Suurnäkki, *Enzymatic hydrolysis of lignocellulosic polysaccharides in the presence of ionic liquids.* Green Chemistry, 2015. **17**(2): p. 694-714.
165. Nasir, M., et al., *Laccase, an Emerging Tool to Fabricate Green Composites: A Review.* BioResources, 2015. **10**(3).
166. Nasir, M., et al., *Laccase application in medium density fibreboard to prepare a bio-composite.* RSC advances, 2014. **4**(22): p. 11520-11527.
167. Henriksson, M. and L.A. Berglund, *Structure and properties of cellulose nanocomposite films containing melamine formaldehyde.* Journal of applied polymer science, 2007. **106**(4): p. 2817-2824.

168. López-Rubio, A., et al., *Enhanced film forming and film properties of amylopectin using micro-fibrillated cellulose.* Carbohydrate Polymers, 2007. **68**(4): p. 718-727.
169. Siddiqui, N., et al., *Production and characterization of cellulose nanofibers from wood pulp.* Journal of Adhesion Science and Technology, 2011. **25**(6-7): p. 709-721.
170. Janardhnan, S. and M.M. Sain, *Targeted disruption of hydroxyl chemistry and crystallinity in natural fibers for the isolation of cellulose nano-fibers via enzymatic treatment.* BioResources, 2011. **6**(2): p. 1242-1250.
171. Pinkert, A., et al., *Ionic liquids and their interaction with cellulose.* Chemical reviews, 2009. **109**(12): p. 6712-6728.
172. Kuzina, S.I., I.A. Shilova, and I.M. Al'fa, *Chemical and radiation-chemical radical reactions in lignocellulose materials.* Radiation Physics and Chemistry, 2011. **80**(9): p. 937-946.
173. Li, J., et al., *Homogeneous isolation of nanocellulose from sugarcane bagasse by high pressure homogenization.* Carbohydrate polymers, 2012. **90**(4): p. 1609-1613.
174. Fukaya, Y., et al., *Cellulose dissolution with polar ionic liquids under mild conditions: required factors for anions.* Green Chemistry, 2008. **10**(1): p. 44-46.
175. Zhu, S., et al., *Dissolution of cellulose with ionic liquids and its application: a mini-review.* Green Chemistry, 2006. **8**(4): p. 325-327.
176. Phanthong, P., et al., *A facile one-step way for extraction of nanocellulose with high yield by ball milling with ionic liquid.* Cellulose, 2017. **24**: p. 2083-2093.
177. Xiao, Y.T., W.L. Chin, and S.B. Abd Hamid. *Facile preparation of highly crystalline nanocellulose by using ionic liquid*. in *Advanced materials research*. 2015. Trans Tech Publ.
178. Lazko, J., et al., *Well defined thermostable cellulose nanocrystals via two-step ionic liquid swelling-hydrolysis extraction.* Cellulose, 2014. **21**: p. 4195-4207.
179. El Achaby, M., et al., *Production of cellulose nanocrystals from vine shoots and their use for the development of nanocomposite materials.* International journal of biological macromolecules, 2018. **117**: p. 592-600.
180. Suhara, P., et al., *Improving cellulose nanofibrillation of non-wood fiber using alkaline and bleaching pre-treatments.* Volume 131, Pags. 203-212, 2019.
181. Kargarzadeh, H., et al., *Effects of hydrolysis conditions on the morphology, crystallinity, and thermal stability of cellulose nanocrystals extracted from kenaf bast fibers.* Cellulose, 2012. **19**(3): p. 855-866.
182. Peng, B.L., et al., *Chemistry and applications of nanocrystalline cellulose and its derivatives: a nanotechnology perspective.* The Canadian journal of chemical engineering, 2011. **89**(5): p. 1191-1206.
183. Xiang, Q., et al. *Heterogeneous aspects of acid hydrolysis of α-cellulose*. in *Biotechnology for Fuels and Chemicals: The Twenty-Fourth Symposium*. 2003. Springer.
184. Rånby, B.G., A. Banderet, and L.G. Sillén, *Aqueous Colloidal Solutions of Cellulose Micelles.* Acta Chemica Scandinavica, 1949. **3**: p. 649-650.
185. Bondeson, D., A. Mathew, and K. Oksman, *Optimization of the isolation of nanocrystals from microcrystalline cellulose by acid hydrolysis.* Cellulose, 2006. **13**: p. 171-180.

186. Dong, X.M., J.-F. Revol, and D.G. Gray, *Effect of microcrystallite preparation conditions on the formation of colloid crystals of cellulose.* Cellulose, 1998. **5**: p. 19-32.
187. Yue, Y., et al., *Comparative properties of cellulose nano-crystals from native and mercerized cotton fibers.* Cellulose, 2012. **19**: p. 1173-1187.
188. Sinko, R., X. Qin, and S. Keten, *Interfacial mechanics of cellulose nanocrystals.* Mrs Bulletin, 2015. **40**(4): p. 340-348.
189. Johar, N., I. Ahmad, and A. Dufresne, *Extraction, preparation and characterization of cellulose fibres and nanocrystals from rice husk.* Industrial Crops and Products, 2012. **37**(1): p. 93-99.
190. Sacui, I.A., et al., *Comparison of the properties of cellulose nanocrystals and cellulose nanofibrils isolated from bacteria, tunicate, and wood processed using acid, enzymatic, mechanical, and oxidative methods.* ACS applied materials & interfaces, 2014. **6**(9): p. 6127-6138.
191. Yu, H.-Y., et al., *Comparison of the reinforcing effects for cellulose nanocrystals obtained by sulfuric and hydrochloric acid hydrolysis on the mechanical and thermal properties of bacterial polyester.* Composites Science and Technology, 2013. **87**: p. 22-28.
192. Amaral-Labat, G., et al., *"Blue glue": A new precursor of carbon aerogels.* Microporous and mesoporous materials, 2012. **158**: p. 272-280.
193. Keerati-U-Rai, M. and M. Corredig, *Effect of dynamic high pressure homogenization on the aggregation state of soy protein.* Journal of Agricultural and Food Chemistry, 2009. **57**(9): p. 3556-3562.
194. Khalil, H.A., et al., *Production and modification of nanofibrillated cellulose using various mechanical processes: a review.* Carbohydrate polymers, 2014. **99**: p. 649-665.
195. Frone, A.N., et al., *Preparation and characterization of PVA composites with cellulose nanofibers obtained by ultrasonication.* BioResources, 2011. **6**(1): p. 487-512.
196. Siró, I. and D. Plackett, *Microfibrillated cellulose and new nanocomposite materials: a review.* Cellulose, 2010. **17**: p. 459-494.
197. Malainine, M.E., M. Mahrouz, and A. Dufresne, *Thermoplastic nanocomposites based on cellulose microfibrils from Opuntia ficus-indica parenchyma cell.* Composites Science and Technology, 2005. **65**(10): p. 1520-1526.
198. Dufresne, A., *Processing of polymer nanocomposites reinforced with polysaccharide nanocrystals.* Molecules, 2010. **15**(6): p. 4111-4128.
199. Qua, E., et al., *Preparation and characterization of poly (vinyl alcohol) nanocomposites made from cellulose nanofibers.* Journal of Applied Polymer Science, 2009. **113**(4): p. 2238-2247.
200. Baheti, V., R. Abbasi, and J. Militky, *Ball milling of jute fibre wastes to prepare nanocellulose.* World Journal of Engineering, 2012. **9**(1): p. 45-50.
201. Barakat, A., et al., *Mechanical pretreatments of lignocellulosic biomass: towards facile and environmentally sound technologies for biofuels production.* Rsc Advances, 2014. **4**(89): p. 48109-48127.
202. Ferrer, A., et al., *Valorization of residual Empty Palm Fruit Bunch Fibers (EPFBF) by microfluidization: production of nanofibrillated cellulose and EPFBF nanopaper.* Bioresource technology, 2012. **125**: p. 249-255.

203. Lee, S.-Y., et al., *Influence of chemical modification and filler loading on fundamental properties of bamboo fibers reinforced polypropylene composites.* Journal of Composite Materials, 2009. **43**(15): p. 1639-1657.
204. Chakraborty, A., M. Sain, and M. Kortschot, *Cellulose microfibrils: a novel method of preparation using high shear refining and cryocrushing.* 2005.
205. Grüneberger, F., et al., *Rheology of nanofibrillated cellulose/acrylate systems for coating applications.* Cellulose, 2014. **21**: p. 1313-1326.
206. Azeredo, H.M., M.F. Rosa, and L.H.C. Mattoso, *Nanocellulose in bio-based food packaging applications.* Industrial Crops and Products, 2017. **97**: p. 664-671.
207. Naderi, A., T. Lindström, and J. Sundström, *Carboxymethylated nanofibrillated cellulose: rheological studies.* Cellulose, 2014. **21**: p. 1561-1571.
208. Brown, E.E., et al., *Potential of nanocrystalline cellulose–fibrin nanocomposites for artificial vascular graft applications.* Biomacromolecules, 2013. **14**(4): p. 1063-1071.
209. Mandal, A. and D. Chakrabarty, *Studies on the mechanical, thermal, morphological and barrier properties of nanocomposites based on poly (vinyl alcohol) and nanocellulose from sugarcane bagasse.* Journal of Industrial and Engineering Chemistry, 2014. **20**(2): p. 462-473.
210. Boufi, S., et al., *Nanofibrillated cellulose as an additive in papermaking process: A review.* Carbohydrate polymers, 2016. **154**: p. 151-166.
211. George, J. and S. Sabapathi, *Cellulose nanocrystals: synthesis, functional properties, and applications.* Nanotechnology, science and applications, 2015: p. 45-54.
212. Kaushik, M. and A. Moores, *Nanocelluloses as versatile supports for metal nanoparticles and their applications in catalysis.* Green Chemistry, 2016. **18**(3): p. 622-637.
213. Lalia, B.S., Y.A. Samad, and R. Hashaikeh, *Nanocrystalline cellulose-reinforced composite mats for lithium-ion batteries: electrochemical and thermomechanical performance.* Journal of Solid State Electrochemistry, 2013. **17**: p. 575-581.
214. Ilyas, R., et al., *Macro to nanoscale natural fiber composites for automotive components: Research, development, and application.* Biocomposite and synthetic composites for automotive applications, 2021: p. 51-105.
215. Asyraf, M., et al., *Integration of TRIZ, Morphological Chart and ANP method for development of FRP composite portable fire extinguisher.* Polymer Composites, 2020. **41**(7): p. 2917-2932.
216. Gama, F., F. Dourado, and S. Bielecki, *Bacterial nanocellulose: from biotechnology to bio-economy*. 2016: Elsevier.
217. Zhao, S.-W., et al., *The preparation and antibacterial activity of cellulose/ZnO composite: A review.* Open Chemistry, 2018. **16**(1): p. 9-20.
218. Justh, N., et al., *Photocatalytic properties of TiO2@ polymer and TiO2@ carbon aerogel composites prepared by atomic layer deposition.* Carbon, 2019. **147**: p. 476-482.
219. Ussia, M., et al., *ZnO–pHEMA nanocomposites: an ecofriendly and reusable material for water remediation.* ACS applied materials & interfaces, 2018. **10**(46): p. 40100-40110.

220. Khalil, A.M., M.L. Hassan, and A.A. Ward, *Novel nanofibrillated cellulose/polyvinylpyrrolidone/silver nanoparticles films with electrical conductivity properties.* Carbohydrate polymers, 2017. **157**: p. 503-511.
221. Lefatshe, K., C.M. Muiva, and L.P. Kebaabetswe, *Extraction of nanocellulose and in-situ casting of ZnO/cellulose nanocomposite with enhanced photocatalytic and antibacterial activity.* Carbohydrate polymers, 2017. **164**: p. 301-308.
222. Hussein, J., et al., *Biocompatible zinc oxide nanocrystals stabilized via hydroxyethyl cellulose for mitigation of diabetic complications.* International journal of biological macromolecules, 2018. **107**: p. 748-754.
223. Khalid, A., et al., *Bacterial cellulose-zinc oxide nanocomposites as a novel dressing system for burn wounds.* Carbohydrate polymers, 2017. **164**: p. 214-221.
224. Shefa, A.A., et al., *Investigation of efficiency of a novel, zinc oxide loaded TEMPO-oxidized cellulose nanofiber based hemostat for topical bleeding.* International journal of biological macromolecules, 2019. **126**: p. 786-795.
225. Chaudhry, Q., et al., *Applications and implications of nanotechnologies for the food sector.* Food additives and contaminants, 2008. **25**(3): p. 241-258.
226. Sorrentino, A., G. Gorrasi, and V. Vittoria, *Potential perspectives of bio-nanocomposites for food packaging applications.* Trends in food science & technology, 2007. **18**(2): p. 84-95.
227. Pirsa, S., T. Shamusi, and E.M. Kia, *Smart films based on bacterial cellulose nanofibers modified by conductive polypyrrole and zinc oxide nanoparticles.* Journal of Applied Polymer Science, 2018. **135**(34): p. 46617.
228. Ko, H.-U., et al., *Fabrication of cellulose ZnO hybrid nanocomposite and its strain sensing behavior.* Materials, 2014. **7**(10): p. 7000-7009.
229. Gullapalli, H., et al., *Flexible piezoelectric ZnO–paper nanocomposite strain sensor.* small, 2010. **6**(15): p. 1641-1646.
230. Sahoo, K., A. Biswas, and J. Nayak, *Effect of synthesis temperature on the UV sensing properties of ZnO-cellulose nanocomposite powder.* Sensors and Actuators A: Physical, 2017. **267**: p. 99-105.
231. Mun, S., et al., *Flexible cellulose and ZnO hybrid nanocomposite and its UV sensing characteristics.* Science and Technology of advanced MaTerialS, 2017. **18**(1): p. 437-446.
232. Pimentel, A., et al., *Ultra-fast microwave synthesis of ZnO nanorods on cellulose substrates for UV sensor applications.* Materials, 2017. **10**(11): p. 1308.
233. Song, P., Y.-H. Wang, and X. Liu, *Flexible physical sensors made from paper substrates integrated with zinc oxide nanostructures.* Flexible and Printed Electronics, 2017. **2**(3): p. 034001.
234. Sahoo, K., et al., *Role of hexamethylenetetramine in ZnO-cellulose nanocomposite enabled UV and humidity sensor.* Materials Science in Semiconductor Processing, 2020. **105**: p. 104699.
235. Sharma, M., et al., *Solar light assisted degradation of dyes and adsorption of heavy metal ions from water by CuO–ZnO tetrapodal hybrid nanocomposite.* Materials Today Chemistry, 2020. **17**: p. 100336.
236. Bentahar, Y., *Caractérisation physico-chimique des argiles marocaines: application à l'adsorption de l'arsenic et des colorants cationiques en solution aqueuse*. 2016, COMUE Université Côte d'Azur (2015-2019); Université Abdelmalek Essaâdi ….

237. Lai, K.C., et al., *Ice-templated graphene oxide/chitosan aerogel as an effective adsorbent for sequestration of metanil yellow dye.* Bioresource technology, 2019. **274**: p. 134-144.
238. Repo, E., et al., *Adsorption of Co (II) and Ni (II) by EDTA-and/or DTPA-modified chitosan: kinetic and equilibrium modeling.* Chemical engineering journal, 2010. **161**(1-2): p. 73-82.
239. Sokolowska-Gajda, J., H.S. Freeman, and A. Reife, *Synthetic dyes based on environmental considerations. Part 2: Iron complexes formazan dyes.* Dyes and pigments, 1996. **30**(1): p. 1-20.
240. Zare, E.N., A. Motahari, and M. Sillanpää, *Nanoadsorbents based on conducting polymer nanocomposites with main focus on polyaniline and its derivatives for removal of heavy metal ions/dyes: a review.* Environmental research, 2018. **162**: p. 173-195.
241. Ezechi, E.H., et al., *Characterization and optimization of effluent dye removal using a new low cost adsorbent: Equilibrium, kinetics and thermodynamic study.* Process Safety and Environmental Protection, 2015. **98**: p. 16-32.
242. Malik, A., *Metal bioremediation through growing cells.* Environment international, 2004. **30**(2): p. 261-278.
243. Mudhoo, A., A. Mudhoo, and D. Beekaroo, *Adsorption of reactive red 158 dye by chemically treated Cocos nucifera L. shell powder*. 2011: Springer.
244. Hethnawi, A., et al., *Polyethylenimine-functionalized pyroxene nanoparticles embedded on Diatomite for adsorptive removal of dye from textile wastewater in a fixed-bed column.* Chemical Engineering Journal, 2017. **320**: p. 389-404.
245. Kant, R., *Textile dyeing industry an environmental hazard. J Nat Sci 4 (1): 22–26*. 2012.
246. Affat, S.S., *Classifications, advantages, disadvantages, toxicity effects of natural and synthetic dyes: a review.* University of Thi-Qar Journal of Science, 2021. **8**(1): p. 130-135.
247. Anliker, R., et al., *Organic dyes and pigments.* Anthropogenic compounds, 1980: p. 181-215.
248. Mishra, G. and M. Tripathy, *A critical review of the treatments for decolourization of textile effluent.* Colourage, 1993. **40**: p. 35-35.
249. Purkait, M., S. DasGupta, and S. De, *Adsorption of eosin dye on activated carbon and its surfactant based desorption.* Journal of environmental management, 2005. **76**(2): p. 135-142.
250. Lefrère, J.-J. and P. Rouger, *Transfusion sanguine, une approche sécuritaire*. 2000: John Libbey Eurotext.
251. Danel, V. and P. Barriot, *Intoxications aiguës en réanimation*. 1999: Arnette.
252. Rafatullah, M., et al., *Adsorption of methylene blue on low-cost adsorbents: a review.* Journal of hazardous materials, 2010. **177**(1-3): p. 70-80.
253. Gulkaya, I., G.A. Surucu, and F.B. Dilek, *Importance of H2O2/Fe2+ ratio in Fenton's treatment of a carpet dyeing wastewater.* Journal of Hazardous Materials, 2006. **136**(3): p. 763-769.
254. Zhenwang, L., C. ZhenLu, and L. Jianyan. *The PT dye molecular structure and its chromophoric luminescences mechanism*. in *15th World Conference on Non-Destructive Testing*. 2000.
255. Fatiha, M. and B. Belkacem, *Adsorption of methylene blue from aqueous solutions using natural clay.* J. Mater. Environ. Sci, 2016. **7**(1): p. 285-292.
256. Lai, K.C., et al., *Environmental application of three-dimensional graphene materials as adsorbents for dyes and heavy metals: Review on ice-templating*

method and adsorption mechanisms. Journal of Environmental Sciences, 2019. **79**: p. 174-199.
257. Dassanayake, R.S., S. Acharya, and N. Abidi, *Recent advances in biopolymer-based dye removal technologies.* Molecules, 2021. **26**(15): p. 4697.
258. Ramade, F., *Dictionnaire encyclopédique des pollutions, Edition: science international.* Paris, 2000. **834**.
259. Dąbrowski, A., *Adsorption—from theory to practice.* Advances in colloid and interface science, 2001. **93**(1-3): p. 135-224.
260. Yagub, M.T., et al., *Dye and its removal from aqueous solution by adsorption: a review.* Advances in colloid and interface science, 2014. **209**: p. 172-184.
261. Pashin, J.C., *Coal as a petroleum source rock and reservoir rock,* in *Applied coal petrology*. 2008, Elsevier. p. 227-262.
262. Leonard, A. and R. Lauwerys, *Carcinogenicity and mutagenicity of chromium.* Mutation Research/Reviews in Genetic Toxicology, 1980. **76**(3): p. 227-239.
263. Mancuso, T. *Consideration of chromium as an industrial carcinogen*. in *International conference on heavy metals in the environment*. 1975. University of Toronto, Institute of Environmental Studies Toronto, Canada.
264. Daniel, S., *The adsorption on metal surfaces of long chain polar compounds from hydrocarbon solutions.* Transactions of the Faraday Society, 1951. **47**: p. 1345-1359.
265. Ahmad, A., et al., *Recent advances in new generation dye removal technologies: novel search for approaches to reprocess wastewater.* RSC advances, 2015. **5**(39): p. 30801-30818.
266. Sham, A.Y. and S.M. Notley, *Adsorption of organic dyes from aqueous solutions using surfactant exfoliated graphene.* Journal of Environmental Chemical Engineering, 2018. **6**(1): p. 495-504.
267. Jawad, A.H., et al., *Chitosan-glyoxal film as a superior adsorbent for two structurally different reactive and acid dyes: Adsorption and mechanism study.* International journal of biological macromolecules, 2019. **135**: p. 569-581.
268. Monama, G.R., et al., *Palladium deposition on copper (II) phthalocyanine/metal organic framework composite and electrocatalytic activity of the modified electrode towards the hydrogen evolution reaction.* Renewable Energy, 2018. **119**: p. 62-72.
269. Xia, L., Z. Wei, and M. Wan, *Conducting polymer nanostructures and their application in biosensors.* Journal of colloid and interface science, 2010. **341**(1): p. 1-11.
270. Shi, B., et al., *Removal of lead (II) ions from aqueous solution using Jatropha curcas L. seed husk ash as a biosorbent.* Journal of environmental quality, 2016. **45**(3): p. 984-992.
271. Nandi, B., A. Goswami, and M. Purkait, *Removal of cationic dyes from aqueous solutions by kaolin: kinetic and equilibrium studies.* Applied Clay Science, 2009. **42**(3-4): p. 583-590.
272. Lu, Y., et al., *Adsorption of Cu (II) and Ni (II) from aqueous solutions by taro stalks chemically modified with diethylenetriamine.* Environmental Science and Pollution Research, 2018. **25**: p. 17425-17433.
273. Dong, J., et al., *Adsorption of copper ion from solution by polyethylenimine modified wheat straw.* Bioresource Technology Reports, 2019. **6**: p. 96-102.

274. Qiu, H., et al., *Removal of Cu 2+ from wastewater by modified xanthan gum (XG) with ethylenediamine (EDA).* Rsc Advances, 2016. **6**(86): p. 83226-83233.
275. Hokkanen, S., E. Repo, and M. Sillanpää, *Removal of heavy metals from aqueous solutions by succinic anhydride modified mercerized nanocellulose.* Chemical engineering journal, 2013. **223**: p. 40-47.
276. Wang, C., H. Wang, and G. Gu, *Ultrasound-assisted xanthation of cellulose from lignocellulosic biomass optimized by response surface methodology for Pb (II) sorption.* Carbohydrate polymers, 2018. **182**: p. 21-28.
277. Saini, S., J.K. Katnoria, and I. Kaur, *A comparative study for removal of cadmium (II) ions using unmodified and NTA-modified Dendrocalamus strictus charcoal powder.* Journal of Environmental Health Science and Engineering, 2019. **17**: p. 259-272.
278. Jasem, N.A., *Removal of copper (II) and cadmium (II) ions from aqueous solutions using banana peels and bentonite clay as adsorbents.* Journal of Engineering and Sustainable Development, 2015. **19**(4): p. 49-68.
279. Siti, N., et al., *Adsorption process of heavy metals by low-cost adsorbent: a review.* World Applied Sciences Journal, 2013. **28**(11): p. 1518-1530.
280. Salleh, M.A.M., et al., *Cationic and anionic dye adsorption by agricultural solid wastes: a comprehensive review.* Desalination, 2011. **280**(1-3): p. 1-13.
281. Edeline, F., *L'épuration physico-chimique, théorie et technologie des eau.* Ed. Cebedoc Sprl, Liège, 1998.
282. Errais, E., *Réactivité de surface d'argiles naturelles: Etude de l'adsorption de colorants anioniques*. 2011, Strasbourg.
283. Bulut, Y. and H. Aydın, *A kinetics and thermodynamics study of methylene blue adsorption on wheat shells.* Desalination, 2006. **194**(1-3): p. 259-267.
284. Meunier, F. and L.-M. Sun, *Adsorption aspects théoriques.* Techniques de l'ingénieur Procédés de traitement des eaux potables, industrielles et urbaines base documentaire: TIB318DUO (ref. article: j2730), 2003.
285. Manole Creanga, C., *Procédé AD-OX d'élimination de polluants organiques non biodégradables: par adsorption puis oxydation catalytique*. 2007, Toulouse, INPT.
286. Dutta, S., et al., *Recent advances on the removal of dyes from wastewater using various adsorbents: A critical review.* Materials Advances, 2021. **2**(14): p. 4497-4531.
287. Kumar, A., et al., *Adsorption of phenol and 4-nitrophenol on granular activated carbon in basal salt medium: equilibrium and kinetics.* Journal of hazardous materials, 2007. **147**(1-2): p. 155-166.
288. Alasadi, A., F. Khaili, and A. Awwad, *Adsorption of Cu (II), Ni (II) and Zn (II) ions by nano kaolinite: Thermodynamics and kinetics studies.* Chemistry International, 2019. **5**(4): p. 258-26.
289. Babarinde, A. and G.O. Onyiaocha, *Equilibrium sorption of divalent metal ions onto groundnut (Arachis hypogaea) shell: kinetics, isotherm and thermodynamics.* Chem. Int, 2016. **2**(3): p. 37-46.
290. Azizian, S., *Kinetic models of sorption: a theoretical analysis.* Journal of colloid and Interface Science, 2004. **276**(1): p. 47-52.
291. Cai, Z., et al., *Electrospun polyindole nanofibers as a nano-adsorbent for heavy metal ions adsorption for wastewater treatment.* Fibers and Polymers, 2017. **18**: p. 502-513.

292. Thilagan, J., S. Gopalakrishnan, and T. Kannadasan, *A study on adsorption of copper (II) ions in aqueous solution by chitosan-cellulose beads cross linked by formaldehyde.* International journal of pharmaceutical and chemical sciences, 2013. **2**(2): p. 1043-1054.
293. Yousefi, T., et al., *Removal of Pb (II) by modified natural adsorbent; thermodynamics and kinetics studies.* Journal of Water and Environmental Nanotechnology, 2018. **3**(3): p. 265-272.
294. Soldatkina, L. and M. Zavrichko, *Equilibrium, kinetic, and thermodynamic studies of anionic dyes adsorption on corn stalks modified by cetylpyridinium bromide.* Colloids and Interfaces, 2018. **3**(1): p. 4.
295. Ho, Y.-S. and G. McKay, *Pseudo-second order model for sorption processes.* Process biochemistry, 1999. **34**(5): p. 451-465.
296. Baby, R., B. Saifullah, and M.Z. Hussein, *Palm Kernel Shell as an effective adsorbent for the treatment of heavy metal contaminated water.* Scientific Reports, 2019. **9**(1): p. 18955.
297. He, Y., et al., *Efficient removal of Pb (II) from aqueous solution by a novel ion imprinted magnetic biosorbent: Adsorption kinetics and mechanisms.* PloS one, 2019. **14**(3): p. e0213377.
298. Giles, C.H., D. Smith, and A. Huitson, *A general treatment and classification of the solute adsorption isotherm. I. Theoretical.* Journal of colloid and interface science, 1974. **47**(3): p. 755-765.
299. Giles, C.H., A.P. D'Silva, and I.A. Easton, *A general treatment and classification of the solute adsorption isotherm part. II. Experimental interpretation.* Journal of colloid and interface science, 1974. **47**(3): p. 766-778.
300. Jebrane, M., *Fonctionnalisation chimique du bois par transesterification des esters d'enol*. 2009, Bordeaux 1.
301. Limousin, G., et al., *Sorption isotherms: A review on physical bases, modeling and measurement.* Applied geochemistry, 2007. **22**(2): p. 249-275.
302. Langmuir, I., *The adsorption of gases on plane surfaces of glass, mica and platinum.* Journal of the American Chemical society, 1918. **40**(9): p. 1361-1403.
303. Duong, D.D., *Adsorption analysis: equilibria and kinetics.* (No Title), 1998.
304. Langmuir, I., *The constitution and fundamental properties of solids and liquids. Part I. Solids.* Journal of the American chemical society, 1916. **38**(11): p. 2221-2295.
305. Özacar, M. and İ.A. Şengil, *Equilibrium data and process design for adsorption of disperse dyes onto alunite.* Environmental Geology, 2004. **45**: p. 762-768.
306. Amirouche, L., *Etude du pouvoir de sorption du cuivre (II), du Zinc (II) et des polyphénols par les bentonites sous l'effet des irradiations micro-ondes*. 2011, UMMTO.
307. Freundlich, H., *Über die adsorption in lösungen.* Zeitschrift für physikalische Chemie, 1907. **57**(1): p. 385-470.
308. Reffas, A., E.M. Bencheikh, and L. Duclaux, *Étude de l'adsorption de colorants organiques (rouge nylosan et bleu de méthylène) sur des charbons actifs préparés à partir du marc de café.* 2017.
309. Schulthess, C. and D. Sparks, *Equilibrium-based modeling of chemical sorption on soils and soil constituents.* Advances in Soil Science: Volume 16, 1991: p. 121-163.

310. Shaker, M.A., *Dynamics and thermodynamics of toxic metals adsorption onto soil-extracted humic acid.* Chemosphere, 2014. **111**: p. 587-595.
311. Özer, A., F. Tümen, and M. Bildik, *Cr (III) removal from aqueous solutions by depectinated sugar beet pulp.* Environmental technology, 1997. **18**(9): p. 893-901.
312. Zhao, Z., et al., *The reaction thermodynamics during plating Al on graphene process.* Materials, 2019. **12**(2): p. 330.
313. Adebayo, G., H. Adegoke, and S. Fauzeeyat, *Adsorption of Cr (VI) ions onto goethite, activated carbon and their composite: kinetic and thermodynamic studies.* Applied Water Science, 2020. **10**(9): p. 1-18.
314. Gorzin, F. and M. Bahri Rasht Abadi, *Adsorption of Cr (VI) from aqueous solution by adsorbent prepared from paper mill sludge: Kinetics and thermodynamics studies.* Adsorption Science & Technology, 2018. **36**(1-2): p. 149-169.
315. An, F.-Q., et al., *Adsorption of heavy metal ions by iminodiacetic acid functionalized D301 resin: Kinetics, isotherms and thermodynamics.* Reactive and Functional Polymers, 2017. **118**: p. 42-50.
316. Salvestrini, S., *Analysis of the Langmuir rate equation in its differential and integrated form for adsorption processes and a comparison with the pseudo first and pseudo second order models.* Reaction Kinetics, Mechanisms and Catalysis, 2018. **123**(2): p. 455-472.
317. Wu, P., et al., *Adsorption mechanisms of five bisphenol analogues on PVC microplastics.* Science of the Total Environment, 2019. **650**: p. 671-678.
318. Jiang, G., et al., *Structure and properties of regenerated cellulose fibers from different technology processes.* Carbohydrate polymers, 2012. **87**(3).
319. Mahmoudian, S., et al., *Preparation of regenerated cellulose/montmorillonite nanocomposite films via ionic liquids.* Carbohydrate Polymers, 2012. **88**(4): p. 1251-1257.
320. Li, H., et al., *Macro-/nanoporous Al-doped ZnO/cellulose composites based on tunable cellulose fiber sizes for enhancing photocatalytic properties.* Carbohydrate polymers, 2020. **250**: p. 116873.
321. Diallo, D., et al., *Étude des constituants des feuilles de Ziziphus mauritiana Lam.(Rhamnaceae), utilisées traditionnellement dans le traitement du diabète au Mali.* Comptes Rendus Chimie, 2004. **7**(10-11): p. 1073-1080.
322. Zhu, Y., et al., *Optimization of enzyme-assisted extraction and characterization of polysaccharides from Hericium erinaceus.* Carbohydrate polymers, 2014. **101**: p. 606-613.
323. Szymańska-Chargot, M., et al., *Isolation and characterization of cellulose from different fruit and vegetable pomaces.* Polymers, 2017. **9**(10): p. 495.
324. Kouadri, I. and H. Satha, *Extraction and characterization of cellulose and cellulose nanofibers from Citrullus colocynthis seeds.* Industrial Crops and Products, 2018. **124**: p. 787-796.
325. Cai, J. and L. Zhang, *Rapid dissolution of cellulose in LiOH/urea and NaOH/urea aqueous solutions.* Macromolecular bioscience, 2005. **5**(6): p. 539-548.
326. Serna, F., J. Lagneau, and J.-M. Carpentier, *La diffraction des rayons X: une technique puissante pour résoudre certains problèmes industriels et technologiques.* Chim. Nouv, 2014: p. 1-12.
327. Ghidan, A.Y., T.M. Al-Antary, and A.M. Awwad, *Green synthesis of copper oxide nanoparticles using Punica granatum peels extract: Effect on green*

peach Aphid. Environmental Nanotechnology, Monitoring & Management, 2016. **6**: p. 95-98.
328. Megashah, L.N., et al., *Modification of cellulose degree of polymerization by superheated steam treatment for versatile properties of cellulose nanofibril film.* Cellulose, 2020. **27**(13): p. 7417-7429.
329. PAQUETON, H. and J. RUSTE, *Microscopie électronique à balayage Principe et équipement.* Techniques de l'ingénieur. Analyse et caractérisation, 2006(P865v2).
330. Ben Mya, O., *Synthèse et caractérisation de la pérovskite La1-x SrxFe0. 7Ni0. 3O3*. 2015, Université Mohamed Khider-Biskra.
331. Inkson, B.J., *Scanning electron microscopy (SEM) and transmission electron microscopy (TEM) for materials characterization*, in *Materials characterization using nondestructive evaluation (NDE) methods*. 2016, Elsevier. p. 17-43.
332. George, G., R. Wilson, and J. Joy, *Ultraviolet Spectroscopy: A Facile Approach for the Characterization of Nanomaterials*, in *Spectroscopic Methods for Nanomaterials Characterization*. 2017, Elsevier. p. 55-72.
333. Mäntele, W. and E. Deniz, *UV–VIS absorption spectroscopy: Lambert-Beer reloaded*. 2017, Elsevier. p. 965-968.
334. Tauc, J. and A. Menth, *States in the gap.* Journal of non-crystalline solids, 1972. **8**: p. 569-585.
335. De Viguerie, L., *Propriétés physico-chimiques et caractérisation des matériaux du 'sfumato'*. 2009, Université Pierre et Marie Curie-Paris VI.
336. GUERRAM, A., *Synthèse verte et caractérisation des nanoparticules de ZnO à l'aide d'extrait des feuilles de Phoenix dactylifera L et leur applications*. 2022, Faculté des Sciences et de la technologie.
337. Ngah, W.W., L. Teong, and M.M. Hanafiah, *Adsorption of dyes and heavy metal ions by chitosan composites: A review.* Carbohydrate polymers, 2011. **83**(4): p. 1446-1456.
338. Lipatova, I.M., L.I. Makarova, and A.A. Yusova, *Adsorption removal of anionic dyes from aqueous solutions by chitosan nanoparticles deposited on the fibrous carrier.* Chemosphere, 2018. **212**: p. 1155-1162.
339. Wei, X., et al., *Bio-inspired functionalization of microcrystalline cellulose aerogel with high adsorption performance toward dyes.* Carbohydrate polymers, 2018. **198**: p. 546-555.
340. Bouzaida, I. and M. Rammah, *Adsorption of acid dyes on treated cotton in a continuous system.* Materials Science and Engineering: C, 2002. **21**(1-2): p. 151-155.
341. Sun, D., et al., *Adsorption of anionic dyes from aqueous solution on fly ash.* Journal of hazardous materials, 2010. **181**(1-3): p. 335-342.
342. Kausar, A., et al., *Dyes adsorption using clay and modified clay: A review.* Journal of Molecular Liquids, 2018. **256**: p. 395-407.
343. Aly-Eldeen, M.A., et al., *The uptake of Eriochrome Black T dye from aqueous solutions utilizing waste activated sludge: Adsorption process optimization using factorial design.* The Egyptian Journal of Aquatic Research, 2018. **44**(3): p. 179-186.
344. Samal, K., N. Raj, and K. Mohanty, *Saponin extracted waste biomass of Sapindus mukorossi for adsorption of methyl violet dye in aqueous system.* Surfaces and Interfaces, 2019. **14**: p. 166-174.

345. Lianou, A., E. Panagou, and G.-J. Nychas, *Microbiological spoilage of foods and beverages*, in *The stability and shelf life of food*. 2016, Elsevier. p. 3-42.
346. Lewis, L., et al., *Aflatoxin contamination of commercial maize products during an outbreak of acute aflatoxicosis in eastern and central Kenya.* Environmental health perspectives, 2005. **113**(12): p. 1763-1767.
347. Angulo, F.J., et al., *Diarrhoeal disease in children due to contaminated food.* 2017.
348. Abatenh, E., et al., *The role of microorganisms in bioremediation-A review.* Open Journal of Environmental Biology, 2017. **2**(1): p. 038-046.
349. Dimitrijević, S.I., et al., *A study of the synergistic antilisterial effects of a sub-lethal dose of lactic acid and essential oils from Thymus vulgaris L., Rosmarinus officinalis L. and Origanum vulgare L.* Food chemistry, 2007. **104**(2): p. 774-782.
350. Provincial, L., et al., *Survival of Vibrio parahaemolyticus and Aeromonas hydrophila in sea bream (Sparus aurata) fillets packaged under enriched CO2 modified atmospheres.* International Journal of Food Microbiology, 2013. **166**(1): p. 141-147.
351. Saraiva, C., et al., *Modelling the fate of Listeria monocytogenes in beef meat stored at refrigeration temperatures under different packaging conditions.* Procedia Food Science, 2016. **7**: p. 177-180.
352. Säde, E., et al., *Exploring lot-to-lot variation in spoilage bacterial communities on commercial modified atmosphere packaged beef.* Food microbiology, 2017. **62**: p. 147-152.
353. Samy, R.P. and S. Ignacimuthu, *Antibacterial effects of the bark of Terminalia arjuna: justification of folklore beliefs.* Pharmaceutical Biology, 2001. **39**(6): p. 417-420.
354. Bazerque, P., C. Perez, and M. Pauli, *Antibiotic assay by the Agar-well Diffusion Method.* Acta Biol Med Exp, 1990. **15**: p. 113-5.
355. Magaldi, S., et al., *Well diffusion for antifungal susceptibility testing.* International journal of infectious diseases, 2004. **8**(1): p. 39-45.
356. Valgas, C., et al., *Screening methods to determine antibacterial activity of natural products.* Brazilian journal of microbiology, 2007. **38**: p. 369-380.
357. Choi, Y., et al., *Antioxidant and antimicrobial activities of propolis from several regions of Korea.* LWT-Food Science and Technology, 2006. **39**(7): p. 756-761.
358. Basli, A., et al., *Activité antibactérienne des polyphénols extraits d'une plante médicinale de la flore d'Algérie: Origanum glandulosum Desf.* Phytothérapie, 2012. **10**(1): p. 2-9.
359. Mouas, Y., F.Z. Benrebiha, and C. Chaouia, *ÉVALUATION DE L'ACTIVITÉ ANTIBACTERIENNE DE L'HUILE ESSENTIELLE ET DE L'EXTRAIT MÉTHANOLIQUE DU ROMARIN ROSMARINUS OFFICINALIS L.* Revue Agrobiologia, 2017. **7**(1): p. 363-370.
360. KADRI, M., et al., *Chromatography analysis, in vitro antioxidant and antibacterial activities of essential oil of Artemisia herba-alba Asso of Boussaâda, Algeria.* Biodiversitas Journal of Biological Diversity, 2022. **23**(9).
361. Wiegand, I., K. Hilpert, and R.E. Hancock, *Agar and broth dilution methods to determine the minimal inhibitory concentration (MIC) of antimicrobial substances.* Nature protocols, 2008. **3**(2): p. 163-175.

362. Boumediri, H., et al., *Extraction and characterization of vascular bundle and fiber strand from date palm rachis as potential bio-reinforcement in composite.* Carbohydrate Polymers, 2019. **222**: p. 114997.
363. Vijay, R., et al., *Characterization of raw and alkali treated new natural cellulosic fibers from Tridax procumbens.* International journal of biological macromolecules, 2019. **125**: p. 99-108.
364. Saravanakumar, S., et al., *Characterization of a novel natural cellulosic fiber from Prosopis juliflora bark.* Carbohydrate polymers, 2013. **92**(2): p. 1928-1933.
365. Liu, R., H. Yu, and Y. Huang, *Structure and morphology of cellulose in wheat straw.* Cellulose, 2005. **12**(1): p. 25-34.
366. Mayandi, K., et al., *A comparative study on characterisations of Cissus quadrangularis and Phoenix reclinata natural fibres.* Journal of Reinforced Plastics and Composites, 2015. **34**(4): p. 269-280.
367. Ilyas, R., et al., *Mechanical testing of sugar palm fiber reinforced sugar palm biopolymer composites*, in *Advanced Processing, Properties, and Applications of Starch and Other Bio-Based Polymers*. 2020, Elsevier. p. 89-110.
368. Jiang, Y., et al., *Tensile properties and structure characterization of palm fibers by alkali treatment.* Fibers and Polymers, 2019. **20**(5): p. 1029-1035.
369. Getie, S., et al., *Synthesis and characterizations of zinc oxide nanoparticles for antibacterial applications.* J Nanomed Nanotechno S, 2017. **8**(004).
370. Suryanto, H., et al. *Effect of alkali treatment on crystalline structure of cellulose fiber from mendong (Fimbristylis globulosa) straw*. in *Key Engineering Materials*. 2014. Trans Tech Publ.
371. Wang, H. and C. Xie, *Effect of annealing temperature on the microstructures and photocatalytic property of colloidal ZnO nanoparticles.* Journal of Physics and Chemistry of Solids, 2008. **69**(10): p. 2440-2444.
372. Cheng, D., et al., *Characterization of potential cellulose fiber from Luffa vine: A study on physicochemical and structural properties.* International Journal of Biological Macromolecules, 2020. **164**: p. 2247-2257.
373. Wada, M., L. Heux, and J. Sugiyama, *Polymorphism of cellulose I family: reinvestigation of cellulose IVI.* Biomacromolecules, 2004. **5**(4): p. 1385-1391.
374. Terea, H., et al., *Preparation and characterization of cellulose/ZnO nanoparticles extracted from peanut shells: effects on antibacterial and antifungal activities.* Biomass Conversion and Biorefinery, 2023: p. 1-12.
375. Guan, Y., et al., *Green one-step synthesis of ZnO/cellulose nanocrystal hybrids with modulated morphologies and superfast absorption of cationic dyes.* International journal of biological macromolecules, 2019. **132**: p. 51-62.
376. Sharma, P.R., et al., *Efficient removal of arsenic using zinc oxide nanocrystal-decorated regenerated microfibrillated cellulose scaffolds.* ACS Sustainable Chemistry & Engineering, 2019. **7**(6): p. 6140-6151.
377. Nam, S., et al., *Segal crystallinity index revisited by the simulation of X-ray diffraction patterns of cotton cellulose Iβ and cellulose II.* Carbohydrate polymers, 2016. **135**: p. 1-9.
378. Adel Salih, A., R. Zulkifli, and C.H. Azhari, *Tensile properties and microstructure of single-cellulosic bamboo fiber strips after alkali treatment.* Fibers, 2020. **8**(5): p. 26.

379. Yu, H.-Y., et al., *New approach for single-step extraction of carboxylated cellulose nanocrystals for their use as adsorbents and flocculants.* ACS Sustainable Chemistry & Engineering, 2016. **4**(5): p. 2632-2643.
380. Heinze, T. and T. Liebert, *Celluloses and polyoses/hemicelluloses.* 2012.
381. Sun, X., et al., *Characteristics of degraded cellulose obtained from steam-exploded wheat straw.* Carbohydrate research, 2005. **340**(1): p. 97-106.
382. Neto, W.P.F., et al., *Extraction and characterization of cellulose nanocrystals from agro-industrial residue–Soy hulls.* Industrial Crops and Products, 2013. **42**: p. 480-488.
383. Poletto, M., H.L. Ornaghi Junior, and A.J. Zattera, *Native cellulose: structure, characterization and thermal properties.* Materials, 2014. **7**(9): p. 6105-6119.
384. Madureira, A.R., et al., *Extraction and characterisation of cellulose nanocrystals from pineapple peel.* International Journal of Food Studies, 2018.
385. Rotaru, R., C. Peptu, and V. Harabagiu, *Viscose-barium titanate composites for electromagnetic shielding.* Cellulose Chem. Tech, 2016. **50**: p. 621-628.
386. Lu, P. and Y.-L. Hsieh, *Preparation and properties of cellulose nanocrystals: rods, spheres, and network.* Carbohydrate polymers, 2010. **82**(2): p. 329-336.
387. Manimaran, P., et al., *Characterization of natural cellulosic fibers from Nendran Banana Peduncle plants.* International Journal of Biological Macromolecules, 2020. **162**: p. 1807-1815.
388. Ravindran, D., S.B. SR, and S. Indran, *Characterization of surface-modified natural cellulosic fiber extracted from the root of Ficus religiosa tree.* International journal of biological macromolecules, 2020. **156**: p. 997-1006.
389. Nurfadlilah, L. and R. Hidayah, *Antibacterial Activity of Sugarcane Bagasse Nanocellulose Biocomposite with Chitosan Against Escherichia coli.* Jurnal Kimia VALENSI Volume, 2021. **7**(1).
390. Mansour, R., A. Abdelaziz, and A.F. Zohra, *Characterization of long lignocellulosic fibers extracted from Hyphaene thebaica L. leaves.* Research Journal of Textile and Apparel, 2018.
391. Vinod, A., et al., *Characterization of untreated and alkali treated natural fibers extracted from the stem of Catharanthus roseus.* Materials Research Express, 2019. **6**(8): p. 085406.
392. Chen, Y., H.-Y. Yu, and Y. Li, *Highly efficient and superfast cellulose dissolution by green chloride salts and its dissolution mechanism.* ACS Sustainable Chemistry & Engineering, 2020. **8**(50): p. 18446-18454.
393. Ibrahim, A.A., et al., *Utilization of carboxymethyl cellulose based on bean hulls as chelating agent. Synthesis, characterization and biological activity.* Carbohydrate polymers, 2011. **83**(1): p. 94-115.
394. Zak, A.K., et al., *Effects of annealing temperature on some structural and optical properties of ZnO nanoparticles prepared by a modified sol–gel combustion method.* Ceramics International, 2011. **37**(1): p. 393-398.
395. Calcott, P.H., *Cyclic AMP and cyclic GMP control of synthesis of constitutive enzymes in Escherichia coli.* Microbiology, 1982. **128**(4): p. 705-712.
396. Xaba, T., P.P. Mongwai, and M. Lesaoana, *Decomposition of bis (N-benzyl-salicydenaminato) zinc (II) complex for the synthesis of ZnO nanoparticles to fabricate ZnO-chitosan nanocomposite for the removal of iron (II) ions from wastewater.* Journal of Chemistry, 2019. **2019**.
397. Jasmani, L. and S. Adnan, *Preparation and characterization of nanocrystalline cellulose from Acacia mangium and its reinforcement potential.* Carbohydrate polymers, 2017. **161**: p. 166-171.

398. Vasconcelos, N.F., et al., *Bacterial cellulose nanocrystals produced under different hydrolysis conditions: Properties and morphological features.* Carbohydrate polymers, 2017. **155**: p. 425-431.
399. Leipner, H., et al., *Structural changes of cellulose dissolved in molten salt hydrates.* Macromolecular Chemistry and Physics, 2000. **201**(15): p. 2041-2049.
400. Shen, C., et al., *Acidified ZnCl2 molten salt hydrate systems as hydrolytic media for cellulose I and II nanocrystal production: from rods to spheres.* Cellulose, 2022. **29**(14): p. 7629-7647.
401. Mohamed, M.A., et al., *Bio-inspired hierarchical hetero-architectures of in-situ C-doped g-C3N4 grafted on C, N co-doped ZnO micro-flowers with booming solar photocatalytic activity.* Journal of Industrial and Engineering Chemistry, 2019. **77**: p. 393-407.
402. Shingange, K., et al., *0D to 3D ZnO nanostructures and their luminescence, magnetic and sensing properties: Influence of pH and annealing.* Materials Research Bulletin, 2017. **85**: p. 52-63.
403. Kukushkin, S. and S. Nemna. *The effect of pH on nucleation kinetics in solutions*. in *Doklady Physical Chemistry*. 2001. Springer.
404. Fu, F., et al., *Interfacial assembly of ZnO–cellulose nanocomposite films via a solution process: a one-step biomimetic approach and excellent photocatalytic properties.* Cellulose, 2017. **24**: p. 147-162.
405. Kian, L.K., et al., *Isolation and characterization of nanocrystalline cellulose from roselle-derived microcrystalline cellulose*. International journal of biological macromolecules, 2018. **114**: p. 54-63.
406. Chowdhury, Z.Z. and S.B. Abd Hamid, *Preparation and characterization of nanocrystalline cellulose using ultrasonication combined with a microwave-assisted pretreatment process.* BioResources, 2016. **11**(2): p. 3397-3415.
407. Pathania, D., S. Sharma, and P. Singh, *Removal of methylene blue by adsorption onto activated carbon developed from Ficus carica bast.* Arabian journal of chemistry, 2017. **10**: p. S1445-S1451.
408. Gouamid, M., M. Ouahrani, and M. Bensaci, *Adsorption equilibrium, kinetics and thermodynamics of methylene blue from aqueous solutions using date palm leaves.* Energy procedia, 2013. **36**: p. 898-907.
409. Yang, S., et al., *Adsorption of Ni (II) on oxidized multi-walled carbon nanotubes: effect of contact time, pH, foreign ions and PAA.* Journal of hazardous materials, 2009. **166**(1): p. 109-116.
410. Adeogun, A.I., et al., *Biowaste-derived hydroxyapatite for effective removal of reactive yellow 4 dye: equilibrium, kinetic, and thermodynamic studies.* ACS omega, 2018. **3**(2): p. 1991-2000.
411. Johnson, B.B., *Effect of pH, temperature, and concentration on the adsorption of cadmium on goethite.* Environmental Science & Technology, 1990. **24**(1): p. 112-118.
412. Sun, X.-F., et al., *Biosorption of Malachite Green from aqueous solutions onto aerobic granules: Kinetic and equilibrium studies.* Bioresource Technology, 2008. **99**(9): p. 3475-3483.
413. Doğan, M., M.H. Karaoğlu, and M. Alkan, *Adsorption kinetics of maxilon yellow 4GL and maxilon red GRL dyes on kaolinite.* Journal of Hazardous Materials, 2009. **165**(1-3): p. 1142-1151.

414. Kargi, F. and S. Ozmıhcı, *Biosorption performance of powdered activated sludge for removal of different dyestuffs.* Enzyme and Microbial Technology, 2004. **35**(2-3): p. 267-271.
415. Errais, E., et al., *Efficient anionic dye adsorption on natural untreated clay: Kinetic study and thermodynamic parameters.* Desalination, 2011. **275**(1-3): p. 74-81.
416. Teka, T. and S. Enyew, *Study on effect of different parameters on adsorption efficiency of low cost activated orange peels for the removal of methylene blue dye.* International Journal of Innovation and Scientific Research, 2014. **8**(1): p. 106-111.
417. Malik, P.K., *Use of activated carbons prepared from sawdust and rice-husk for adsorption of acid dyes: a case study of Acid Yellow 36.* Dyes and pigments, 2003. **56**(3): p. 239-249.
418. Mane, V.S., I.D. Mall, and V.C. Srivastava, *Kinetic and equilibrium isotherm studies for the adsorptive removal of Brilliant Green dye from aqueous solution by rice husk ash.* Journal of environmental management, 2007. **84**(4): p. 390-400.
419. Ho, Y.S. and G. McKay, *The kinetics of sorption of divalent metal ions onto sphagnum moss peat.* Water research, 2000. **34**(3): p. 735-742.
420. Nekouei, F., et al., *Kinetic, thermodynamic and isotherm studies for acid blue 129 removal from liquids using copper oxide nanoparticle-modified activated carbon as a novel adsorbent.* Journal of Molecular Liquids, 2015. **201**: p. 124-133.
421. Gong, R., et al., *Removal of cationic dyes from aqueous solution by adsorption on peanut hull.* Journal of hazardous materials, 2005. **121**(1-3): p. 247-250.
422. Islam, M.A., et al., *Methylene blue adsorption on factory-rejected tea activated carbon prepared by conjunction of hydrothermal carbonization and sodium hydroxide activation processes.* Journal of the Taiwan Institute of Chemical Engineers, 2015. **52**: p. 57-64.
423. Hameed, B.H., *Spent tea leaves: a new non-conventional and low-cost adsorbent for removal of basic dye from aqueous solutions.* Journal of hazardous materials, 2009. **161**(2-3): p. 753-759.
424. Ks, G. and S. Belagali, *Removal of heavy metals and dyes using low cost adsorbents from aqueous medium-, a review.* IOSR journal of Environmental Science, toxicology and food technology, 2013. **4**(3): p. 56-68.
425. Mustapha, S., et al., *Adsorption isotherm, kinetic and thermodynamic studies for the removal of Pb (II), Cd (II), Zn (II) and Cu (II) ions from aqueous solutions using Albizia lebbeck pods.* Applied water science, 2019. **9**: p. 1-11.
426. Goudarzi, A., et al., *Ammonia-free chemical bath deposition of nanocrystalline ZnS thin film buffer layer for solar cells.* Thin Solid Films, 2008. **516**(15): p. 4953-4957.
427. Tsade Kara, H., et al., *Removal of methylene blue dye from wastewater using periodiated modified nanocellulose.* International Journal of Chemical Engineering, 2021. **2021**: p. 1-16.
428. EL-Mekkawi, D.M., F.A. Ibrahim, and M.M. Selim, *Removal of methylene blue from water using zeolites prepared from Egyptian kaolins collected from different sources.* Journal of Environmental Chemical Engineering, 2016. **4**(2): p. 1417-1422.

429. Pasichnyk, M., et al., *Development of polyester filters with polymer nanocomposite active layer for effective dye filtration.* Scientific Reports, 2022. **12**(1): p. 973.
430. Jawad, A.H., N.S.A. Mubarak, and A.S. Abdulhameed, *Hybrid crosslinked chitosan-epichlorohydrin/TiO 2 nanocomposite for reactive red 120 dye adsorption: kinetic, isotherm, thermodynamic, and mechanism study.* Journal of Polymers and the Environment, 2020. **28**: p. 624-637.
431. AlOthman, Z.A., et al., *Valorization of two waste streams into activated carbon and studying its adsorption kinetics, equilibrium isotherms and thermodynamics for methylene blue removal.* Arabian Journal of Chemistry, 2014. **7**(6): p. 1148-1158.
432. Chebli, D., et al., *Valorization of an agricultural waste, Stipa tenassicima fibers, by biosorption of an anionic azo dye, Congo red.* Desalination and Water Treatment, 2015. **54**(1): p. 245-254.
433. Ramdani, A., et al., *Lead and cadmium removal by adsorption process using hydroxyapatite porous materials.* Water practice and Technology, 2020. **15**(1): p. 130-141.
434. Belaid, K.D. and S. Kacha, *Étude cinétique et thermodynamique de l'adsorption d'un colorant basique sur la sciure de bois.* Revue des Sciences de l'eau, 2011. **24**(2): p. 131-144.
435. Elmoubarki, R., et al., *Adsorption of textile dyes on raw and decanted Moroccan clays: Kinetics, equilibrium and thermodynamics.* Water resources and industry, 2015. **9**: p. 16-29.
436. HPS, A.K., et al., *A review on chitosan-cellulose blends and nanocellulose reinforced chitosan biocomposites: Properties and their applications.* Carbohydrate polymers, 2016. **150**: p. 216-226.
437. Nieß, A., M. Siemann-Herzberg, and R. Takors, *Protein production in Escherichia coli is guided by the trade-off between intracellular substrate availability and energy cost.* Microbial Cell Factories, 2019. **18**(1): p. 1-10.
438. Padmavathy, N. and R. Vijayaraghavan, *Enhanced bioactivity of ZnO nanoparticles—an antimicrobial study.* Science and technology of advanced materials, 2008.
439. Abebe, B., et al., *PVA assisted ZnO based mesoporous ternary metal oxides nanomaterials: synthesis, optimization, and evaluation of antibacterial activity.* Materials Research Express, 2020. **7**(4): p. 045011.
440. Candan, F., et al., *Antioxidant and antimicrobial activity of the essential oil and methanol extracts of Achillea millefolium subsp. millefolium Afan.(Asteraceae).* Journal of ethnopharmacology, 2003. **87**(2-3): p. 215-220.
441. Bougherra, H.H., et al., *Pistacia lentiscus essential oil has repellent effect against three major insect pests of pasta.* Industrial Crops and Products, 2015. **63**: p. 249-255.
442. Kanagasubbulakshmi, S. and K. Kadirvelu, *Green synthesis of iron oxide nanoparticles using Lagenaria siceraria and evaluation of its antimicrobial activity.* Defence Life Science Journal, 2017. **2**(4): p. 422-427.
443. Ahmad, W., K. Kumar Jaiswal, and M. Amjad, *Euphorbia herita leaf extract as a reducing agent in a facile green synthesis of iron oxide nanoparticles and antimicrobial activity evaluation.* Inorganic and Nano-Metal Chemistry, 2021. **51**(9): p. 1147-1154.

444. Kim, S.H., B.L. Schneider, and L. Reitzer, *Genetics and regulation of the major enzymes of alanine synthesis in Escherichia coli.* Journal of bacteriology, 2010. **192**(20): p. 5304-5311.
445. Ahmad, W., K.K. Jaiswal, and S. Soni, *Green synthesis of titanium dioxide (TiO2) nanoparticles by using Mentha arvensis leaves extract and its antimicrobial properties.* Inorganic and Nano-Metal Chemistry, 2020. **50**(10): p. 1032-1038.
446. Ahmad, W. and D. Kalra, *Green synthesis, characterization and anti microbial activities of ZnO nanoparticles using Euphorbia hirta leaf extract.* Journal of King Saud University-Science, 2020. **32**(4): p. 2358-2364.
447. Kontiza, I., et al., *New metabolites with antibacterial activity from the marine angiosperm Cymodocea nodosa.* Tetrahedron, 2008. **64**(8): p. 1696-1702.
448. Paramita, D.A.K., N.S. Antara, and I.B.W. Gunam, *INHIBITION ACTIVITY of ESSENTIAL OIL of LEMONGRASS LEAVES (Cymbopogon citratus) ON THE GROWTH OF Escherichia coli, Staphylococcus aureus, AND Vibrio cholerae.* Jurnal Rekayasa Dan Manajemen Agroindustri, 2014. **2**(1): p. 29-38.

General Conclusion

This work aims to exploit agricultural waste, specifically peanut shells and pea shells, for the synthesis of nanocomposite cellulose/zinc oxide (CNC/ZnO NPs). Several preliminary treatments were conducted on the waste to obtain pure cellulose, followed by acid chemotherapy with H2SO4 to convert it into nanocellulose.

The chemical method Sol-Gel was used to synthesize the ZnO NPs on the CNCs in two different states. Consequently, CNC/ZnO NPs were obtained using two methods: the first method involved cellulose dissolution with an alkaline solution (a mixture of NaOH and urea), while the second method used CNCs without any adjustments.

Various characterization techniques were employed to confirm and analyze the CNC/ZnO NPs prepared using the two different methods. The optical properties, visible ultraviolet radiation, and FTIR analysis demonstrated distinctive absorption ranges, confirming the formation of ZnO NPs on CNCs. Additionally, FTIR analysis revealed differences across all stages, from the peanut and pea shells (the source of cellulose production) to the CNC/ZnO NPs. These differences proved the effectiveness of removing non-cellulose materials and the presence of the Zn-O bond, validating the successful formation of CNC/ZnO NPs.

XRD analysis results exhibited common peaks in all Cs and CNCs samples derived from peanut and pea shells, as well as distinct peaks indicating ZnO formation in CNC/ZnO NPs samples from both methods.

SEM analysis indicated different forms of the prepared nano compound using the two methods. In the first method, ZnO NPs covered every point on the CNCs surface, resulting in a smooth surface without any abnormalities. In contrast, the second method showed random and scattered positions of ZnO NPs on CNCs. Additionally, chemical element analysis corresponded with the XRD results, confirming the purity of all prepared samples and the absence of impurities, thereby enhancing the success of the preparation steps and methods.

The adsorption experiments demonstrated that the adsorption capacity of BM dye on cellulose samples and CNC/ZnO NPs was directly proportional to most of the studied variables (mass, time, pH, and initial concentration).

Also, the increase in temperature has a direct effect on the CNC/ZnO NPs, but an inverse effect on Cs. Adsorption isotherm modeling revealed that the Freundlich model is the most suitable for describing the isotherm in all Cs and CNC/ZnO NPs samples. Adsorption kinetic modeling demonstrated that the pseudo-second-order model is the most appropriate for describing the adsorption kinetics. Thermodynamic results indicated that the adsorption on cellulose was an endothermic process, while on the nanocomposite it was exothermic. The values of $\Delta H°$ were less than 60 KJ/mol, and the negative $\Delta G°$ confirmed the physical and favorable adsorption of MB dye on Cs and CNC/ZnO NPs.

The antimicrobial activities of all Cs and CNC/ZnO NPs samples were evaluated, and it was observed that the hybridization of cellulose with ZnO NPs significantly enhanced its effectiveness against both Gram-positive and Gram-negative bacteria as well as fungi. The results were highly promising and satisfactory, as they demonstrated the inhibition of bacterial and fungal growth. Furthermore, the activity was strongly influenced by the method used for the synthesis of CNC/ZnO NPs, with higher antimicrobial activity observed in samples prepared using the first method.

The obtained results have proven that:

- Regardless of the number of sources used in the extraction of cellulose, the resulting cellulose is chemically the same. However, there are differences in its physical properties, such as size, shape, color, and hardness. This was demonstrated by its behavior and effects observed in the study of adsorption, antibacterial, and antifungal properties.
- The hybridization process of cellulose with ZnO NPs did not enhance its effectiveness in removing methyl blue dye from aqueous solutions. The results obtained using cellulose alone as an adsorbent were better than those obtained using CNC/ZnONPs.
- The successful hybridization of cellulose with ZnO NPs was evident in its antibacterial and antifungal activity. The results obtained using CNC/ZnONPs were better than those obtained using cellulose alone.
- Based on these findings, cellulose, and CNC/ZnONPs can be utilized as active agents for the purification and removal of dyes from aqueous solutions. This promising application opens new horizons for the use of cellulose and its

derived nanomaterials in improving water quality and environmental protection.

- CNC/ZnO NPs offer interesting properties that make them excellent alternatives for targeted drug delivery and controlling the growth of microorganisms and toxins in food.

SCIENTIFIC

PUBLICATIONS

Articles on 'A' Class Journals

Terea, H., Selloum, D., Rebiai, A., Bouafa, A. & Ben Mya, O. *Preparation and characterization of cellulose/ZnO nanoparticles extracted from peanut shells: Efects on antibacterial and antifungal activities*. Biomass Convers. Biorefnery, https://doi.org/10.1007/s13399-023-03959-7 (2023)

Terea, H., Selloum, D., Rebiai, A., Atia, D., Kouadri, I., Ben Seghir., &. Messaoudi, M. Characterization, biological, and antimicrobial propertiesof nanocellulose isolated from peanut shells (Arachis hypogaea L.). Biomass Convers. Biorefnery, https://doi.org/10.1007/s13399-023-04792-8 (2023)

International Seminars

Hafdha Terea, Djamel Selloum, Abdelkrim Rebiai, "*Synthesis and characterization of cellulose/ZnO nanocomposite from plant wastes"*, internationalseminaronmaterials synthesis and environmental monitoring(ISMSEM22)07-09February2022, Ouergla, Algérie. ***(Oral Communication)***

Hafdha Terea, Djamel Selloum, Abdelkrim Rebiai, " *Isolation and characterization of nanocellulose by treating plant waste (for Archis Hypogaea L)*", 1 st International Conference on Chemical Maters and Environment Preservation (IC-CMEP22), 22-23 February2022, Ouergla, Algérie. ***(Poster Communication)***

Hafdha Terea, Djamel Selloum, Abdelkrim Rebiai, " *Adsorbtion of MB on cellulose extracted from plant wasts*", International Conference on Valuation of Alternative Plants and Degraded and Marginal Lands, 10-11 may 2022 , EL-Oued, Algérie. ***(Poster Communication)***

Hafdha Terea, Djamel Selloum, Abdelkrim Rebiai, " *Synthesis the biocomposite Cellulose/Zinc oxide Nanocomposite (CNC/ZnO NPs)* ", 3rd International Conference on Engineering and Applied Natural Sciences, January 14-17, 2023, Konya, Turkey. ***(Oral Communication)***.

Hafdha Terea, Djamel Selloum, Abdelkrim Rebiai, " *Extraction and characterization the cellulose from peanut shells and application in adsorption of Methylene Bluedye from aqueous solutions* ", The first international Seminar on

Catalysis, Chemical Engineering & Green Chemistry, (CaCEG-2023) , February 22-23, 2023 – El Oued, Algeria. ***(Poster Communication)***.

National Seminars

Hafdha Terea, Djamel Selloum, Abdelkrim Rebiai, " *Extraction of cellulose from plant wastes Arachis hypogaea L to preparation of cellulose nanofibers*", 1ER SÉMINAIRE NATIONAL EN GÉNIE DES PROCÉDÉS, (SNGP2021), 08 December 2021, Ouergla, Algérie. ***(Poster Communication)***.

Hafdha Terea, Djamel Selloum, Abdelkrim Rebiai, " *Preparation and characterization of bio-nanocomposites from plant residues (archis hypogaea L)* ", The first National Seminar on Green Chemistry and Natural Products, (NGCNP2022), 14-15 March 2022, EL-Oued, Algérie.***(Poster Communication)***.

Hafdha Terea, Djamel Selloum, Abdelkrim Rebiai, " *Préparation et caractérisation de la cellulose extraite de déchets végétaux comme adsorbant de colorants à partir de solutions aqueuses* ", The first National Conference on chemical procese and environemental engineering**,** 15-16 December 2021, EL-Oued, Algérie.***(Oral Communication)***.

Hafdha Terea, Djamel Selloum, Abdelkrim Rebiai,Allag Nassiba and Berra Djamila**,** " *Synthesis and Characterization of Cellulose/ZnO Nanocomposite (CNC/ZnO NPs) from peanut shells* ",Proceedings of 1st National Conference of Materials sciences And Engineering, (MSE'22), 28-29 june 2022, Khenchla, Algérie. ***(Oral Communication)***.

Berra Djamila, **Hafdha Terea**,and Allag Nassiba ," *Synthesis and Characterization of copper mixed oxides (CuO/CuO2) nanoparticule produced from the leaves of Phoenix dactylifera L*",Proceedings of 1st National Conference of Materials sciences And Engineering, (MSE'22), 28-29 june 2022, Khenchla, Algérie. ***(Poster Communication)***.

Study Day

Hafdha Terea, Djamel Selloum, Abdelkrim Rebiai, "*Preparationand characterization of cellulose extracted from plant waste",* The First Study Day of Materials Science & Applications (1JE-MSA'21), 08 décembre 2021, El Oued, Algérie. ***(Poster Communication)***